12-2012

ON-LINE TRANSIENT STABILITY STUDIES INCORPORATING WIND POWER

Zhenhua Wang
Clemson University, zhenhuw@clemson.edu

ON-LINE TRANSIENT STABILITY STUDIES INCORPORATING WIND POWER

A Dissertation
Presented to
the Graduate School of
Clemson University

In Partial Fulfillment
of the Requirements for the Degree
Doctor of Philosophy
Electrical Engineering

---

by
Zhenhua Wang
December 2012

Accepted by:
Dr. Elham B. Makram, Committee Chair
Dr. John N. Gowdy
Dr. Richard E. Groff
Dr. Peter Kiessler

ABSTRACT

Transient stability is a major concern in power system security and reliability because it is the most common type of instability and its impacts can cause greatest economic losses. For enhancing the energy security, it requires the power system operation to be evaluated during both the planning and the operation stage. Many online/offline transient stability assessment techniques have already been developed for this purpose. However, due to the increase in energy demand, the modern power system has grown to a very sophisticated and large system for which extent transient stability assessment methods may not be able to handle. In addition, the new published regulation rules and new concepts such as the smart grid have also pushed the requirement for transient stability assessment to a higher level. Thus, this dissertation is intended to study large scale power system transient stability. It starts from establishing an analytical approach for power system transient stability assessment. Based on the results, the disadvantages of traditional concepts used in transient stability assessment have been discussed. In order to overcome the difficulties encountered by classical approaches, a new technique for estimating the generator rotor angle difference in multi-machine power system is developed. It is more practical and has been applied to study the impact of wind power generation on power system transient stability afterwards. Since recently there is a significant increase in the importance of renewable energy and its related optimizations in power systems, the final goal of this dissertation focuses on the power system optimal power flow technique with wind power penetration and transient stability constrains. For making results more convincible, the South Carolina offshore wind speed data is used as

the availability of wind power. An approach for maintaining the power system economic operation within the security range has been given at the end of this dissertation.

DEDICATION

To my wonderful parents, Shiguang Wang and Jiqing Rong for all of their love, support and guidance; to my fiancée, Zhao Liu for her continuous encouragement and help.

ACKNOWLEDGMENTS

I would like to thank late Dr. Adly A. Girgis, for all of his tutorial and guidance, my advisor, Dr. Elham B. Makram, for her hard work and support on my Ph.D. study and Dr. G. Kumar Venayagamoorthy for his help and suggestions in my research. I would also like to thank Dr. John N. Gowdy, Dr. Richard E. Groff and Dr. Peter Kiessler for their willingness to be part of the committee and valuable advice.

I am grateful to my fellow graduate students in CUEPRA power group for their assistance.

TABLE OF CONTENTS

Page

Table of Contents (Continued)

Page

LIST OF TABLES

LIST OF FIGURES

List of Figures (Continued)

Figure Page

List of Figures (Continued)

Figure Page

CHAPTER ONE

INTRODUCTION

1.1 Motivation for power system transient stability assessment

The complexity of the modern power system has required new techniques to enhance the stability. In August 2003 the blackout affected 61,800 MWs of load and an area of 50 million people in the states of Ohio, Michigan, Pennsylvania, New York, Vermont, Massachusetts, Connecticut, New Jersey and the Canadian state of Ontario. The total losses were about 4 to 10 billion dollars [1]. Investigation has revealed that the reason for the blackout was failure to maintain the system within secure operating limits. Unfortunately, studies have also pointed out that the 2003 blackout was not an isolated incident. Actually the study found that the entire North American power system was operating close to the critical margin. For preventing severe blackout and for national energy security, a more efficient technique for rapidly detecting and responding to the potential dangerous scenarios is urgently needed. Real time power system stability assessment is the key to this technique. One of the biggest problems in realizing the fast dynamic security assessment technique is the heavy computation burden. Usually the power system dynamic security assessment involves differential equation sets which are solved by iteration methods such as Runge-Kutta method and some other given references. When these approaches are applied to fast response stability applications with the power system which contains thousands of buses, the required time is not acceptable.

The development of power systems has required new techniques to enhance the stability. The Federal Energy Regulatory Commission (FERC) issued a final rule, Order No. 888 [2] in response to provisions of the Energy Policy Act (EPACT) of 1992. It requires utilities which own, control and operate transmission lines to file non-discriminatory open access tariffs that offer others the same electricity transmission service they provide themselves. The second final rule, Order No. 889 [3], requires a real-time information system to assure that transmission owners and their affiliates do not have an unfair competitive advantage in using transmission to sell power. With these rules and other actions an increase in the demand for transmission services is expected. However, they also elevate the requirements of power system operations to maintain the reliability and security. Previously the power system was monopolized by a few utilities. This mechanism easily allowed the utility to establish procedures for system operation and control to prevent overloading and other emergencies. However, with a more competitive power market and a more deregulated power system, it can no longer make arbitrary plans to let the system withstand contingencies and avoid any severe static and dynamic system disturbances. In a deregulated system, the efficient utilization of the transmission system and maximum utilization of revenue would further push the power system to the stability limit.

The optimal operation of the power system has required new techniques to enhance the stability. According to [4], if the oscillatory response of the power system during the transient period following such disturbances is damped and the system settles in a finite time to a new steady operating condition, the system is considered stable. With

the absence of a proper real time stability assessment technique, until recently the power system operators still have to control the system according to the result from offline study of the transmission planning process. Usually the offline study generates the operating thresholds such as maximum power flow on transmission lines, minimum bus voltages and maximum generator angle differences. Some utilities perform their offline dynamic security simulations every day with the operating conditions forecasted for the next day. The results of these studies, which are usually performed overnight, are provided to power system operators. For the reason of ensuring safe operations, these thresholds determined by offline studies are often conservative which contradict to the purpose of economic operation. If the system limits are calculated based on actual conditions rather than hypothetical offline studies, the power system can be operated more efficiently. This will increase the transfer capability of the power grid and enhance the wholesale trade of the power industry.

During past years, great efforts have been put into the study of power system stability, especially the transient stability. According to the above context, there are two major obstacles which limit the development in this field. The first difficulty is the requirement of the real-time analysis. For real-time control, the stability assessment time frame usually requires about less than 10 seconds [5]. Unfortunately, the offline study showed that to finish such simulation needs several minutes or even hours. This makes it impossible to help power system operators to make decisions within a short period of time. The second difficulty is the complexity of the modern power system structure and operation pattern. The stability assessment is like pattern recognition which classifies the

stable and unstable scenarios according to the operation status. Finding proper characters to distinguish the state of a complex system is a very difficult task. Beyond these, to handle such a large scale power system also requires more sophisticated measurement and communication techniques.

The motivation of this research is to develop new techniques for large scale power system transient stability assessment and its related studies. It focuses on studying the generator rotor angle behavior in the multi-machine power system and finding more efficient characters to determine the system operating conditions.

1.2 Difficulty in power system transient stability assessment techniques

The power system stability problem includes three aspects which are: transient stability, voltage stability and frequency stability [6]. Transient stability is a major concern in power system security and reliability because it is the most common type of instability and its impacts can cause greatest economic losses. Transient stability assessment has been part of electric utility guidelines for more than two decades. Generally speaking, transient stability refers to the synchronism of generators rotor angles in the power system. The result of transient stability assessment is used for preventing the occurrence of instability and correcting the potential dangerous scenarios to enhance the reliability. The effectiveness of transient stability assessment in a real-time environment is based on the speed and accuracy. Early methods developed for the power system transient stability utilize the out-of-step relay [7]. Besides, there were also lots of analytical methods designed for transient stability assessment. Except for their performance, the major concern with these methods is the simplification involved in the

calculation. Usually the simplification refers to reducing a power system which contains multiple generators to a simple system which only contains two generators or so called one machine infinite bus (SMIB) system.

Commonly the disturbance (such as short circuit fault, losing of generation or load changing) induces a sudden oscillation of energy redistribution in power system. It causes a change in generator output power. Meanwhile the generator input energy cannot be adjusted instantaneously according to the new power distribution and it results in an energy mismatch at the generator, which could accelerate generator rotor's rotating speed. Because generators are located in different places, effects of the disturbance to each generator also cannot be the same. With the different generator inertias, after the disturbance there are always some generators gaining higher rotor speed so that they could finally deviate from the other generators (details will be demonstrated by the equal area criteria in Chapter Two). Since the steam turbine is designed to operate within a narrow speed range, slightly faster than nominal speed for a while can damage the turbine or trigger serious accidents. For protecting expensive equipment, it is required that unstable generators quit operation or that the power grid be split into islands immediately. On the other hand if control actions for protecting the system are too aggressive, the excessive amounts of generator offline can induce further losses of generation which will intensify the disturbance and cause extra economic losses. Thus, the goal of power system transient stability assessment lies in identifying unstable generators as fast as possible to minimize the impact of disturbance on the power system.

The basic thought of power system transient stability assessment comes from two-machine system and the equal area criteria. People tried to expand this idea to multi-machine system by using the SMIB equivalent system. The SMIB system worked well with traditional power systems since these systems are simple in topology and small in scale. However, for the modern power system, the technique used before seemed no longer adequate. The modern power system has become much more sophisticated both in the topology and the operation state variations. The simple SMIB equivalent system does not have enough accuracy to represent the operation of modern power systems.

1.3 Contributions

The research in this dissertation is focused on power system transient stability related problems. Techniques developed in this dissertation are aimed on the following features:

a. Faster speed in solving large scale power systems and the ability to handle the complexity of the large-scale power system operation
b. Better performance than traditional methods
c. Power system economic operation under stability constrains with renewable energy sources

1.3.1 Power system transient stability assessment using catastrophe theory

Chapter Four starts with the classical power system transient stability assessment technique. Compared with previous direct methods, the proposed technique in Chapter Four has greatly improved the performance of transient stability assessment techniques

by using the catastrophe theory. In Chapter Four, a more appropriate character for classifying the stable and unstable operations in large scale power systems has been proposed. It used the continuity of the generator rotor maximum swing angle to determine the stability conditions instead of actual value of regular parameters, such as the voltage profile, the generator rotor angle and the generator output power. This approach will help to reduce the difficulty of handling numerous operation states which occur in modern power systems. This simulation result clearly shows that the proposed technique's performance is much better than previous methods. However, the study also proves the inadequacy of classical ideas in power system stability studies such as the SMIB system and the associated center of inertia (COI). Hence, in the following research, a new concept for power system transient stability assessment has been developed to overcome difficulties discovered in Chapter Four.

1.3.2 Generator rotor angle difference estimation for multi-machine power system

Instead of power system stability, Chapter Five is mainly focused on processing the signal from power system measurement devices. Due to the unpredictability of the large scale power system, the classical angle reference for calculating the rotor angle difference between a single generator and the system is no longer acceptable. In Chapter Five the research purpose is aimed on finding a "true" generator rotor angle difference to evaluate the multi-machine power system transient stability.

1.3.3 Transient stability constrained power system optimization with wind power generation

Chapter Six discusses applying the technique developed in Chapter Five with renewable energy sources and an approach for power system economic operation. In the past, renewable energy such as wind and solar only obtains a small portion of the total generation. The impact of renewable energy on power system stability is negligible. In recent years, for the reason of energy sustainability and security, countries all over the world are seeking to increase the percentage of the renewable energy in their power generation. However, the study of the impact of the renewable energy penetration on power system transient stability still remains not well established. The purpose of Chapter Six is to develop the preliminary work of studying the impact of wind turbines to power system with South Carolina off shore wind speed. Based on this, it will introduce a feasible approach of optimizing the power system operation including wind power and transient stability constrains.

CHAPTER TWO

POWER SYSTEM TRANSIENT STABILITY

Chapter Two is a brief introduction of basics elements in the power system transient stability assessment.

2.1 The generator swing function and power system transient stability assessment

The objective of transient stability study is to determine if the generator rotor can return to constant speed after a disturbance. Using the simple equivalent model of synchronous generator, the equation representing the synchronous generator rotor motion is given as

$$J\frac{d^2\theta}{dt^2} = T_m - T_e \tag{2.1}$$

where

J Generator's moment inertia ($kg - m^2$)

θ The angular displacement of the rotor with respect to a stationary axis on generator stator (rad)

t time (s)

T_m The input mechanical torque (N-m)

T_e The output electrical torque (N-m)

If the generator's internal friction losses and the heating losses are neglected, to maintain synchronous speed under ideal operation situation, the input mechanical torque

T_m and the output electrical torque T_e should be equal. When the input mechanical torque is greater than the output electrical torque, the generator rotor will accelerate and vice versa. Fig. 2.1 is a simplified diagram of the synchronous generator. It illustrates the stator, rotor, input mechanical torque and output electrical torque. The ω_m is the synchronous speed of generator. In 60 Hz power system, it equals to 120π rad/s and in 50 Hz power system it equals to 100π rad/s.

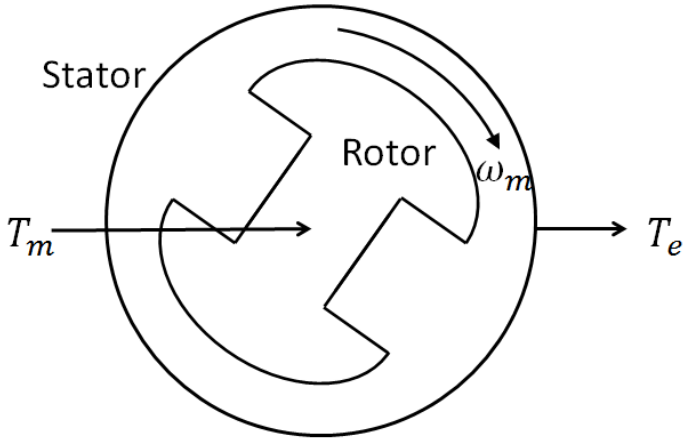

Fig.2.1 Simplified diagram of the synchronous generator

In power systems, most of the generators are synchronous generators driven by the steam turbine. The input torque T_m of this kind of generator is controlled by the turbine governor. The governor adjusts the amount of steam entering the steam turbine according to the generator output power. The output torque T_e is the equivalent torque which relates to the power fed into the power system. It reflects the instantaneous power system operation status. Due to the physical nature of the steam turbine, the generator input torque cannot be adjusted immediately. After the disturbance, because of the slow response speed of the input torque, when the output torque is less than the input torque, it

is possible that the generator will gain enough energy to keep its rotor accelerating forever. This is the innate nature of power system transient stability – the balance of generator input and output torque (power).

The generator output torque cannot be directly obtained because only the generator electric power output can be measured. The electric power equals the torque multiplies the angular velocity. When the generator is synchronous with the power grid, the angular velocity is called synchronous speed ω_m. The relation between generator electric power and the output torque is illustrated in (2.2):

$$P_G = T_G * \omega_m \tag{2.2}$$

Substitute (2.2) into (2.1) yields to:

$$J\omega_m \frac{d^2\theta}{dt^2} = P_m - P_e \tag{2.3}$$

where

P_m Input mechanical power

P_e Output electric power

The angle θ in (2.3) is measured with respect to a stationary reference axis on the stator. This means its value is increasing continuously with time. The most common way of describing the change of generator rotor angle is to use the synchronous speed as the reference. Therefore, (2.4) defines the generator rotor angle displacement with respect to the synchronous speed:

$$\delta_m = \theta - \omega_m t \tag{2.4}$$

δ_m is called electric angle for the purpose of distinguishing the θ and δ_m.

The second order derivative of (2.4) with respect of time is:

$$\frac{d^2\delta_m}{dt^2} = \frac{d^2\theta}{dt^2} \tag{2.5}$$

Substitute (2.5) into (2.3) yields to the generator swing function used for transient stability studies.

$$M\frac{d^2\delta_m}{dt^2} = P_m - P_e \tag{2.6}$$

where

M The coefficient which equals to $J\omega_m$

In (2.6) P_m can be measured at the prime mover of the generator. P_e is the electrical power output which is calculated by the power flow equation.

Assuming there is a small power system which contains only two generators G1 and G2. The bus admittance matrix for this system is given as:

$$Y_{bus} = \begin{bmatrix} Y_{11} & Y_{12} \\ Y_{21} & Y_{22} \end{bmatrix} \tag{2.7}$$

where

Y_{ij} Nodal admittance between node i and j

The injected complex power of generator G1 is calculated as:

$$P_{G1} + jQ_{G1} = E_1 \sum_{k=1}^{2} (Y_{1k}E_k)^* \tag{2.8}$$

When define:

$$E_i = |E_i|\angle\delta_i \qquad Y_{ij} = G_{ij} + jB_{ij} = |Y_{ij}|\angle\theta_{ij}$$

Equation (2.8) yields to:

$$P_{G1} = |E_1|^2 G_{11} + |E_1||E_2||Y_{12}|\cos(\theta_{12} + \delta_2 - \delta_1) \quad (2.9)$$

$$Q_{G1} = -|E_1|^2 B_{11} - |E_1||E_2||Y_{12}|\sin(\theta_{12} + \delta_2 - \delta_1) \quad (2.10)$$

Equation (2.9) is the active power output of generator G1. It can be rewritten as;

$$P_{G1} = |E_1|^2 G_{11} + |E_1||E_2||Y_{12}|(\cos(\theta_{12})\cos(\delta_2 - \delta_1) + \sin(\theta_{12})\sin(\delta_1 - \delta_2)) \quad (2.11)$$

For simplicity, if assuming the admittance Y_{ij} between node i and j is approximately equal to pure susceptance, $cos(\theta_{12}) = 0$ and $sin(\theta_{12}) = 1$. Therefore (2.11) becomes:

$$P_{G1} = |E_1|^2 G_{11} + |E_1||E_2||Y_{12}|\sin(\delta_1 - \delta_2) \quad (2.12)$$

The active power exchanged between node 1 and 2 is:

$$P_{12} = |E_1||E_2||Y_{12}|\sin(\delta_1 - \delta_2) \quad (2.13)$$

Equation (2.13) can be expanded to a system with n generators, the total active power exchange between generator 1 and other generators is given as:

$$P_1 = |E_1|^2 G_{11} + \sum_{\substack{j=1 \\ j \neq i}}^{n} |E_i||E_j||Y_{ij}|\sin\left(\delta_i - \delta_j\right) \quad (2.14)$$

Substitute (2.14) into (2.6) yields to the generator swing equation:

$$M_i \frac{d^2\delta_i}{dt^2} = P_m - |E_i|^2 G_{ii} - \sum_{\substack{j=1 \\ j \neq i}}^{n} |E_i||E_j||Y_{ij}|\sin\left(\delta_i - \delta_j\right) \quad (2.15)$$

Therefore, for a power system with *n* generators, each generator is represented by a swing equation given by (2.15). The transient response of the power system is described by a differential equation set which contains *n* functions and variables. The initial

condition of the differential equation set is obtained by the power flow and it is solved by Rung-Kutta or some other step by step iteration methods. Then the generator angle δ_i can be plotted for the purpose of transient stability assessment.

The generator swing function given by (2.15) is called second order model which is the simplest model. For higher accuracy, higher order generator models can be employed such as the third order model [8] showed by (2.16) and (2.17).

$$M_i \frac{d^2\delta_i}{dt^2} = P_m - P_e \tag{2.16}$$

$$T'_{do} \frac{dE'_q}{dt} = E_f - E'_q + I_d(X_d - X'_d) \tag{2.17}$$

where

E'_q Transient quadrature axis voltage

E_f Field voltage

X'_d Transient direct axis impedance

X_d Direct axis impedance

I_d Direct axis current

T'_{do} Direct axis open circuit time constant

In addition, the load and other components in the power system should be modeled in detail for higher accuracy. All these more accurate models will greatly increase the number of differential functions representing the power system. For a large

scale power system, it is impossible to calculate the generator rotor angle in real time for transient stability assessment.

2.2 Analytical method for power system transient stability assessment

The process of solving the power system dynamic response in section 2.1 is also known as time-domain method. Due to its high computation burden, the analytical method has been developed to study the power system transient stability. The equal area criterion is the fundamental of the analytical method.

2.2.1 Equal area criterion

The derivation of the equal area criterion is based on SMIB equivalent system. The infinite bus refers a power system whose capacity is much bigger than the generator under study. The swing equation for the generator connected to the infinite bus is:

$$M\frac{d^2\delta}{dt^2} = P_m - P_e \tag{2.18}$$

The angular velocity of the generator rotor relative to the synchronous speed is defined as:

$$\omega_m = \frac{d\delta}{dt} = \omega - \omega_s \tag{2.19}$$

Substitute (2.19) into (2.18) yields:

$$M\frac{d\omega_m}{dt} = P_m - P_e \tag{2.20}$$

Multiplying both sides of (2.20) by $\omega_m = \frac{d\delta}{dt}$ yields to:

$$M\omega_m\frac{d\omega_m}{dt} = (P_m - P_e)\frac{d\delta}{dt} \tag{2.21}$$

Rewritten the (2.21) as:

$$\frac{M}{2}\frac{d{\omega_m}^2}{dt} = (P_m - P_e)\frac{d\delta}{dt} \tag{2.22}$$

Multiply by *dt* and integrating (2.22) yields to:

$$\frac{M}{2}({\omega_{m2}}^2 - {\omega_{m1}}^2) = \int_{\delta_1}^{\delta_2}(P_m - P_e)d\delta \tag{2.23}$$

In (2.23) ω_{r2} is the angular velocity when the generator rotor angle equals to δ_2 and ω_{r1} is the angular velocity when the generator rotor angle equals to δ_1. δ_1 is the initial rotor angle before disturbance. Assuming the power system operation is ideal, since there is no oscillation, $\omega_{r1} = 0$. After the disturbance, when the rotor angle has changed to δ_2 with angle velocity ω_{r2}, if the system can go back to synchronous and δ_2 is the maximum value of the generator rotor angle, $\omega_{r2} = \omega_{r1} = 0$. Under this condition, (2.23) becomes:

$$0 = \int_{\delta_1}^{\delta_2}(P_m - P_e)d\delta \tag{2.24}$$

Equation (2.24) can be applied with any two points δ_1 and δ_2. In power system the disturbances which cause transient stability problem are usually suddenly increase/decrease of load or generation and power oscillations due to the disturbance and following tie line tripping. For the reliability issue, the system should be designed to withstand the most severe disturbance [9]. Therefore, the three-phase to ground fault on the tie line and tripping the faulty line is usually selected as disturbance for the power system transient stability studies. Since before and after tripping the tie line, the power system topology and corresponding generator electrical power output P_e are changed, the integration of (2.24) should be separated into two steps. Assume the generator rotor angle

before the disturbance is δ_1, the tie line is tripped when it reaches δ_c and the maximum value it can reach is δ_m, Eq. (2.24) can be modified as:

$$\int_{\delta_1}^{\delta_c}(P_m - P_e)d\delta + \int_{\delta_c}^{\delta_m}(P_m - P_e)d\delta = 0 \quad (2.25)$$

Or $$\int_{\delta_1}^{\delta_c}(P_m - P_e)d\delta = \int_{\delta_c}^{\delta_m} -(P_m - P_e)d\delta \quad (2.26)$$

The equal area criterion is illustrated by the power angle diagram in Fig. 2.2. The sinusoidal curves represent the active power output of the generator with respect to the generator rotor angle δ. The straight line is the generator mechanical power input P_m. The shaded Area 1 is given by the left-hand side of Eq. (2.26) and the shaded area 2 is given by the right-hand side of Eq. (2.26). The size of Area 1, which depends on the fault clearing time, refers to the acceleration energy gained during the fault. It is the energy made the generator asynchronous. Likewise the Area 2 refers to the deceleration energy after the disturbance. It counters the acceleration energy and pulls the generator back to synchronous.

A late tripping of the faulty line results in a bigger δ_c. It will increase the size of Area 1 in Fig. 2.2. This requires a bigger Area 2 to neutralize the acceleration energy. The size of Area 2 can also be increased by moving δ_m to the left in Fig. 2.2. However, δ_m cannot go beyond 180^o if the system is stable. This is because the generator electric power output P_e is less than 0 after it passes 180^o. It can never be greater than the mechanical power input P_m. In this situation the generator rotor will continue to accelerate. Thus the transient stability status can be determined by comparing the size of Area 1 and the maximum possible size of Area 2.

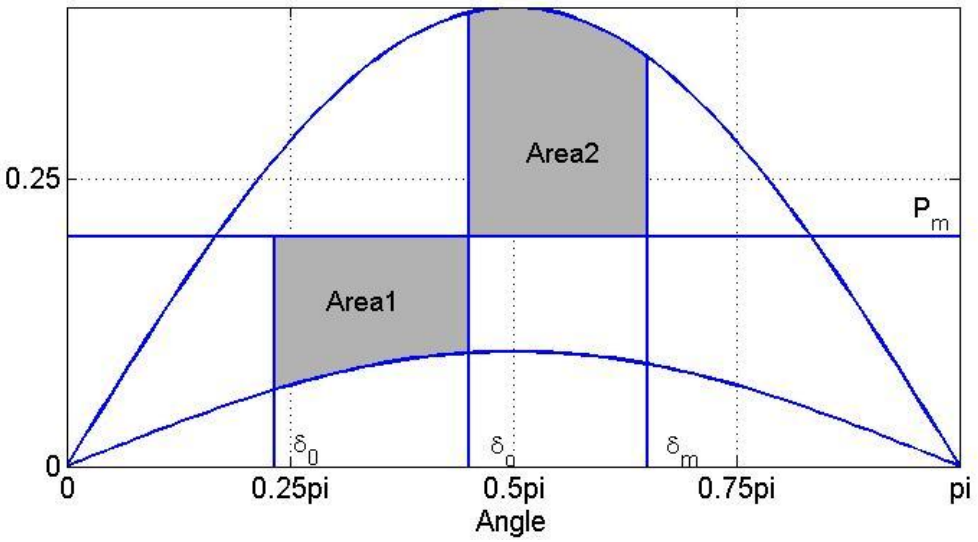

Fig. 2.2 Equal area criterion

The equal area criterion provides an analytical approach to study the power system transient stability. Most of the extant techniques developed for transient stability assessment are based on the equal area criterion. However it is valid under following assumptions:

a. The mechanical power input does not change after the disturbance
b. The voltage behind the generator transient reactance does not change after the disturbance

Actually these assumptions are valid only during a short period after the disturbance and in the SMIB system. The following chapters will discuss the limitation of using these assumptions for large scale power system transient stability assessment.

2.2.2 Equal area criterion in time domain

The balance between the acceleration energy and the deceleration is usually described by the energy conservation law: $(P_m - P_e)$ is the net power gained by the generator. If during time $t_m - t_0$ the net energy is 0, the generator will keep synchronous. But the power is integrated with rotor angle δ in equation (2.26). The following process will explain this.

Firstly multiplying each side of (2.18) by $\frac{d\delta}{dt}$:

$$\frac{d\delta}{dt} M \frac{d^2\delta}{dt^2} = (P_m - P_e) \frac{d\delta}{dt} \tag{2.27}$$

Equation (2.27) can be rearranged as:

$$d\left[\left(\frac{d\delta}{dt}\right)^2\right] = \frac{2}{M}(P_m - P_e)d\delta \tag{2.28}$$

Integrating both sides of (2.28):

$$\left(\frac{d\delta}{dt}\right)^2 = \frac{2}{M}\int_{\delta_0}^{\delta_m}(P_m - P_e)d\delta \tag{2.29}$$

Equation (2.29) can be rearranged as:

$$\frac{d\delta}{dt} = \left(\frac{2}{M}\int_{\delta_0}^{\delta_m}(P_m - P_e)d\delta\right)^{0.5} \tag{2.30}$$

When the system is stable, $\frac{d\delta}{dt}$ should equal to 0. This gives equation (2.25) and (2.26).

CHAPTER THREE

LITERATURE REVIEW

This chapter is the brief discussion of the recent progress on power system transient stability and its related studies. The advantage and disadvantage of these approaches will be summarized and discussed for demonstrating the research motivation of this dissertation.

3.1 Transient stability assessment techniques

There are three common approaches developed for transient stability studies, namely: time domain simulation methods, automatic learning methods and direct methods. Each of these approaches has its unique advantages and disadvantages. Following sections will explain details and cite existing achievements of these three approaches.

3.1.1 Time domain simulation techniques

In time domain simulation, the power system is described by differential equations. When the operation state has changed, differential equations are solved for each Δt so that the pending operation state can be obtained. Without the consideration of speed, the time domain simulation is the most dependable approach for studying power system transient stability problems because it simulates the behavior of entire power system. Its accuracy only depends on the equivalent model of the power system components. However, when the ability of real time application has been emphasized, the

time domain simulation method suffers from either the speed or the error from system simplifications.

Reference [10] is a typical example of using time domain simulation for obtaining the power system operating state after the disturbance. The system snapshot comes from a real time EMS (Energy Management System). A real time power system simulator uses this data to forecast the possible operating states. The result from the simulator is then used to determine the stability. This scheme is the most dependable approach. However, the ability of real time EMS and real time power system simulator are still not achieved.

For improving the performance of time domain simulation, some simplifications on power system components have been devised. Reference [11] presented a faster implicitly decoupled PQ integration technique to predict the post disturbance dynamics. The author has introduced constant load equivalent and constant transfer admittance equivalent in this paper to simplify the power system.

If the computation technology can be greatly improved, the time domain simulation would be the most promising approach for power system transient stability studies. The recently development of PMU has enabled some possibility of the time domain simulation in real time applications [12]. At present the most popular approaches in this area is still experience/training based automatic learning methods and power system operating character extraction based direct methods.

3.1.2 Automatic learning techniques

The advantage of automatic learning technique is to obtain the impending operating states without doing power system simulations. However, this kind of method

requires large amount of operation data to train the decision making system. When the power system is large, the effort for constructing the decision making system and training is unacceptable. Also the training may not be able to handle the unexpected situation and results in false decisions.

Reference [13] introduced a self-adaptive method for solving the unexpected situations in the power system transient stability assessment. The decision tree (DT) used in this paper is trained offline and updated online during the stability assessment process. For the offline DT building, the prospected operating conditions have been obtained by short period load forecasting or unit commitment programs which reflect the expected power flow and system topology. The decision tree is then updated while it is working on the security assessment. For each running cycle, if there is no new operating condition occurred, the decision tree is kept frozen. If new operating condition occurred, the decision tree will be updated according to the new operating condition. The data used for training the decision tree and assessing the stability are voltage and current phasors which are measured by PMU, the type of the disturbance and location of the disturbance. Reference [14] provides a similar decision making technique for the power system transient stability assessment.

Like the DT approach, many other automatic learning techniques have been applied to power system transient stability assessment such as the support vector [15-16] and neural networks [17].

3.1.3 Direct methods.

Direct method is the most popular approach in power system transient stability studies. It refers to those methods which utilize a theory or a concept to map the power system operation from one space to another so that it is easier to find characters or analytical solutions to forecast the system operating condition. For reducing the complexity, these kinds of approaches usually use equivalent systems to represent the actual power system [18].

Reference [19] is an early paper on multi-machine power system transient stability studies. It generally gives the idea of using the weighted average of generator rotor angle to reduce the multi-machine power system to the two-machine equivalent model and using the equal area criteria for the transient stability analysis. The idea of two-machine equivalent model has been widely used in the following researches.

Reference [20] studied the voltage phase angle and the generator transient energy by the "action principle" for the power system transient stability. The COI is used as the reference and it is calculated by the generator terminal voltage phase angle. The generator transient energy is evaluated by the equal area criteria introduced in Chapter Two.

Reference [21] gave an approach of using PMU for power system transient stability assessment. Because the PMU can measure 30 times every second which is much faster than classical measurements, the author in this paper has applied a piecewise constant current load equivalent technique (PCCLE) to predict the transient stability. The disturbance in this paper is assumed to be removed instantaneously so that the fault on stage can be ignored and only pre-fault and post-fault stages need to be considered. The

classical generator model with the static composite constant impedance load model is used to represent the power system. The generator terminal voltage phase angle, rotor angle and rotor angle speed are measured/estimated by using PMU data. The system operation trajectory is then plotted piece wisely. Then the stability is studied according this trajectory.

Reference [22] introduced a similar approach which is using the characteristic ellipsoid method for monitoring power system dynamic trajectory. It defines an N dimensional closed surface that represents the trajectory of one system parameters such as voltage magnitude, frequency or power flow on transmission lines. Each POI (point of interest) represents one dimension. Power system operation from pre-disturbance period to post-disturbance period is studied for stability assessment. The function of this method is to evaluate the system dynamic behavior by the trajectory of those operation parameters.

Reference [23-24] have proposed power system transient stability indices for stability assessment. The index in [25] is defined as the drop in synchronous power after the disturbance. Equation (3.1) and (3.2) illustrate the drop in synchronous power is actually the weighted average of power variation before and after the disturbance.

$$DP = \sum[M_i|P_{di}|/(\sum M_i)] \tag{3.1}$$

$$P_{di} = \frac{P_{ci}-P_{oi}}{M_i} - \frac{\sum P_{ci}-P_{oi}}{\sum M_i} \tag{3.2}$$

where

P_{ci} Generator output power after the disturbance

P_{oi} Generator output power before the disturbance

M_i Inertia

Reference [26] is a very useful paper. It gives an applicable approach of applying the COI in the power system swing equation. The modified swing equation could be used to calculate the unbalance between generator input and output energy with respect to COI. This modified swing equation is also used in Chapter Four with catastrophe theory. There are also many papers like [27-29] which use the generator swing equation to study the generator output energy. For the purpose of simplifying the power system which contains multiple generators, the concept of COI is also used along with the generator swing equation in these papers.

Besides studying generator output energy with the swing equation and COI, the Eigen value has also been used to determine the power system transient stability [30-31]. When the system scale is large, this approach has the disadvantage that it may cause unacceptable time consumptions.

3.2 Optimal power flow considering transient stability constrains

The most direct purpose of power system stability and security studies is the system optimal operation. This is the reason why Chapter Six is focused on the transient stability constrained optimal power flow.

Reference [32] introduces a power system optimization technique to increase the critical fault clearing time. This approach is to find the critical machine or cluster of critical machines, then reduce the system to two parts which are the critical machines and the rest of the system. The most serious fault on the terminal of critical machine is used to test the equivalent system and obtain the stability constrains. The optimization in this

paper is similar to the regular optimal power flow process. Both pre and post contingency limits such as the power flow on transmission lines have been added into inequality constrains so that the system operation can maintain a distance from the critical point. In addition, this paper has also mentions the difficulty of convergence when security constrains have been included into the optimization.

Reference [33] and [34] are about power system dynamic security dispatch. These approaches are constructed as regular optimal power flow plus the transient stability constrains. Typically, the limit of generator rotor angle difference is treated as the transient stability constrains. One thing should be noted is that the rotor angle difference in these papers is based on COI.

3.3 Conclusions

Although the literature review demonstrated completely different mathematical tools for power system transient stability studies, there are two common things among most of the references. One is the application of generator swing equations to link the generator rotor angle with the generator output power. The other is using the COI to simplify the multi-machine power system to the SMIB system. This dissertation will start with complying on these two ideas. Then it will analyze the major problems these literatures may encounter and try to make improvements. The result from the improvement will be used for power system operation optimizations which is the final goal of this dissertation. Chapter Four will start with the catastrophe theory and the COI for power system transient stability assessment. Chapter Five will switch to discuss the drawback of COI and propose a new technique to replace the COI for power system

transient stability studies. Based on the discoveries in Chapter Four and Five, Chapter Six will use the technique proposed in Chapter Five to study the impact of wind energy on power system transient stability and develop a power system optimal power flow technique with transient stability constrains for the wind power penetration.

CHAPTER FOUR

TRANSIENT STABILITY ASSESSMENT USING CATASTROPHE THEORY

As discussed in Chapter Three, the time domain analysis and automatic learning methods are considered to be difficult to realize due to the speed requirement for real time analysis, uncertainty and complexity of the power system. Literature review also revealed that the most popular approach is the direct method which usually refers to locating system operation characters and identifying thresholds for stability margin by using the generator swing equation. However, to determine the optimum threshold is a difficult task in large scale power system because of the various operating states and associated uncertainties. Significant efforts have been taken to improve the direct method and threshold modeling [35 -38]. In all these methods the intricacy still arises from finding a balance between the speed and the accuracy. Recently, people started to use PMU in power system monitoring and control. It can provide more information than the traditional SCADA system. With the help of PMU data, the purpose of this chapter is to design a new approach which can handle complex operating conditions in large scale power system.

4.1 Phasor measurement unit

The PMU is a measurement device with GPS satellite synchronization. It is used to measure voltage and current phasors in wide area power system. Before the invention of PMU, there was no practical way to measure the phase angle directly. This is because a small mismatch in measurement devices' sampling time would cause huge error in the 60Hz AC power system. Without PMU, when the phase angle was needed, a time

consuming power system state estimation program was used to be executed first. However with the GPS satellite synchronization, all measurement devices in power system will measure at the same time, no matter how far they are scattered.

The application of PMU brought significant improvement to real time power system applications. It enables utilizing the voltage and current phase angle in real time. This extra information can be added to develop new technologies for power system stability assessment.

4.2 Catastrophe theory

Catastrophe theory was initially used to study the sudden changes in system operation behaviors. Instead of representing the system operation by parameter values (in power system they could be voltage, current, generator rotor angle and etc.), the catastrophe theory analyzes the operational discontinuity of the system [39]. Suppose a system is defined by

$$y = F(x, s) \tag{4.1}$$

Where x represents the control variable vector and s represents the state variable vector. According to [40] the equilibrium set is:

$$\nabla_x F(x, s) = 0 \tag{4.2}$$

According to [40] the equilibrium set defines a multi-dimensional plane which has the same dimension as control variable x. The singularity set is a sum of all degenerate critical points of the equilibrium set. It is given by:

$$\nabla_x{}^2 F(x,s) = 0 \tag{4.3}$$

In catastrophe theory, variables which satisfy (4.3) define the discontinuity boundary. The discontinuity boundary is projected on a two-dimensional plane and partitions the plane into several regions. Each region represents one operation state [39]. In catastrophe theory there are four common manifolds used as the discontinuity boundary when the number of control variables is less than or equal to two. Table 4.1 lists these manifolds.

Table 4.1 Manifolds in Catastrophe Theory

Manifold	Singularity Set
Fold	$x^2 + a$
Cusp	$x^3 + ax + b$
Swallowtail	$x^4 + ax^2 + bx + c$
Butterfly	$x^5 + ax^3 + bx^2 + cx + d$

Fig. 4.1 is an example of the equilibrium set, singularity set of cusp manifold and its projection on a 2-D plane. In Fig. 4.1 the projection of singularity set divides the 2-D plane into two regions. According to catastrophe theory when the operation trajectory travels only inside one region, it means the system operation state is experiencing a slow and smooth change. In reality this behavior correlates to stable oscillations. To the contrary, the system operation trajectory crossing the equilibrium set represents that the system operation state was under sudden changes which related to the unstable operation. This is known as the discontinuity in catastrophe theory. The operation continuity can be used for stability assessment.

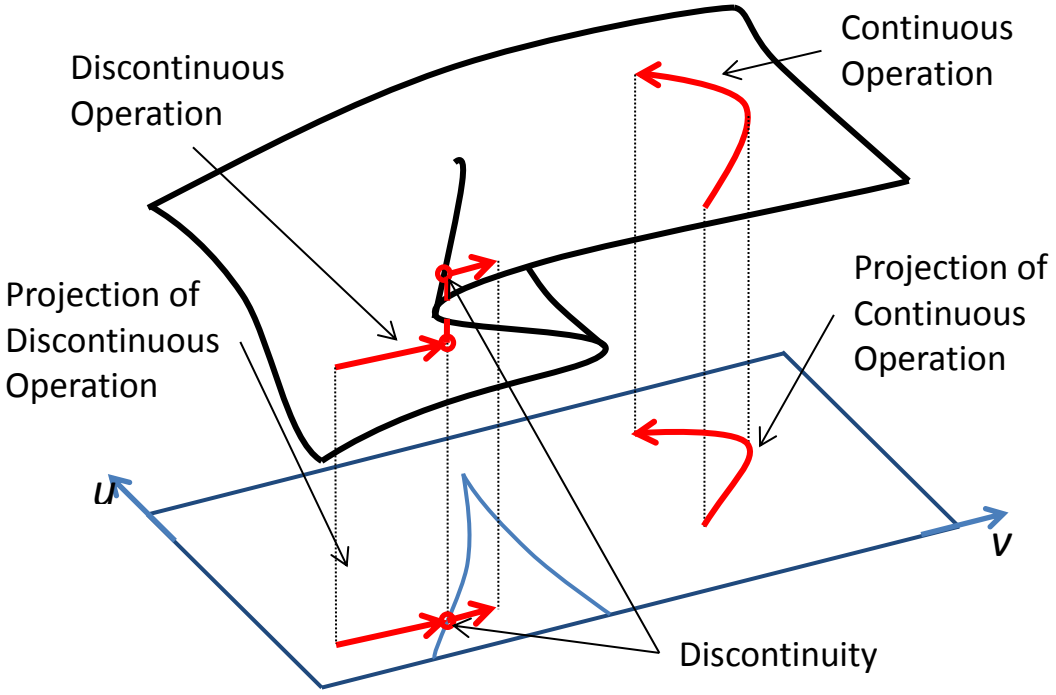

Fig. 4.1 Operation trajectory and its projection

The operation continuity in catastrophe theory provides a great advantage for stability assessment in complex large scale power systems. The common approach to stability assessment begins with modeling the system and selecting parameters to represent operation. Then thresholds for these parameters are determined to classify the operation states. Some of the states are assigned to the unstable group and some are assigned to the stable group. However, due to the uncertainty and complexity of the large scale power system, there are numerous operation states. It is difficult for classical direct methods to choose proper parameters and thresholds to distinguish all possible operating conditions. Catastrophe theory can category all operating conditions into continuous

operation and discontinuous operation, which directly correlate with the system stability. Also compared with automatic learning techniques, catastrophe theory only requires mapping the operational trajectory from one space to another space. Its computation takes less time than the training process. With above two advantages, the catastrophe theory method could be a great improvement in the development of power system stability assessment.

4.3 Catastrophe theory with transient stability assessment

A two-machine system (Fig. 4.2) and equal area criterion are taken as the example to illustrate the basic idea of finding the discontinuity in power system operation for transient stability assessment. The P-δ curve of generator A in a two-machine system [41] is shown in Fig. 4.3. The sinusoidal curve in Fig. 4.3 indicates the relation between generator active power output P_e and the rotor angle difference between two generators. In the ideal case without disturbance, the active power output is constant. It stays at the intersection of the P-δ curve and the mechanical power input, which denoted as "Point a" in Fig. 4.3. The correlated value of rotor angle difference equals δ_0. When the disturbance occurs, the rotor angle difference starts to increase. δ_c is the rotor angle difference when the disturbance has been cleared. If the two generators can return to synchronous, the rotor angle difference would increase until it reaches the maximum value δ_m and then starts to decrease. δ_m is called maximum swing angle. The flat line in Fig. 4.3 is the mechanical power input. It is assumed as constant after disturbance. Before disturbance, generator A follows the "Normal Operation Curve". After of the disturbance, generator A's active

power output suddenly drops to the "During Fault Operation Curve" when rotor angle difference equals to δ_0. Thus the energy mismatch would force the generator A's rotor to accelerate. Area 1 indicates this acceleration energy. At the time when rotor angle difference equals to δ_c, the disturbance was removed and the P-δ curve went back to the "Normal Operation Curve". At this time the electrical power output becomes greater than the mechanical power input. This would result in decreasing of generator A's rotor speed. Due to the generator A's inertia, the speed gained by Generator A during disturbance cannot be reduced to zero immediately. The rotor angle difference in this case would keep increasing until it reaches δ_m, where the total acceleration energy is canceled. Area 2 indicates this deceleration energy. Then due to the inertia, the rotor angle difference would continue to decrease after it reaches δ_0. It will go back and forth around "Point a" until the oscillation is damped out.

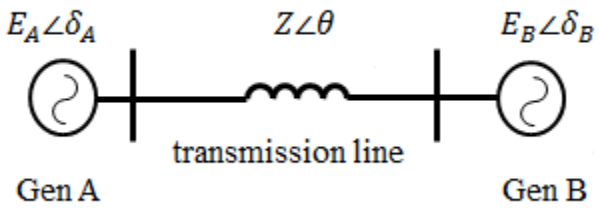

Fig. 4.2 Two-machine system

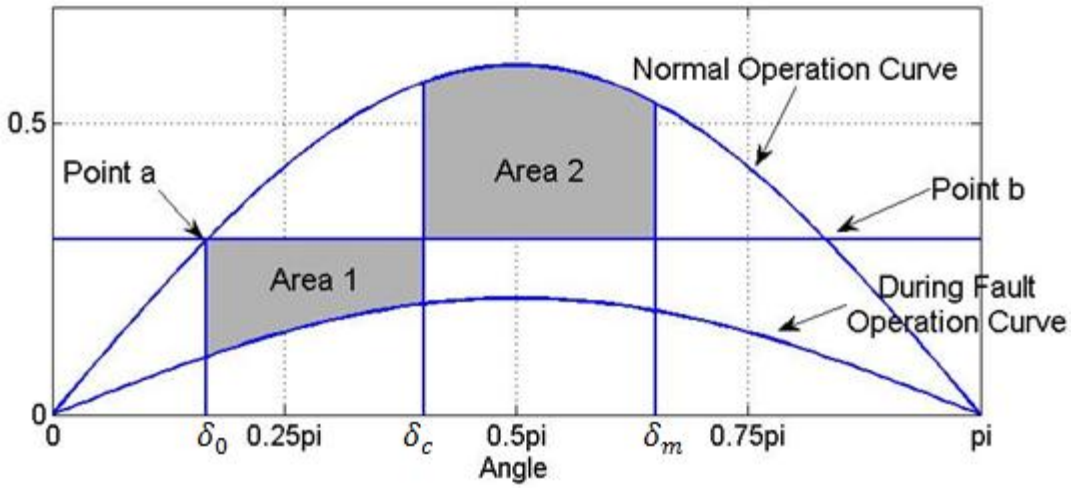

Fig. 4.3 Generator P-δ curve

The following interprets the system behavior of unstable cases. After clearing the disturbance, the generator goes back to the "Normal Operation Curve" and the rotor angle difference continues to increase. Once the angle difference reaches "Point b", the active power output can never be greater than the mechanical power input. In this case nothing can stop the monotonically increasing of rotor angle difference, and the expected value of maximum swing angle becomes infinite. In other words, from the stable state to the unstable state the value of maximum swing angle δ_{m} has changed suddenly from bounded (the equal area criterion in section 2.2.1 has showed δ_{m} must be less than 180^{o}) to unbounded. This phenomenon matches the concept of continuity defined in catastrophe theory. Thus, in this chapter, catastrophe theory is used to determine the sudden change of maximum swing angle δ_{m}.

Generally speaking, conditions which affect the power system transient stability includes line impedance, the type and location of the disturbance, the operation status before the disturbance and the time disturbance has been removed (fault clearing time). Obviously the first three categories are predetermined for a specific disturbance. The only condition can be changed is the fault clearing time. In Fig. 4.3 the fault clearing time is reflected by the fault clearing angle δ_c. It can be inferred from the equal area criteria that a later fault clearing time results in a bigger δ_c, which reduces the size of the deceleration Area 2. This action makes it less probable for the system to neutralize the acceleration energy gained before the disturbance is removed. In other words, it is the fault clearing time which determines the transient stability of a given system. In catastrophe theory, this can be described as the fault clearing angle δ_c which determines the continuity of maximum swing angle δ_m.

When using catastrophe theory for transient stability assessment, the maximum swing angle can form an operation trajectory with different value of δ_c. Since by increasing the value of δ_c, the generator finally becomes unstable, it is expected that the trajectory will cross the discontinuity boundary when the generator becomes unstable. The value of δ_c correlates to the transition point is the estimation of critical clearing angle. In catastrophe theory, the trajectory and the discontinuity boundary are projected to a 2-D plane for easier observation.

In reference [41 - 44], catastrophe theory has been applied for power system transient stability assessment. Different from the approach proposed in this chapter, they

concluded when the system is unstable the critical clearing angle (CCA) does not exist and vice versa. The discontinuity in [41 - 44] is linked with the existence of CCA. In this chapter, the CCA is considered as always existing. Its value varies from a positive number to zero depending on the severity of the disturbance. The value of CCA equal to zero does not mean the CCA does not exist. And it is also not guaranteed that there must be a sudden change before the CCA reaches zero. Hence, it is more appropriate to apply the catastrophe theory with the maximum swing angle for transient stability assessment. Following sections will demonstrate the procedure of using catastrophe theory to obtain the discontinuity of maximum swing angle.

4.4 Multi-machine system transient stability assessment using catastrophe theory

The transient stability assessment in multi-machine system is different from two-machine system because it needs to find a reference to represent the effect of multiple generators' rotor angles. COI is a commonly used concept in multi-machine system as the generator rotor angle reference [45]. In this section, a COI based modified generator swing equation has been introduced to study the multi-machine system transient stability assessment. The PMU measurements are used here to estimate the real time generator rotor angle for calculating the COI [46].

The COI is weighted average of all generator rotor angles in the system. It is defined as:

$$\delta_{COI} = \frac{\sum M_i \delta_i}{\sum M_i} \tag{4.4}$$

where

M_i = The coefficient which equals to $J_i \omega_{mi}$

δ_i = generator rotor angle of generator *i*

Suppose the stability of generator *t* is under evaluation. The rotor angle of generator *t* is defined as δ_t and the system equivalent rotor angle is defined as δ_s. δ_s is calculated as:

$$\delta_s = \frac{\sum_{\substack{i=1 \\ i \neq t}}^{N} M_i \delta_i}{\sum_{\substack{i=1 \\ i \neq t}}^{N} M_i} \tag{4.5}$$

The modified energy function, which is introduced by [26], is based on the COI to accommodate multi-machine system analysis. The modified energy function is given by:

$$P_m - P_e = M_t(\ddot{\delta}_t - \ddot{\delta}_s) = P_{mt} - \frac{M_t}{M_s}\sum_{j \in s} P_{mj} - P_{et} + \frac{M_t}{M_s}\sum_{j \in s} P_{ej} \tag{4.6}$$

where

M_t = coefficient which equals to $J_t \omega_{mt}$

M_S = $M_s = \sum_{\substack{i=1 \\ i \neq t}}^{N} M_i$

In (4.6) P_m and P_e are mechanical power input and electrical power output of the generator. They are obtained by power flow equations:

$$P_{mt} = E_t^2 G_{tt} + \sum_{\substack{i=1 \\ i \neq t}}^{N} E_t E_i G_{ti} \cos(\delta_{ji}(t)) + \sum_{\substack{i=1 \\ i \neq t}}^{N} E_t E_i B_{ti} \sin(\delta_{ji}(t)) \tag{4.7}$$

$$P_{mj} = E_j^2 G_{jj} + \sum_{\substack{i=1 \\ i \neq j}}^{N} E_j E_i G_{ji} \cos(\delta_{ji}(t)) + \sum_{\substack{i=1 \\ i \neq j}}^{N} E_j E_i B_{ji} \sin(\delta_{ji}(t)) \tag{4.8}$$

$$P_{et} = E_t^2 G_{tt} + \sum_{\substack{i=1 \\ i \neq t}}^{N} E_t E_i G_{ti} \cos(\delta_{ji}(t)) + \sum_{\substack{i=1 \\ i \neq t}}^{N} E_t E_i B_{ti} \sin(\delta_{ji}(t)) \quad (4.9)$$

$$P_{ej} = E_j^2 G_{jj} + \sum_{\substack{i=1 \\ i \neq j}}^{N} E_j E_i G_{ji} \cos(\delta_{ji}(t)) + \sum_{\substack{i=1 \\ i \neq j}}^{N} E_j E_i B_{ji} \sin(\delta_{ji}(t)) \quad (4.10)$$

Where

E_m = Field armature voltage generator *m*

G_{mn} = Real term of Y_{mn}in admittance matrix

B_{mn} = Imaginary term of Y_{mn}in admittance matrix

$\delta_{mn}(t)$ = Generator rotor angle difference between generator *m* and *n* at time *t*.

Define P_e by:

$$P_e = P_{et} - \frac{M_t}{M_s} \sum_{j \in s} P_{ej} \quad (4.11)$$

By assuming the COI represents the system over all generator rotor angle behavior, the rotor angle difference between generator *t* and other generators can be defined as $\delta = \delta_t - \delta_{COI}$ and the rotor angle difference between other two generators is 0. Substituting equation (4.9) and (4.10) into equation (4.11) the electrical power output of generator *t* with respect to COI is obtained as:

$$P_e = \left(E_t^2 G_{tt} - \frac{M_t}{M_s} \sum_{\substack{i=1 \\ i=t}}^{N} E_i^2 G_{ii} \right) - \frac{M_t}{M_s} \sum_{\substack{i=1 \\ i \neq j}}^{N} E_j E_i G_{ji} + \sum_{\substack{i=1 \\ i \neq t}}^{N} E_t E_i G_{ti} \cos\delta + \sum_{\substack{i=1 \\ i \neq t}}^{N} E_t E_i B_{ti} \sin\delta \quad (4.12)$$

This equation is simplified as:

$$P_e(\delta) = P + A_1 cos\delta + A_2 sin\delta \quad (4.13)$$

where

$$A_1 = \sum_{\substack{i=1 \\ i \neq t}}^{N} E_t E_i G_{ti}$$

$$A_2 = \sum_{\substack{i=1 \\ i \neq t}}^{N} E_t E_i G_{ti}$$

$$P = \left(E_t^2 G_{tt} - \frac{M_t}{M_s} \sum_{\substack{i=1 \\ i=t}}^{N} E_i^2 G_{ii} \right) - \frac{M_t}{M_s} \sum_{\substack{i=1 \\ i \neq j}}^{N} E_j E_i G_{ji}$$

Note that due to the change in power system operating condition, the value of A_1, A_2 and P in (4.13) before the disturbance and after the disturbance will be different. Thus, for post disturbance clearing these parameters are denoted as A_1', A_2' and P' accordingly. Since the proposed method evaluated the transient stability based on the measurement of first few cycles after the disturbance, the assumption of constant P_m is valid [4].

Similar to equations in [41 - 44], the balance of mechanical power and electrical power has been used as the equilibrium set. With modified energy (4.6) and (4.13), the equilibrium set for multi-machine system transient stability assessment is given as:

$$\int_{\delta_0}^{\delta_c} (P_m - P_e(\delta)) d\delta + \int_{\delta_c}^{\delta_m} (P_m - P_e(\delta)) d\delta = 0 \tag{4.14}$$

where

$$P_m = P_{mt} - \frac{M_t}{M_s} \sum_{j \in s} P_{mj}$$

The following relationship is obtained by substituting (4.13) into (4.14) and solving the integration:

$$A_2' \cos\delta_m - A_1' \sin\delta_m + (P_m - P')\delta_m + K = 0 \tag{4.15}$$

where

$$K = (\delta_0 - \delta_c)P + \delta_c P' - \delta_0 P_m - A_1 \sin\delta_c + A_2 \cos\delta_c + A_1' \sin\delta_c - A_2' \cos\delta_c + A_1 \sin\delta_0 - A_2 \cos\delta_0$$

The equation (4.15) can be expanded by Taylor series:

$$\cos\delta_m = 1 - \frac{1}{2!}\delta_m^{\,2} \tag{4.16}$$

$$\sin\delta_m = \delta_m - \frac{1}{3!}\delta_m^{\,3} \tag{4.17}$$

Fig. 4.4 shows the accuracy of second order Taylor series expansion for *sin(x)*. It can be found when the angle $\delta < 90°$ the sinusoidal curve and the second order Taylor series approximation are very close. Because in most cases the maximum angle difference cannot significantly exceed 90°, the second order Taylor series would have enough accuracy for power system transient stability study.

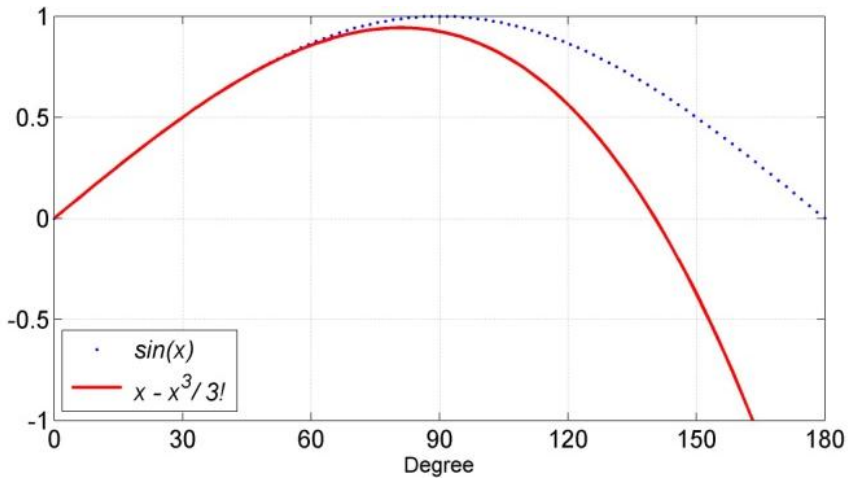

Fig. 4.4 Accuracy of Taylor series expansion

Substituting (4.16), (4.17) into (4.15) gives

$$\delta_m^{\,3} + B_1\delta_m^{\,2} + B_2\delta_m + B_3 = 0 \tag{4.18}$$

where

$$B_1 = (-\frac{3A_2'}{A_1'})$$

$$B_2 = (\frac{P_m - P' - A_1'}{\frac{1}{6}A_1'})$$

$$B_3 = (\frac{A_2' + K}{\frac{1}{6}A_1'})$$

By defining $\delta_m = y - \frac{B_1}{3}$, (4.18) can be rearranged as a standard cusp catastrophe manifold:

$$y^3 + uy + v = 0 \tag{4.19}$$

Where *u* and *v* can be obtained as:

$$u = -\frac{1}{3}B_1^2 + B_2 \tag{4.20}$$

$$v = \frac{2}{27}B_1^3 - \frac{1}{3}B_2B_1 + B_3 \tag{4.21}$$

Similar to [41], the degenerate critical point set is calculated as:

$$3y^2 + u = 0 \tag{4.22}$$

By substituting (4.22) into (4.19), the cusp manifold has been mapped to the 2-D plane with *u*-*v* coordinate as (4.23). In this dissertation (4.23) is the discontinuity boundary for transient stability assessment:

$$4u^3 + 27v^2 = 0 \tag{4.23}$$

After the disturbance has been detected, the trajectory of maximum swing angle δ_m, which is defined by (4.20) and (4.21), is plotted together with the discontinuity

boundary (4.23). By increasing the fault clearing angle δ_c, the trajectory would gradually approach the discontinuity boundary. Continue increasing δ_c until the trajectory crosses the discontinuity boundary, the value of δ_c at the intersection is the estimation of CCA. The transient stability can be obtained by comparing the estimated CCA with the actual fault clearing angle. PMU is used here again to provide the actual fault clearing angle.

The computation burden of the proposed method is low. It is noticed from (4.20) and (4.21) that obtaining the operational trajectory of the maximum swing angle δ_m requires only simple calculations. The cusp manifold, which is used as discontinuity boundary, is fixed all the time. Compared with traditional transient stability assessment methods, there is no need of obtaining specific cusp manifolds in each step of calculation. This can eliminates the time for iterations and convergence in traditional techniques. The catastrophe theory method has a better performance in satisfying the speed requirement for real time analysis in large scale power systems.

4.5 Numerical results and conclusion

The IEEE 39-bus system [47] shown in Fig. 4.5 is used to test the proposed method. The simulation is done by PSS/E (Power System Simulator for Engineering). A three-phase to ground fault was applied to the transmission line as the disturbance. The fault was cleared by removing the faulted transmission lines. The first part of simulation is for testing the stability assessment for generators by using the proposed method. The second part of the simulation is designed to test the accuracy of CCA estimation. The

estimated CCA is compared with actual CCA which is obtained from simulation. The estimation error of the proposed method is compared with the method developed by [36].

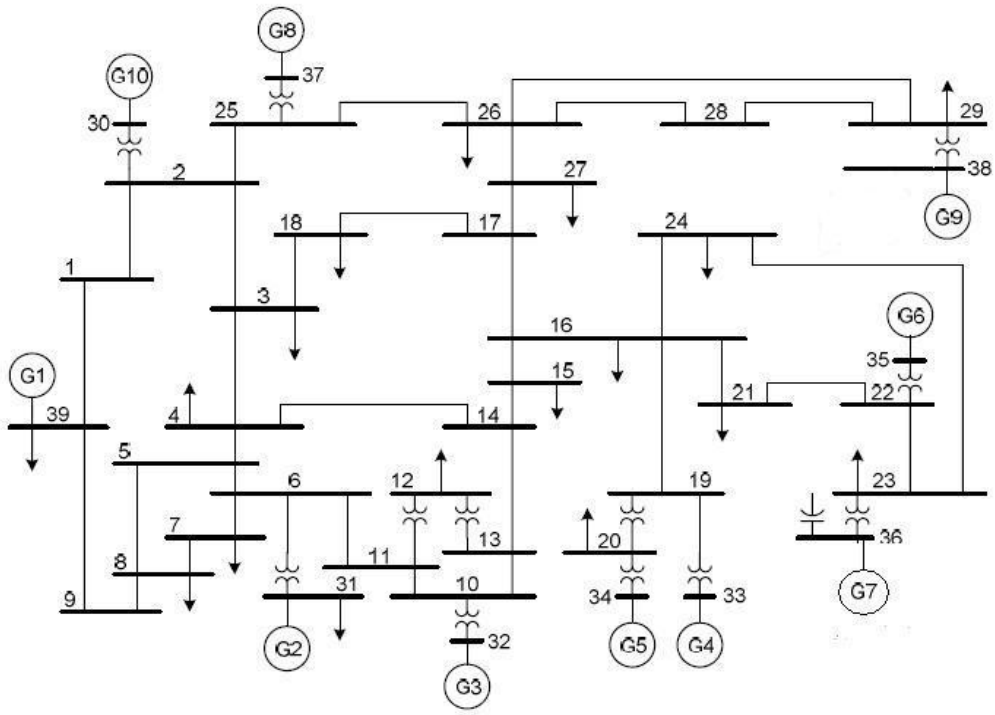

Fig. 4.5 IEEE 39 bus system

Following Table 4.2 is the result of stability assessment. The first row shows the generator name. The first column shows the location of disturbance. The disturbance occurs on the transmission line between the two buses given in the fault location column. All disturbances are three-phase to ground fault at 50% of the line and the fault is cleared by removing the faulty line. The fault lasts for 0.3 second. In Table 4.2, symbol "S" means generators in the system remain synchronous. Symbol "U" means generators in the system cannot maintain synchronous. When the assessment does not match the simulation, the result is noted with a "*".

Table 4.2 Stability Estimation in IEEE 39-BUS System by Catastrophe Theory

Fault location	Assessment result	Simulation result
01-02	S	S
02-03	U	U
02-25	U	U
03-04	U	U
03-18	U	U
04-05	U	U
15-16	U	U
16-17	U	U
17-18	U	U
17-27	U	U
21-22	U	U
22-23	U	U
23-24	U*	U
25-26	U	U
26-27	U	U

* The stability assessment suggested generator G7 is stable but the simulation showed generators in that case cannot maintain synchronous.

The proposed method gave specific critical clearing angles (CCA) for each generator in Table 4.3. This is not like traditional methods which gave a single CCA for all generators. This makes the proposed method more reasonable since effects of disturbance on different generators are not the same due to generators' locations and physical conditions. Although noticeable error in CCA estimation is observed, compared with the result given by [36], the accuracy of proposed method has already improved significantly.

Table 4.3 CCA Estimation by Catastrophe Theory

Fault Location	Generator	Simulation (Degree)	Prediction (Degree)	Prediction Error in proposed method (Degree)	Prediction Error in [36] (Degree)
Fault between bus 02-03	G4	8.65	10.80	-2.15	N/A
	G5	5.55	6.84	-1.29	
Fault between bus 04-05	G4	11.46	15.12	-3.66	N/A
	G5	6.44	11.88	-5.44	
Fault between bus 04-14	G5	9.68	22.32	-12.64	121.00
	G7	17.28	19.08	-1.80	
	G9	12.44	2.16	10.28	
Fault between bus 17-27	G4	24.57	14.76	9.81	124.50
	G5	15.79	31.32	-15.53	
	G7	26.25	27.72	-1.47	
Fault between bus 22-23	G4	7.05	4.32	2.73	124.20
	G6	17.49	41.40	-23.91	
	G8	0.89	2.16	-1.27	
Fault between bus 26-29	G4	0.99	0.72	0.27	66.2
	G8	3.95	2.15	1.80	
	G9	7.21	1.82	5.39	

The possible reason for errors in proposed method could be the COI. When generator rotor angles in the system are close to each other the weighted average of generator rotor angles can accurately represent their behaviors. However, when generator rotor angles are very different from each other the COI would have significant error. Thus, for improving the performance of the proposed method, the deficiency of COI must be remedied.

4.6 Discussion on improving the performance of proposed method

One interesting phenomena in power system stability is that after disturbance, generators usually self-organize themselves into several clusters based on their rotor angular velocity. Because generators belong to the same cluster are approximately synchronous, their COI can reasonably represent the generators' rotor angle. Then the difference of COI between generator clusters will properly reflect the rotor angle interaction between these clusters [48-52]. Therefore, for improving the performance of the proposed method, catastrophe theory can be used to study the transient stability of generator clusters. The COI at this time is not between one generator and the rest system, but between generator clusters.

Numerical simulations showed that the stability assessment result is slightly improved with generator clusters. However, this is only theoretically feasible because in reality the generator clustering is unpredictable. Usually the definite generator clustering behavior appears several seconds after the disturbance. This does not satisfy the time frame for real-time analysis. If the clustering prediction is not accurate, generators will

not be assigned to clusters properly. The result of stability assessment may be even worse than the result for single generator as introduced before.

This part of research shows the effort made on large scale power system real time transient stability assessment. It achieved the purpose of finding simplest characters to represent the stable and unstable conditions in complex power systems. The numerical results have proved that continuity of the generator maximum swing angle is a good simplification for power system transient stability assessment. Due to the limitation of COI, catastrophe theory method does not provide perfect result in critical clearing angle prediction. Unfortunately, the COI is still widely used in recently published papers for transient stability related problems. The following chapter will develop a new way in obtaining the generator rotor angle difference without using the COI. This method does not require the information of actual generator rotor angle. Therefore, it also has the potential to be applied with those renewable energy sources which do not have rotating parts.

CHAPTER FIVE

GENERATOR ROTOR ANGLE DIFFERENCE ESTIMATION

The previous chapters have demonstrated classical approaches for multi-machine power system transient stability assessment. Except for the time domain methods and automatic learning methods, nearly all the direct methods have employed following assumptions [4] to simplify the power system operating conditions for decision making:

a. Mechanical power input is constant;
b. Constant voltage behind transient reactance model for the synchronous machines is valid;
c. The mechanical rotor angle of a machine coincides with the angle of the voltage behind the transient reactance;
d. Loads are represented by passive impedance;
e. System stability is determined by the first swing of generator rotor angle.

Initially these assumptions were used in transient stability studies with small power systems. However, for modern large scale power system, they may not be appropriate. In this chapter the COI for multi-machine power system transient stability assessment will be further investigated. An alternative solution will be introduced to replace the COI in order to improve the performance of multi-machine power system transient stability related studies.

5.1 Introduction

Obviously the most straightforward approach for power system transient stability assessment is to evaluate the rotor angle difference between generators. This is usually explained by the example with the two-machine system: after choosing one generator as the reference, the system's transient stability condition is obtained by investigating the rotor angle difference between the generator and the reference. But applying this approach to the actual power system operation is unrealistic because it is hard to select a fair reference among multiple generators. For transient stability assessment in multi-machine power system, the common solution is to reduce the system to the SMIB equivalent system and evaluate the rotor angle difference between one generator and the infinite bus. Like the approach in Chapter Four, the COI is used to represent the rotor angle of the equivalent generator connected to the infinite bus. It is generally believed that the COI satisfies the accuracy of roughly reflecting the value of that equivalent generator's rotor angle. Until recently, most of the studies on transient stability assessment and its related power system operation optimizations have been still based on COI [53-54]. Although statistically the COI seems to be acceptable for representing the overall system equivalent rotor angle, no proof has been provided to verify the true feasibility of COI for power system transient stability assessment. In fact, the relation between COI and the power system transient stability still remains unclear.

Even if COI is truly a proper system equivalent rotor angle for transient stability assessment, difficulties still remain in satisfying the requirement of real-time analysis. Obtaining COI often requires great effort: not all of the generators are equipped with

proper devices to measure the accurate rotor angle, nor does the communication system always have enough capability to enable the transmission of rotor angle information for calculating COI in real-time.

In following sections the performance of COI for power system transient stability assessment will be discussed. The numerical example has revealed that COI actually is not a suitable reference for evaluating the transient stability of the multi-machine power system. After this, a new technique used for obtaining the "true" rotor angle difference between the generator and the system was introduced to replace the COI for power system transient stability assessment. The proposed technique directly calculates the rotor angle difference via the generator's electric power output. In addition, instead of treating COI as a common reference, the proposed technique allows each generator to have its own reference for obtaining their rotor angle differences. This is a more reasonable idea due to the fact that the power grid topology is not uniform and the distances between the disturbance location and generators in the system are not the same. Also, the proposed technique has the potential to calculate a virtual rotor angle difference for generation units that do not have the physical rotating structure. This feature allows the proposed technique to be applied with studying the impact of renewable energy sources on power system transient stability.

5.2 COI for multi-machine power system transient stability assessment

This section will discuss the performance of COI in transient stability assessment and the difficulty of using COI for real-time analysis.

5.2.1 The performance of COI

COI is calculated by (4.4). For simplicity, the generator rotor angle is assumed to be accurately measured without any delay. The precondition of using COI based rotor angle difference to evaluate power system transient stability depends on the assumption that COI can represent the equivalent system rotor angle. If this is at least partially true, the rotor angle difference between COI and the generator can be used to evaluate the transient stability of the power system. Unfortunately, it is impossible to verify this conclusion directly because, at present, COI is the only way to obtain the rotor angle of the equivalent system. In this section, an alternate method by which to verify the validity of COI for multi-machine system transient stability assessment is provided.

The inherent nature of power system transient stability is not the rotor angle difference but the mismatch of generator's mechanical power input, P_m, and the electrical power output, P_e. The P_e can be either measured at the generator terminal or calculated by generator's power output equation. Taking a two-machine system containing generators 1 and 2 as an example, P_e of generator 1 is approximately calculated by (5.1).

$$P_{e1} = E_1 E_2 B_{12} \sin(\delta_1 - \delta_2) \tag{5.1}$$

where

E_n Voltage behind the transient reactance of generator *n*

B_{12} Susceptance between generators 1 and 2

$\delta_1 - \delta_2$ Rotor angle difference between generators 1 and 2

When assuming that the P_m is forced to remain constant, the generator's energy mismatch would only depend on the P_e. Meanwhile, (5.1) also indicates that the P_e is the function of the rotor angle difference between the two generators. Therefore, the rotor angle difference, which caused the fluctuation of P_e, is used to evaluate the transient stability as well. In addition the actual P_e measured at the generator terminal should always be close to the P_e calculated by using the rotor angle difference in (5.1). Fig. 5.1 illustrates the relationship between transient stability, generator output power (P_e) and rotor angle difference.

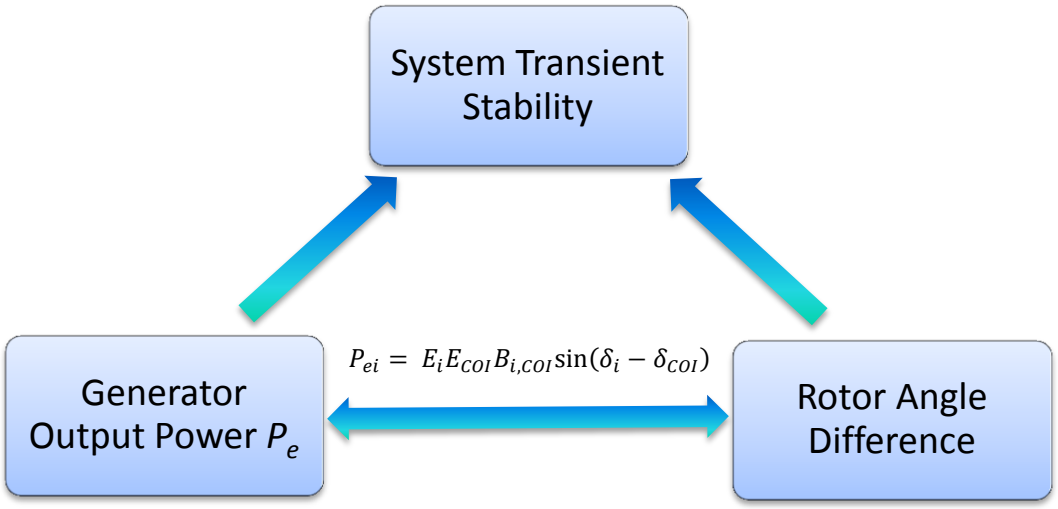

Fig. 5.1 Relationship between transient stability, P_e and rotor angle difference

The above conclusion worked well with the two-machine system, and the P_e curve from the measurement is very close to the P_e curve calculated by (5.1). However, in the multi-machine system, when the rotor angle difference between the generator and COI is used to evaluate the transient stability, it can be regarded as reducing the multi-machine system to the two-machine system. The reduced two-machine system contains

one generator and an equivalent system whose rotor angle equals COI. As discussed above, if COI is appropriate for evaluating the transient stability in the multi-machine system, it is expected that the P_e curve calculated by (5.1) when δ_2 is replaced by δ_{COI} should also be similar to the actual P_e curve measured at the generator terminal.

If the impact of the disturbance and the resulted system oscillation are small, equation (5.1) indicates that the COI is close to the equivalent system rotor angle. However, when the disturbance is strong, the numerical simulation does not support the same conclusion. The IEEE 39-bus system is used to demonstrate the multi-machine power system's transient behavior. A three phase to ground fault is generated at 50% of the transmission line between bus 16 and 19 as the disturbance. The fault lasted for 0.1 second and was cleared by removing the faulty line. The P_e of the generator at bus 33, which is directly obtained by simulation, has been compared with the P_e calculated by (5.2) with COI. The governor in the simulation is forced to output constant mechanical power. To minimize the effect of the load's dynamic response, loads are converted to constant impedance. The two P_e curves are unified to 1 by dividing their own maximum values in order to compare their shapes.

Fig. 5.2 shows that no similarity exists between the two P_e curves. This reveals that sometimes in multi-machine systems, the angle difference obtained by COI is incapable for reflecting the variation of P_e and COI is not an appropriate equivalent system rotor angle for transient stability assessment.

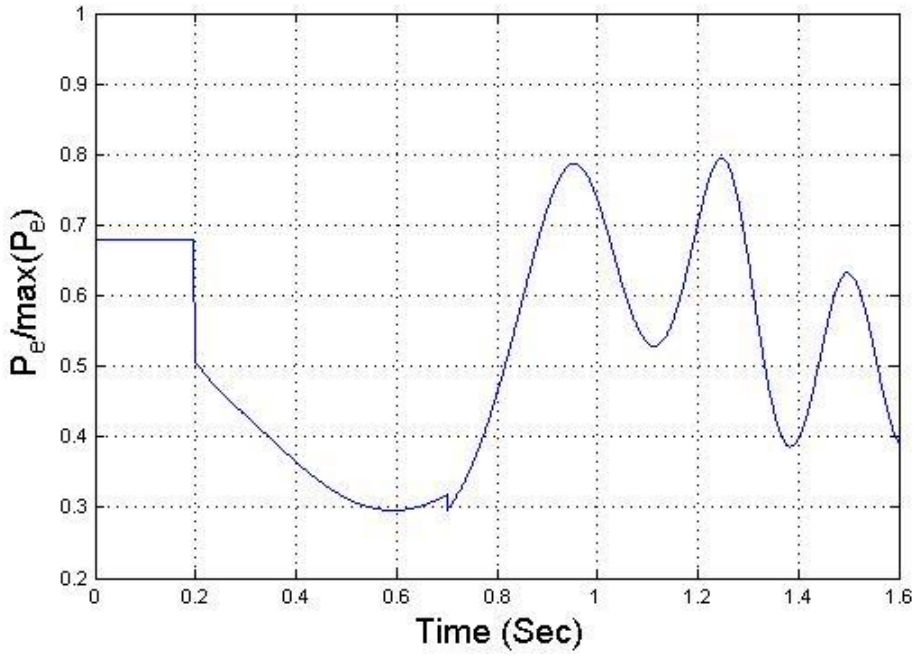

(a)

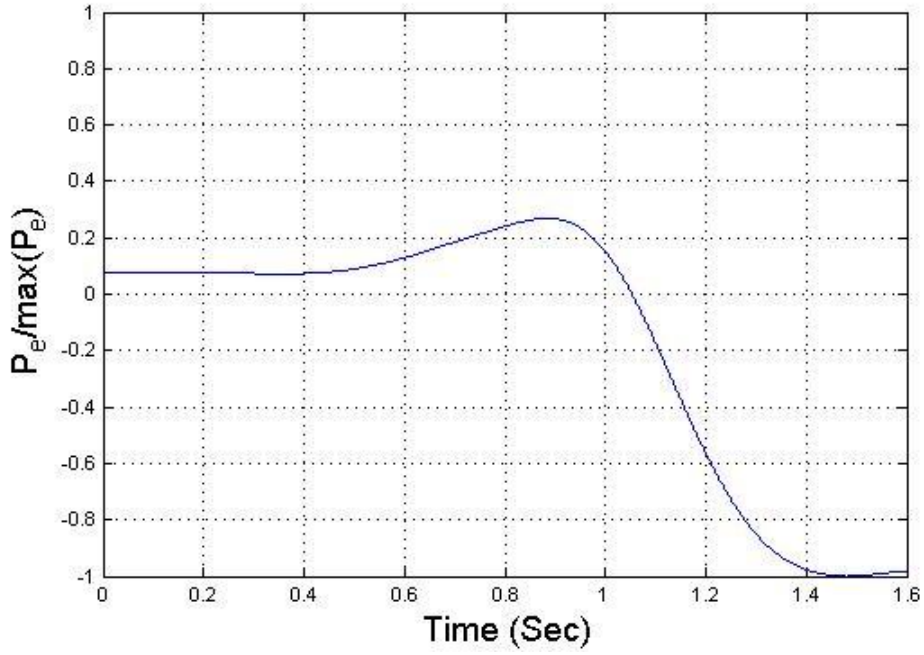

(b)

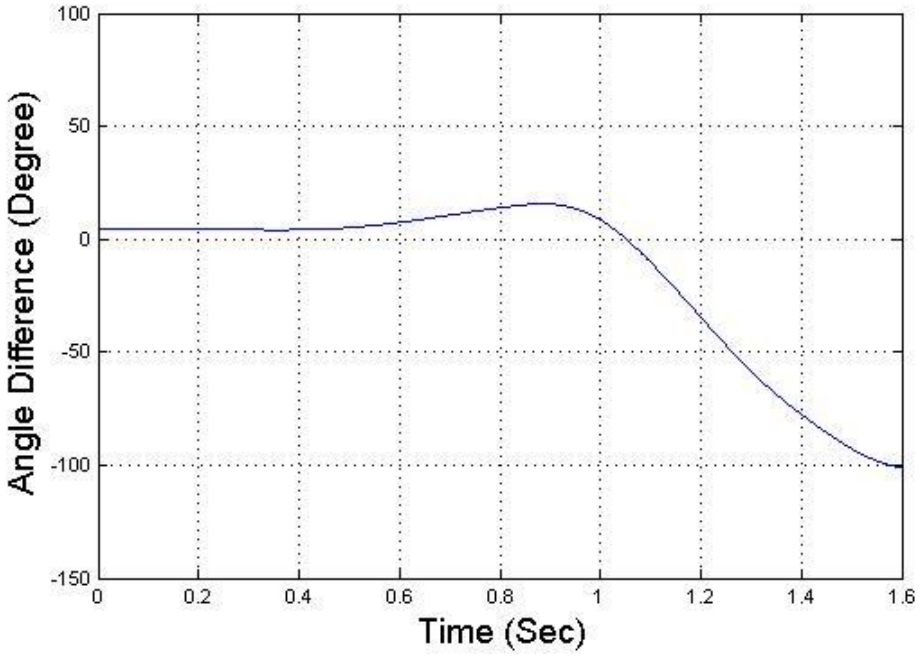

(c)

Fig. 5.2 (a) Electric power output of the generator G4 at bus 33; (b) Generator electric power calculated by COI; (c) Generator angle difference calculated by COI.

This example proves the ineffectiveness of COI as the reference for evaluating the multi-machine system's transient stability. As discussed before, the COI can represent the equivalent system behavior in stable scenarios. Since the main purpose of power system transient stability assessment is to identify potentially unstable scenarios, the result would not be convincing if COI were applied to real power system operations with noticeable disturbances.

Chapter Four has tried the generator cluster's COI for improving the performance of the proposed method in multi-machine system transient stability assessment. By this approach, the entire system's COI is replaced by the generator cluster's COI [55], and the power system transient stability is studied according to the angle difference between

generator clusters. This is because after the disturbance, generators belonging to the same cluster are relatively synchronous so that the generator cluster's COI is able to correctly represent the equivalent rotor angle of that cluster. Theoretically, this alternative can prevent the problem showed by Fig. 5.2. However, the difficulty of estimating generator clusters has restricted the effectiveness of COI in the on-line decision making for multi-machine system transient stability assessment.

5.2.2 The difficulty of obtaining COI in real time

The calculation of the generator rotor angle in real time without dedicated rotor angle measurements is usually based on the assumption of first swing stability. This assumption concludes that during the period of first swing, the generator's rotor angle is considered to be proportional to its terminal voltage phase angle. Thus, if only focusing on the first swing, the generator's rotor angle can be estimated easily with measurements such as the phasor measurement units (PMU). Unfortunately, this assumption does not work well with the multi-machine system. An example of using the first swing stability and equal area criteria for multi-machine system transient stability assessment is demonstrated in [56]. Its stability criterion is based on the input/output energy balance of the "first swing" [57]. Repeating this approach with the IEEE 39-bus system proved that the "first swing" does not always dependable for determining the final status of the transient stability.

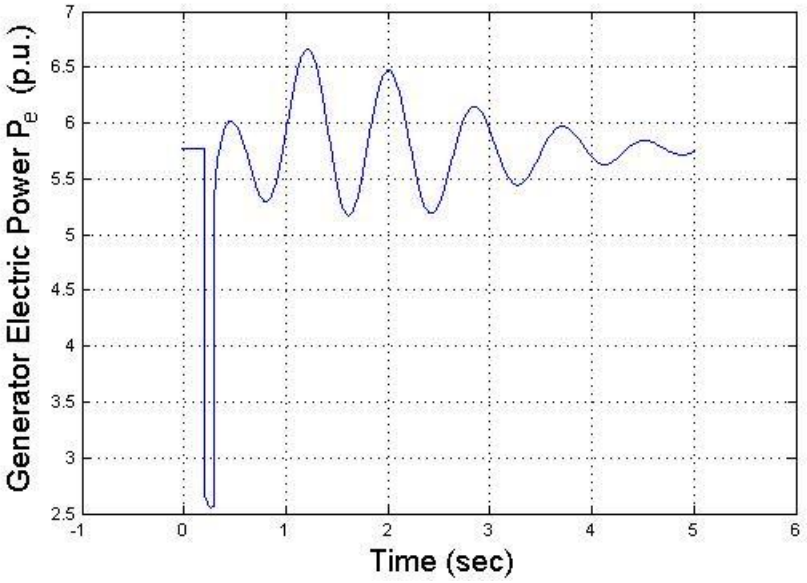

Fig. 5.3 Generator electric power output in multi-machine power system

According to the equal area criteria, the first swing in Fig. 5.3 has indicated that this is an unstable oscillation because the total input power is greater than the total output power during the first swing (t < 1 sec). The energy mismatch makes the generator's rotor to accelerate continuously. However, a sudden, huge increase in the output power P_e is observed just after the first swing. This increase has finally neutralized the excess input power gained during the first swing and re-stabilizes the generator. This is because the transient period of the generator in multi-machine power system is the interaction between generator and multiple generators after the disturbance. There could be some generators which response to the disturbance slower than the other generators but cause the biggest impact. It is not guaranteed that the oscillation initiated by the first generator or generator cluster in multi-machine systems produces the biggest effect and determines the final result of the stability condition. Therefore, the concept of first swing stability only applies to the two-machine system.

Other than time domain simulation, there is no efficient way to accurately forecast the situation illustrated by Fig. 5.2. So without the assumption of first swing stability and result from time domain solution, it is expected to take longer time to determine the transient stability status in the multi-machine system. Beyond the first swing, the generator's rotor angle is no longer proportional to its terminal voltage phase angle, which complicates the application of COI in on-line analysis.

Thus, due to the performance and difficulty to obtain, COI is insufficient for on-line transient stability studies in multi-machine power system. This is the motivation of finding a better approach to replace COI. In this paper, the rotor angle difference obtained by the proposed method is a more reasonable indicator for on-line applications of multi-machine power system transient stability study.

5.3 Rotor angle difference estimation

Although COI is not an adequate system equivalent rotor angle for transient stability studies, it does not deny the existence of the equivalent system. The generator itself does not have the capability to know the power system's structure. So its dynamic response is only the response to the disturbance effect appeared on the generator terminal bus. In this paper we assume the real generator behavior during disturbance can be considered as the interaction between the individual generator and an equivalent system with unknown parameters. Fig. 5.4 illustrates the interaction between generator *A* and the multi-machine power system. The equivalent system connected to *A* can be assumed to be an equivalent transmission line with impedance $Z\angle\theta$ and an equivalent generator

which is named *S*. The equivalent generator here represents the aggregated effects of all components in the system except for generator *A*.

Debate may arise from this assumption because after the disturbance, generators with similar angular velocity often form clusters but this assumption does not reflect the interaction between generators belong to the same cluster. Actually the proposed technique assumes the rest system is a whole part. There is nothing to do with the individual generator's rotor angle. Otherwise, since there will always be a generator whose rotor angle lags all other generators, from the swing equation, it should absorb power instead of generating power. However, it injects power to the power system. The proposed technique explains the interaction between an individual generator and the rest system the equivalent system by assuming that the system equivalent rotor angle lags that generator. Since the rest part of the system is lumped together, the transmission line in Fig. 5.4 is the equivalent transmission line which does not need to be modeled as π section model.

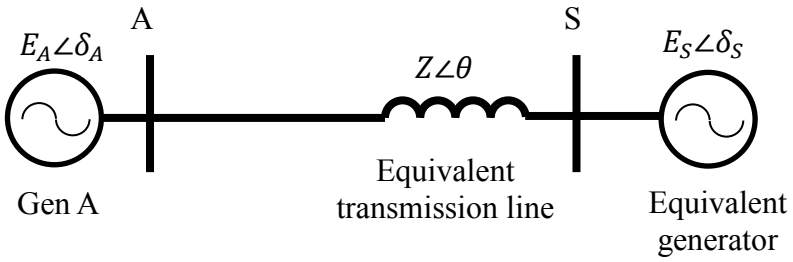

Fig. 5.4 Equivalent system diagram

With unknown parameters, the complex power output of generator A is calculated as:

$$S_A = E_A\angle\delta_A\left(\frac{E_A\angle\delta_A - E_S\angle\delta_S}{Z\angle\theta}\right)^* + G_{AA}|E_A|^2 \tag{5.2}$$

where

E_n	Voltage behind the transient reactance of generator *n*
δ_A	Rotor angle of generator A
δ_S	Rotor angle of equivalent generator (unknown)
$Z\angle\theta$	Impedance of the equivalent transmission line (unknown)
G_{AA}	Self-conductance of the generator terminal bus

The active and reactive power injections were calculated from (5.2) as:

$$P_A = \frac{|E_A|^2}{|Z|}\cos(\theta) - \frac{|E_A E_S|}{|Z|}\cos(\theta)\cos(\delta_A - \delta_S) + \frac{|E_A E_S|}{|Z|}\sin(\theta)\sin(\delta_A - \delta_S) \tag{5.3}$$

$$Q_A = \frac{|E_A|^2}{|Z|}\sin(\theta) - \frac{|E_A E_S|}{|Z|}\cos(\theta)\sin(\delta_A - \delta_S) - \frac{|E_A E_S|}{|Z|}\sin(\theta)\cos(\delta_A - \delta_S) \tag{5.4}$$

If the transmission line resistance is neglected, then in (5.3) and (5.4), $\sin(\theta)$ equals 1 and $\cos(\theta)$ equals 0. So, (5.3) and (5.4) become:

$$P_A = \frac{|E_A E_S|}{|Z|}\sin(\delta_A - \delta_S) \tag{5.5}$$

$$Q_A = \frac{|E_A|^2}{|Z|} - \frac{|E_A E_S|}{|Z|}\cos(\delta_A - \delta_S) \tag{5.6}$$

Except for the output active power P_A and the reactive power Q_A in (5.5) and (5.6), which can be measured accurately at the generator terminal, all other parameters are unknown. $\delta_{AS}(t) = \delta_A(t) - \delta_S(t)$ is the rotor angle difference between generator A and

the assumed equivalent generator. In this paper, $\delta_{AS}(t)$ is modeled as having a nonlinear relation with time *t*.

Compared with $\delta_{AS}(t)$, the voltage magnitude behind the generator transient reactance, the system structure that affects G_{AA} and the equivalent impedance, $Z\angle\theta$, does not change dramatically. If the measurement device's sampling rate is sufficiently fast during one sampling cycle, $\frac{|E_A E_S|}{|Z|}$ and $\frac{|E_A|^2}{|Z|}$ can be considered constant. Therefore, solving the derivative for (5.5) and (5.6) will cancel the first term in (5.5) and (5.6):

$$P'_A(t_P) = \delta'_{AS}(t_P)\frac{|E_A E_S|}{|Z|}\cos(\delta_{AS}(t_P)) \tag{5.7}$$

$$Q'_A(t_Q) = \delta'_{AS}(t_Q)\frac{|E_A E_S|}{|Z|}\sin(\delta_{AS}(t_Q)) \tag{5.8}$$

When t_P and t_Q are equal, (5.7) and (5.8) are combined by (5.9) to cancel the sinusoidal term and obtain the amplitude:

$$\sqrt{P'_A(t_P)^2 + Q'_A(t_Q)^2} = |\delta'_{AS}(t)|\frac{|E_A E_S|}{|Z|} \tag{5.9}$$

Equation (5.9) is valid if the *error* in (5.10) equals zero.

$$error = 1 - \sqrt{(sin'(t))^2 + (cos'(t))^2} \tag{5.10}$$

When the sampling rate of $P_A(t)$ and $Q_A(t)$ is high enough, t_P and t_Q could be very close. Therefore the error in (5.10) approximately equals to 0. Two 1Hz sinusoidal signal *sin(t)* and *cos(t)* are used to illustrate the error versus the sampling rate in (5.10). Fig. 5.5 shows that when the sampling rate is 50 times higher than the signal frequency, the error of (5.10) will be less than 0.001%. 50 times higher than the signal frequency can be

easily achieved by PMU or extent relay protection devices because their A/D sampling rate usually cat get to at least more than 1000Hz, and the oscillation frequency of the generator's output power observed in out simulation is much lower than this rate.

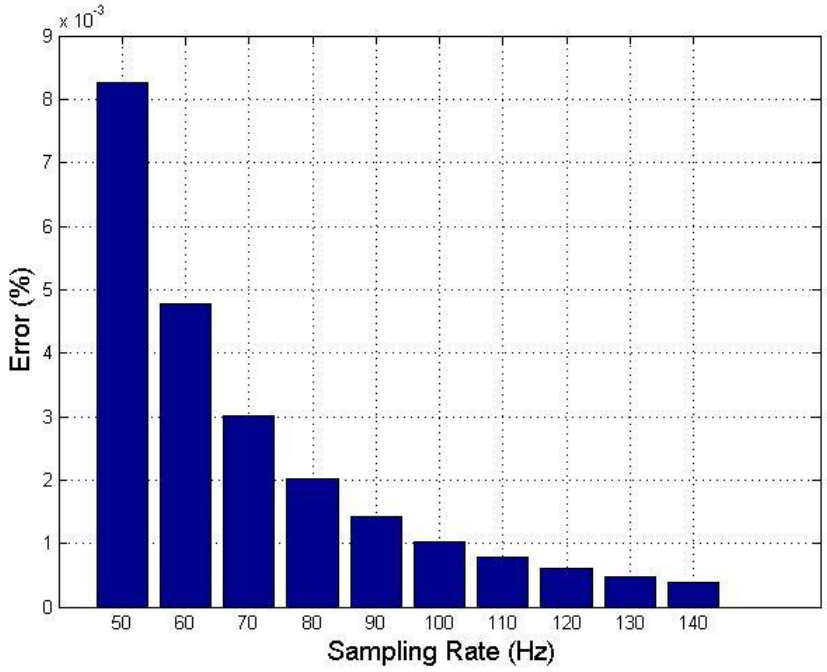

Fig. 5.5 Error versus sampling rate in equation (11)

Therefore using t to replace t_P and t_Q and dividing (5.8) by the amplitude obtained in (5.9) yields to the value of the pure sinusoidal function of the angle difference δ_{AS}:

$$\frac{Q'_A(t)}{\sqrt{P'_A(t)^2+Q'_A(t)^2}} = \frac{\delta'_{AS}(t)}{|\delta'_{AS}(t)|}\sin(\delta_{AS}(t)) \tag{5.11}$$

For unstable cases, because $\delta_{AS}(t)$ is continuously increasing, $\delta'_{AS}(t) > 0$ and $\frac{\delta'_{AS}(t)}{|\delta'_{AS}(t)|}$ equals 1. Therefore, (5.11) becomes:

$$\frac{Q'_A(t)}{\sqrt{P'_A(t)^2+Q'_A(t)^2}} = \sin(\delta_{AS}(t)) \tag{5.12}$$

However, for stable cases, $\delta_{AS}(t)$ fluctuates back and forth. When $\delta_{AS}(t)$ is increasing, $\delta'_{AS}(t) > 0$ and $\frac{\delta'_{AS}(t)}{|\delta'_{AS}(t)|}$ equals 1; however, when $\delta_{AS}(t)$ is decreasing, $\delta'_{AS}(t) < 0$ and $\frac{\delta'_{AS}(t)}{|\delta'_{AS}(t)|}$ equals -1. Thus, for stable cases (5.11) should be written as:

$$\frac{Q'_A(t)}{\sqrt{P'_A(t)^2+Q'_A(t)^2}} = \pm\sin(\delta_{AS}(t)) \tag{5.13}$$

The actual sign before $sin(\delta_{AS}(t))$ is difficult to determine. An applicable solution is to calculate the absolute value of (5.13) and then adjust the sign according to the envelope of P_e. This is because (5.5), which approximately equals P_e, has the same pattern as $y(t) = sin(\delta_{AS}(t))$. In addition, obtaining the actual value of $\delta_{AS}(t)$ by $arcsin(y(t))$ is not necessary because the $sin(\delta(t))$ curve is already enough to illustrate the trend of the rotor angle difference. Calculating $arcsin(y(t))$ will increase the difficulty of identifying the angle in the range between [0 °, 90 °] and [90 °, 180 °] or between [180 °, 270 °] and [270 °, 360 °].

The above calculation process showed that the proposed technique obtains the rotor angle difference $\delta_{AS}(t)$ for generator A in Fig. 5.4 only by its own active and reactive power output. Although it requires the measurement device to maintain a high sampling rate, which results in a high data transmitting rate, it does not add any additional burden to the power system communication channels. On the contrary, using COI for real-time transient stability assessment requires generators to upload their rotor

angle frequently. So, it could be easier to physically realize the proposed technique than COI.

5.4 Numerical results

5.4.1 Rotor angle difference estimation in two-machine system

The validity of the proposed technique is examined by a two-machine system because the actual rotor angle difference between the two generators can be used for comparison with the rotor angle difference estimated by the proposed technique. The two-machine system is modified from the IEEE 9-bus system. The generator on bus 3 has been removed and shunt capacitor has been added to maintain the voltage on all buses above *0.98 p.u.* As discussed previously, the proposed technique provides $sin(\delta_{AS}(t))$ instead of $\delta_{AS}(t)$. To compare their values, the actual difference between the two generator rotor angles measured from simulation is converted to $sin(\delta_{AS}(t))$ to match the estimated rotor angle difference. Because the oscillation ceased slowly in the stable case, its plot had five seconds to show the shrinking envelope of the rotor angle difference. However, in unstable cases, due to the fast and continuously increasing rotor angle difference, it is better to plot a shorter time period so that the curve is not densely squeezed.

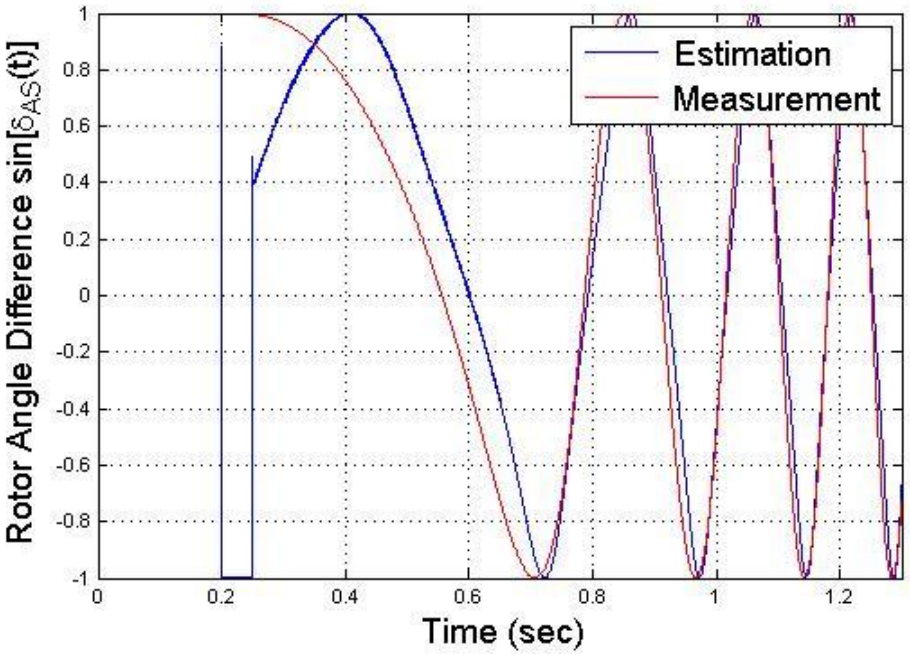

Fig. 5.6 Rotor angle difference of unstable case

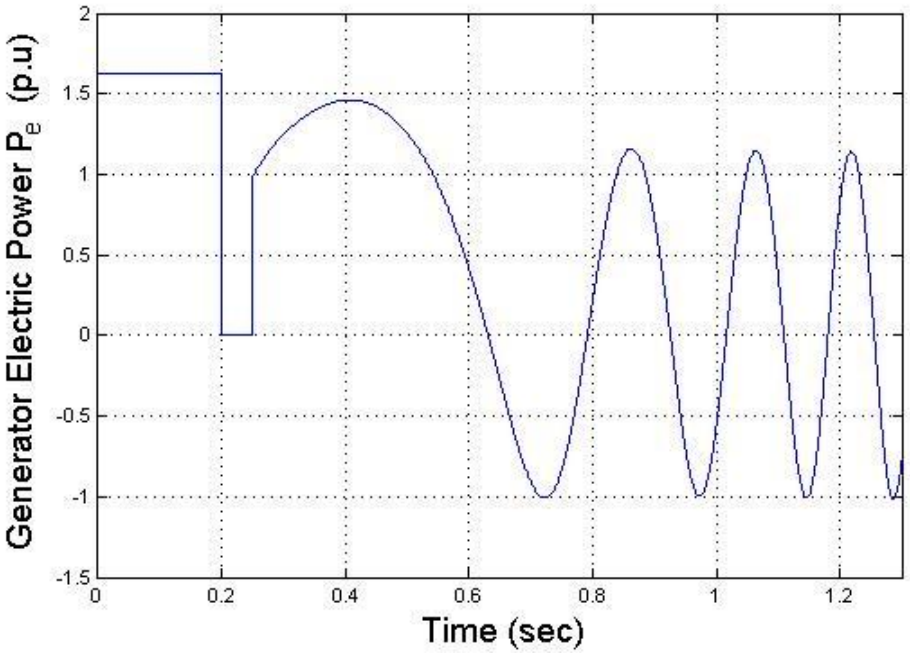

Fig. 5.7 Generator's electrical power output of unstable case

The above is an unstable case generated by the two-machine system. It can be expected that the continuously increasing rotor angle difference causes $|sin(\delta_{AS}(t))|$ to oscillate between -1 and 1.

The estimated and measured rotor angle differences are quite close to each other in Fig. 5.6. This proves that the equivalent system given in Fig. 5.4 and equation (5.9) is reasonable. Because the load in transient stability is a damping factor and the proposed technique assumes that the equivalent rotor angle is the aggregating effect of all components in the system, the value of the rotor angle difference form estimation would be smaller than the actual angle difference. This is reflected as a small lag in the time domain. Additionally, the envelopes of both rotor angle difference curves are also consistent with the P_e shown in Fig. 5.7.

Fig.5.8 shows the rotor angle difference from a stable case in a two-machine system. The oscillation caused by the disturbance is ceased slowly in this example. As in the unstable case, the two rotor angle difference curves plotted in Fig. 5.8 are also matched very well. Similar to the phenomena depicted in Fig. 5.6, the estimated rotor angle difference is smaller than the actual rotor angle difference due to the damping effect from the load. However, the difference between the two rotor angle difference curves in Fig. 5.7 is not as significant as the difference in Fig. 5.6. This is because the disturbance and resulting rotor angle fluctuation in the stable situation is much smaller than in the unstable situation. In addition, the active power output curve in Fig. 5.9 also shows the same envelope as the rotor angle difference curves in Fig. 5.8

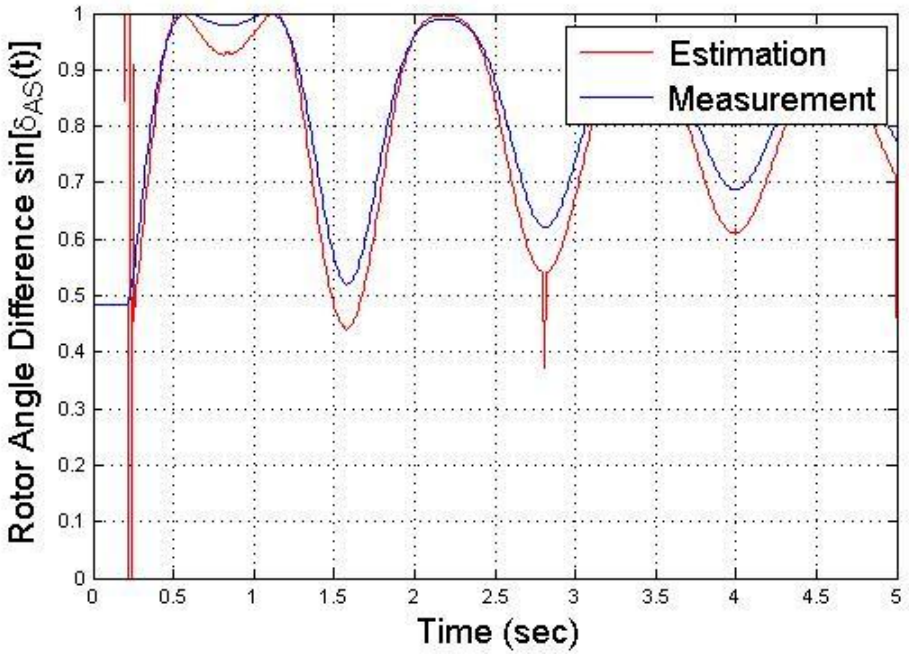

Fig. 5.8 Rotor angle difference of stable case

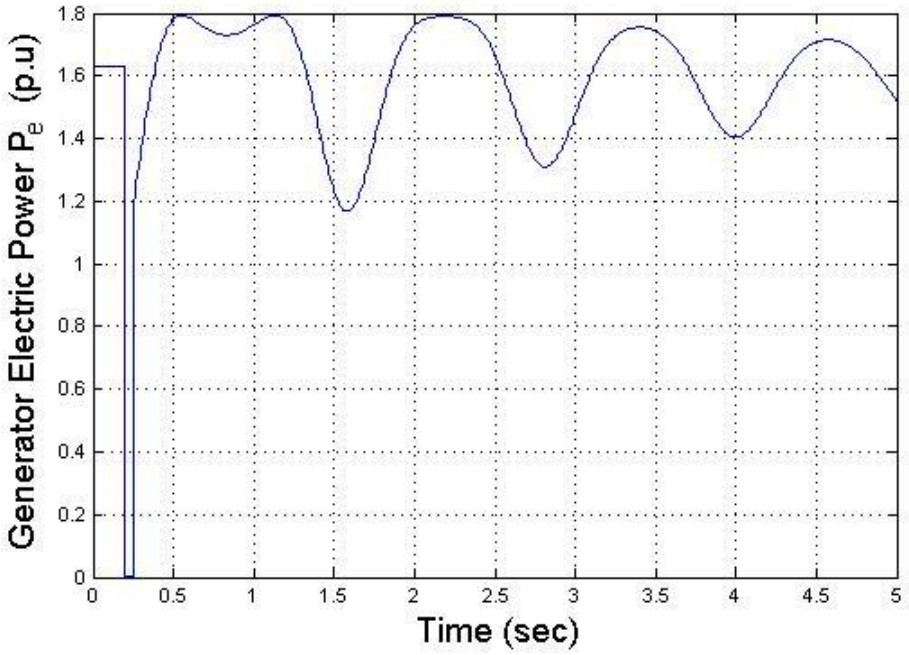

Fig. 5.9 Generator's electrical power output of stable case

Above two examples illustrate the effectiveness of the proposed technique. It proves that the proposed technique can provide an accurate rotor angle difference between the generator and the equivalent system. Later on, the proposed technique will be examined with the IEEE 39-bus system, and its performance will be compared with that of COI.

5.4.2 Rotor angle difference estimation using a PSS/E case study [58]

In this section, the IEEE 39-bus system is simulated by PSS/E. A three-phase to ground fault is applied to 50% of the transmission line between bus 4 and 14 as the disturbance. The rotor angle difference of the generator at bus 34 estimated by the proposed technique and calculated using COI are compared, as well as the generator's electrical power output. In Fig. 5.10b, the rotor angle difference obtained by the proposed technique closely matches the envelope of P_e in Fig. 5.10 (a). However, the rotor angle difference obtained by COI in Fig. 5.10c appears totally dissimilar to the P_e in Fig. 5.10 (b). In addition, after 1.6s, the rotor angle difference in Fig. 5.10 (b) reaches 180^o. This suggests that the ongoing oscillation is unstable. At the same time, the rotor angle difference in Fig. 5.10 (c) has just surpassed 90^o which does not clearly indicate the stability margin.

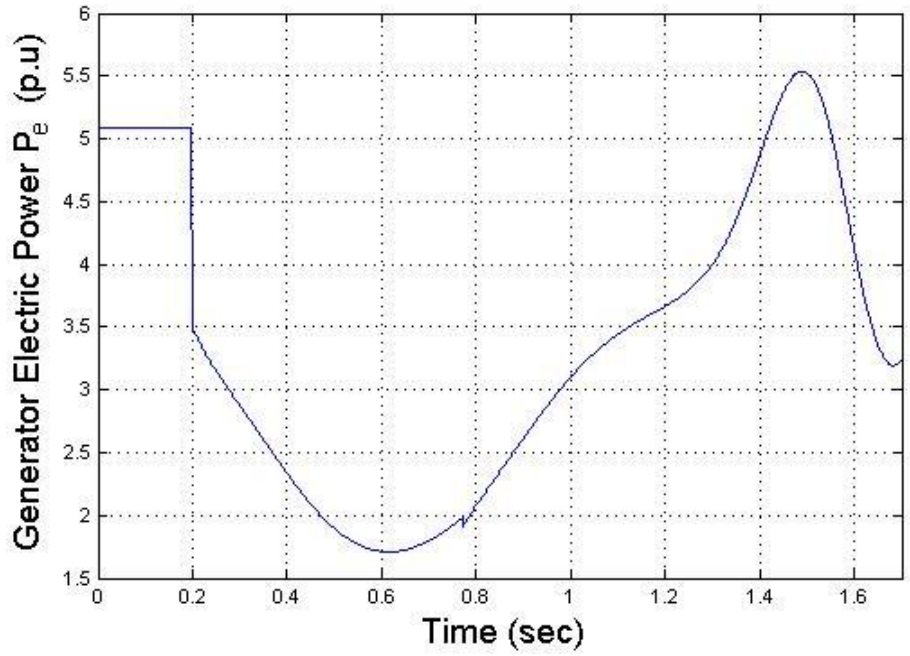
Generator Electric Power P_e (p.u)
Time (sec)
6
5.5
5
4.5
4
3.5
3
2.5
2
1.5
0
0.2
0.4
0.6
0.8
1
1.2
1.4
1.6

(a)

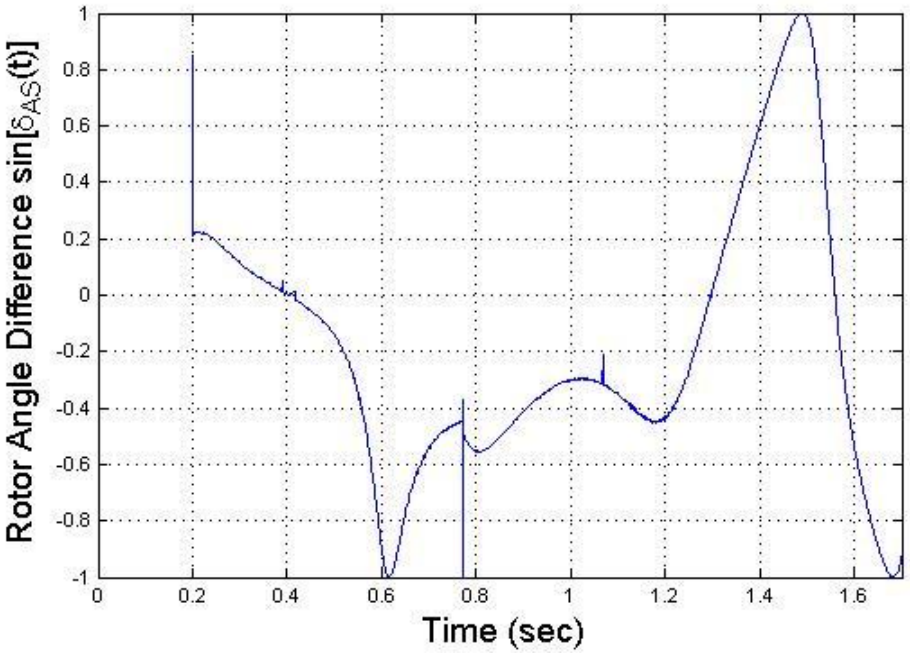
Rotor Angle Difference sin[δ_{AS}(t)]
Time (sec)
1
0.8
0.6
0.4
0.2
0
-0.2
-0.4
-0.6
-0.8
-1
0
0.2
0.4
0.6
0.8
1
1.2
1.4
1.6

(b)

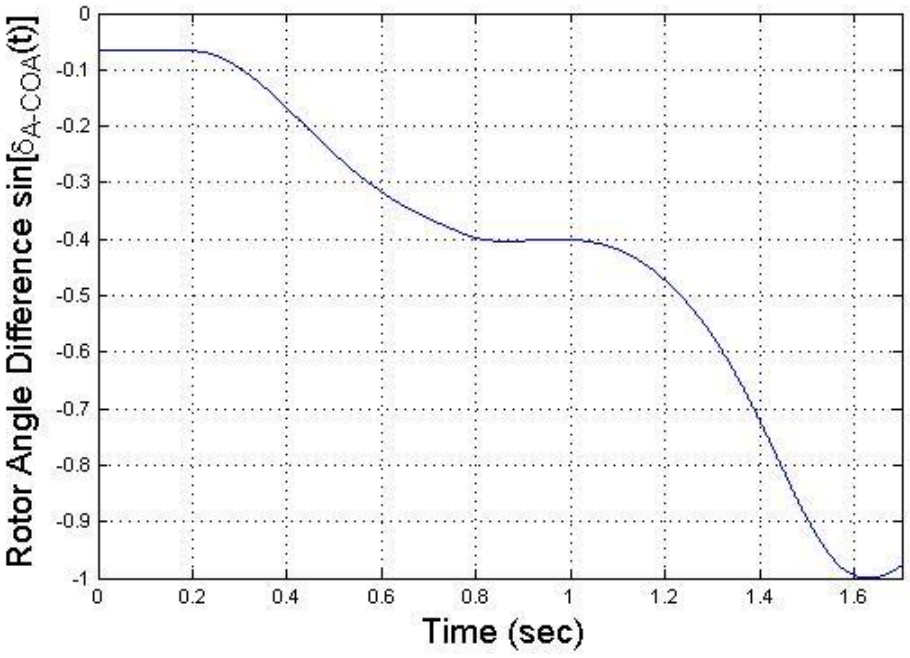

(c)

Fig. 5.10 (a) Electric power output of the generator G5 at bus 34; (b) Generator rotor angle difference obtained by the proposed method; (c) Generator rotor angle difference calculated by the COI.

With the same disturbance Fig. 5.11 illustrates the rotor angle difference of the generator at bus 37. In Fig. 5.11 (a) and (b), the generator active power output and the rotor angle difference obtained by the proposed method show similar patterns and they are totally irrelevant to the COI based rotor angle difference in Fig. 5.11 (c). Fig. 5.11 (c) also indicates that at 1.6s the rotor angle difference is less than 90° which could not confirm that the generator is unstable.

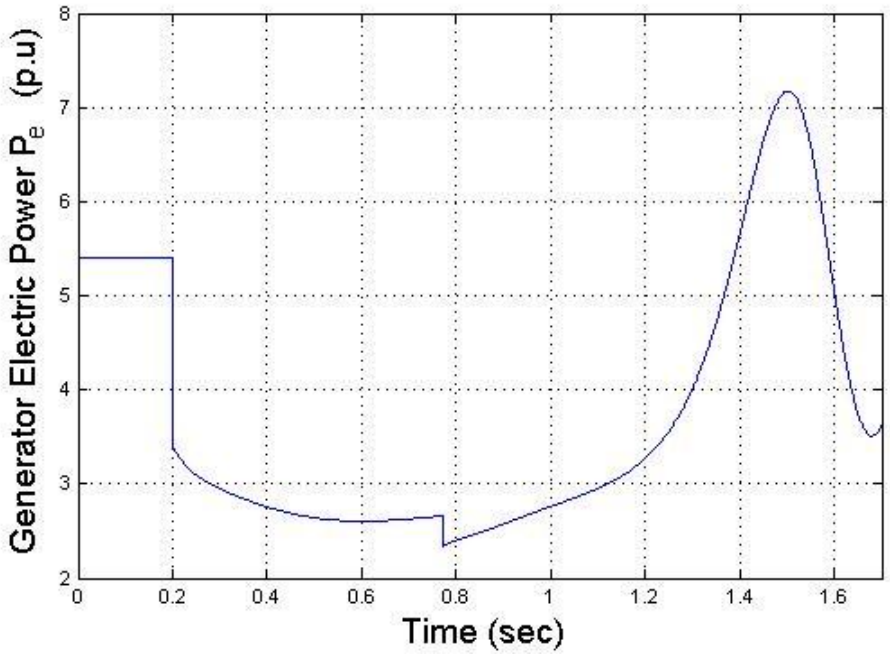
Generator Electric Power P_e (p.u)
Time (sec)
8
7
6
5
4
3
2
0
0.2
0.4
0.6
0.8
1
1.2
1.4
1.6

(a)

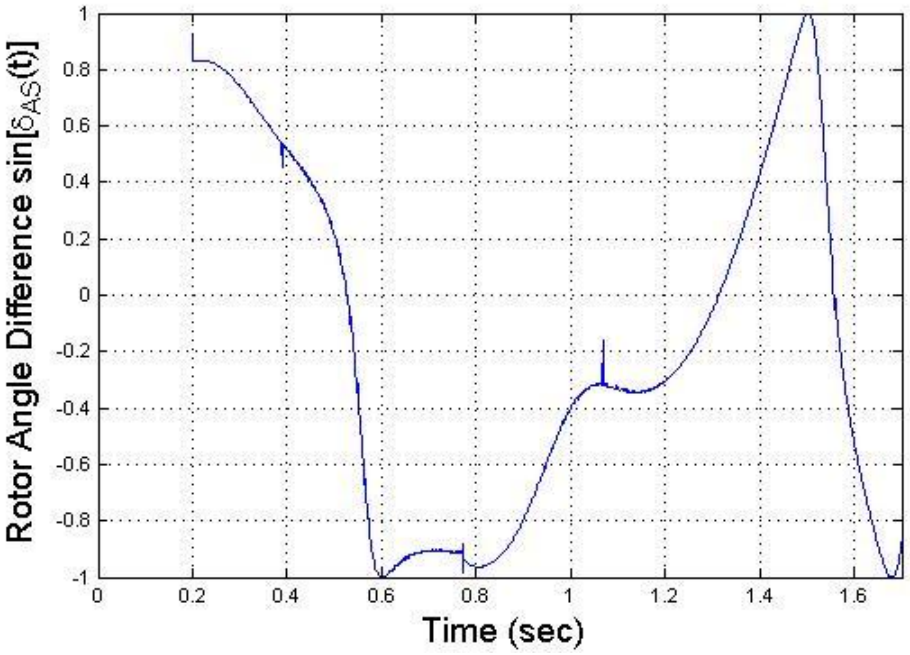
Rotor Angle Difference sin[δ_{AS}(t)]
Time (sec)
1
0.8
0.6
0.4
0.2
0
-0.2
-0.4
-0.6
-0.8
-1
0
0.2
0.4
0.6
0.8
1
1.2
1.4
1.6

(b)

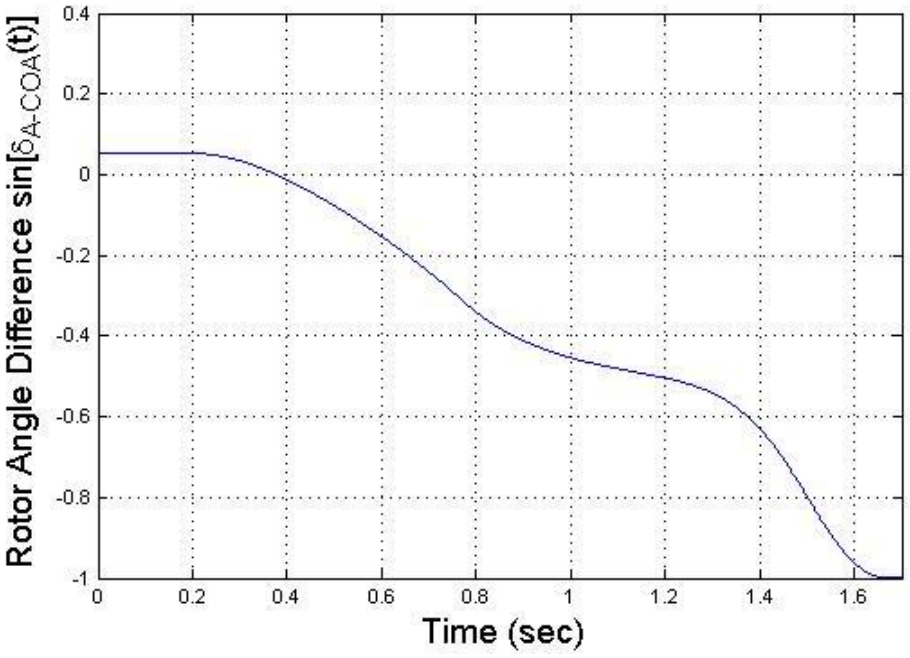

(c)

Fig. 5.11 (a) Electric power output of the generator G8 at bus 37; (b) Generator rotor angle difference obtained by the proposed method; (c) Generator rotor angle difference calculated by the COI.

5.4.3 Rotor angle difference estimation using a real-time digital simulator (RTDS) case study [59]

In Section 5.4.2 the proposed technique was compared with the COI in a PSS/E simulation, revealing that the proposed technique is more reasonable and accurate than COI in evaluating the transient stability. In section 5.4.3, the validity of the proposed technique will be further verified by RTDS simulation. The RTDS has detailed electro-magnetic model for the generator, it can provide more realistic results than PSS/E. Fig.

5.12 illustrates the active power output of the generator at bus 30 in the IEEE 39-bus system. The three-phase to ground fault is applied to 50% of the transmission line between bus 16 and 19 as the disturbance. It is simulated both by RTDS and PSS/E. Unlike in the PSS/E result given by Fig. 5.12 (b), the RTDS result in Fig. 5.12 (a) contains sub-transient components. This caused excessive fluctuations on the rotor angle difference curve which is displayed in Fig. 5.13 (a). However, with the sub-transient components fading out, both of the curves in Fig. 5.13 (a) and (b) started to show similar trends. The RTDS results again supported the effectiveness of the proposed technique in estimating the generator rotor angle difference of the multi-machine system.

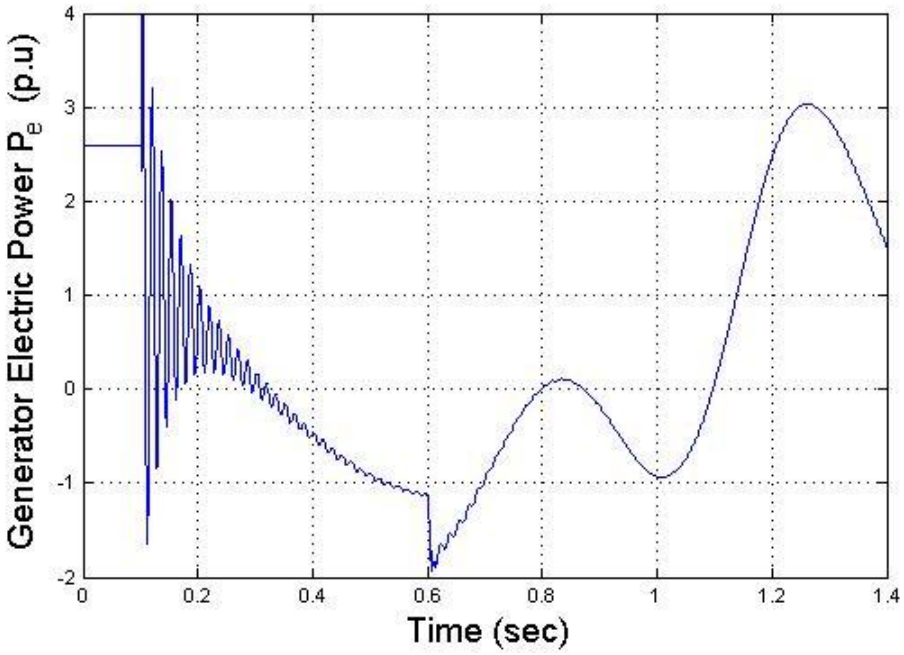

(a)

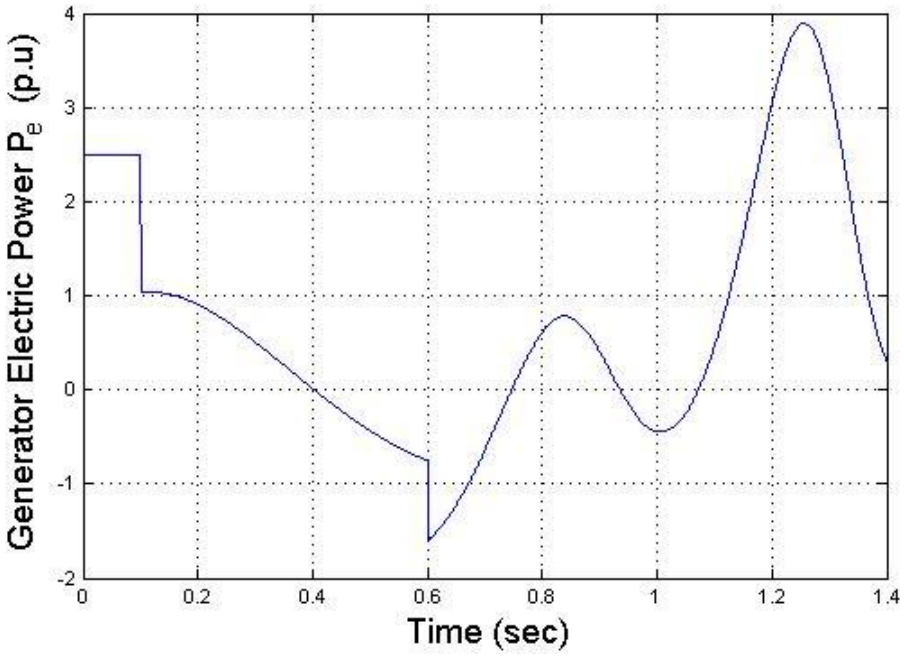

(b)

Fig. 5.12 (a) Electric power output of the generator G1 at bus 30 (RTDS); (b) Electric power output of the generator G1 at bus 30 (PSS/E).

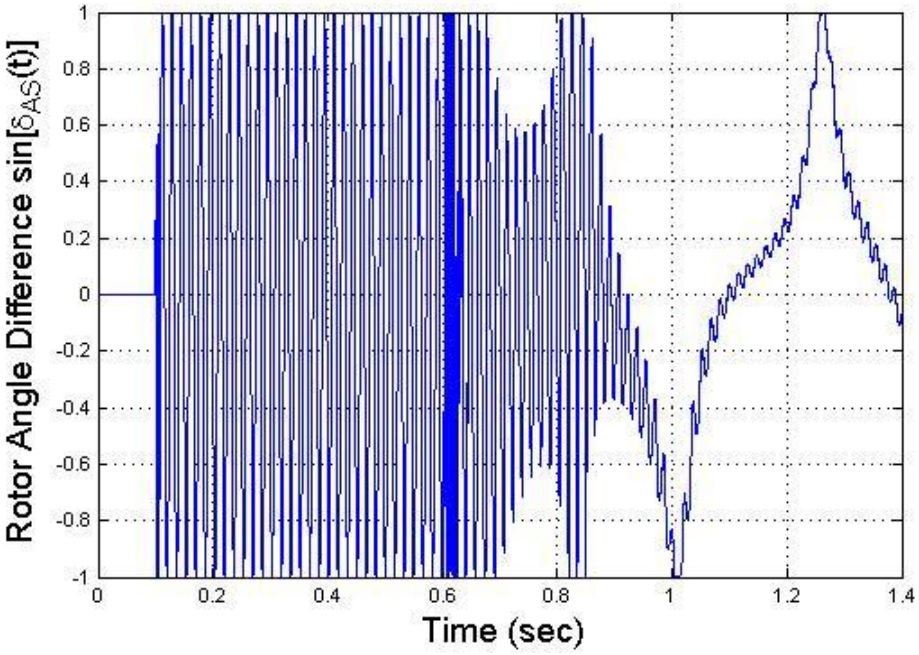

(a)

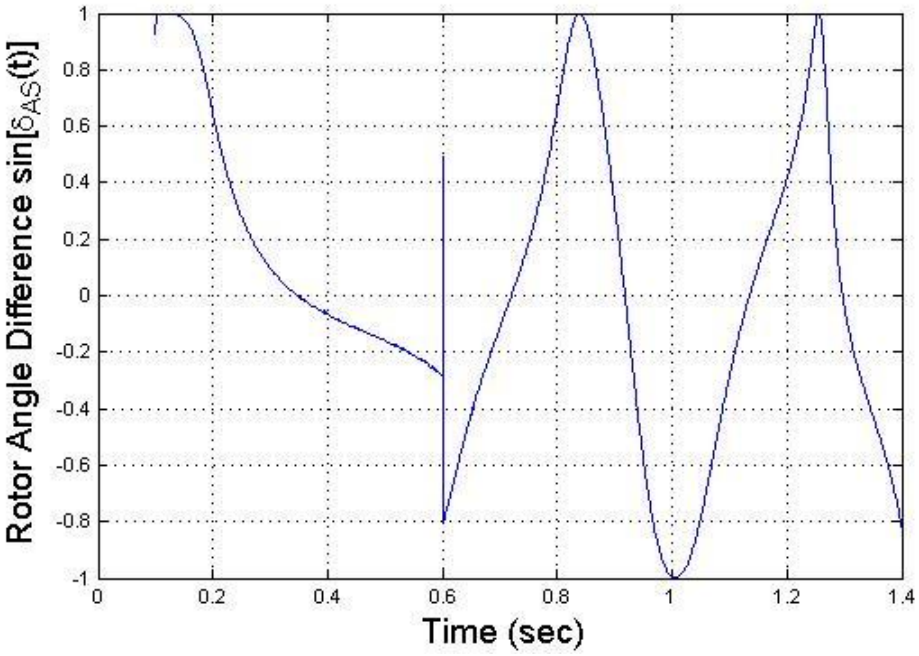

(b)

Fig. 5.13 (a) Rotor angle difference obtained by the proposed method using RTDS data; (b) Rotor angle difference obtained by the proposed method using PSS/E data

With the same disturbance, following Fig. 5.14 and Fig. 5.15 give the rotor angle difference of the generators on bus 37. Fig. 5.14 (a) and Fig. 5.14 (b) illustrate the active power outputs which are simulated by RTDS and PSS/E respectively. Similarly the excessive fluctuations in Fig. 5.15 (a) have deteriorated the rotor angle difference estimation result. With the decreasing of sub transient components, the Fig. 5.15 (a) and Fig. 5.15 (b) start to have similar trends.

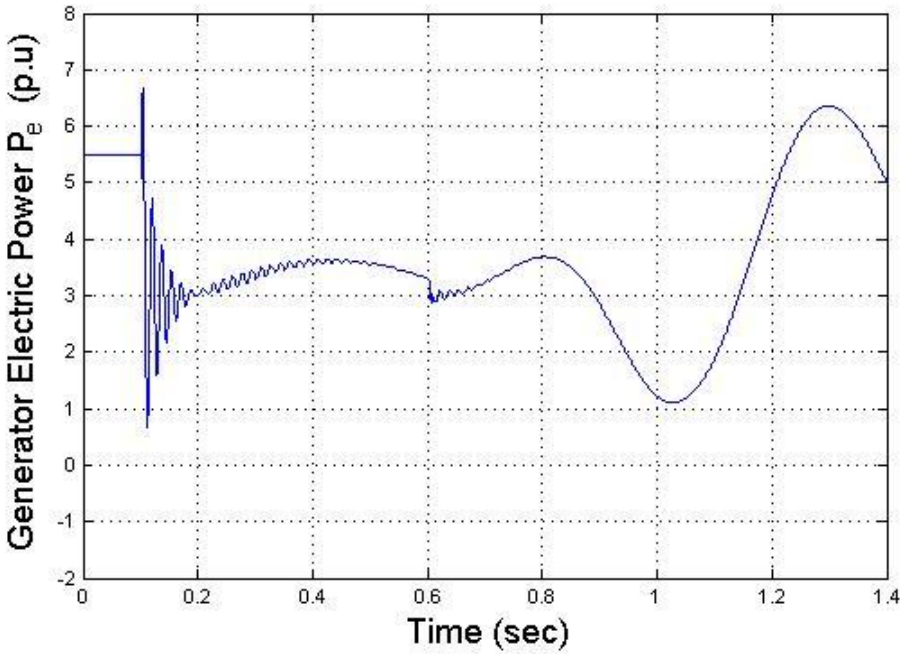

(a)

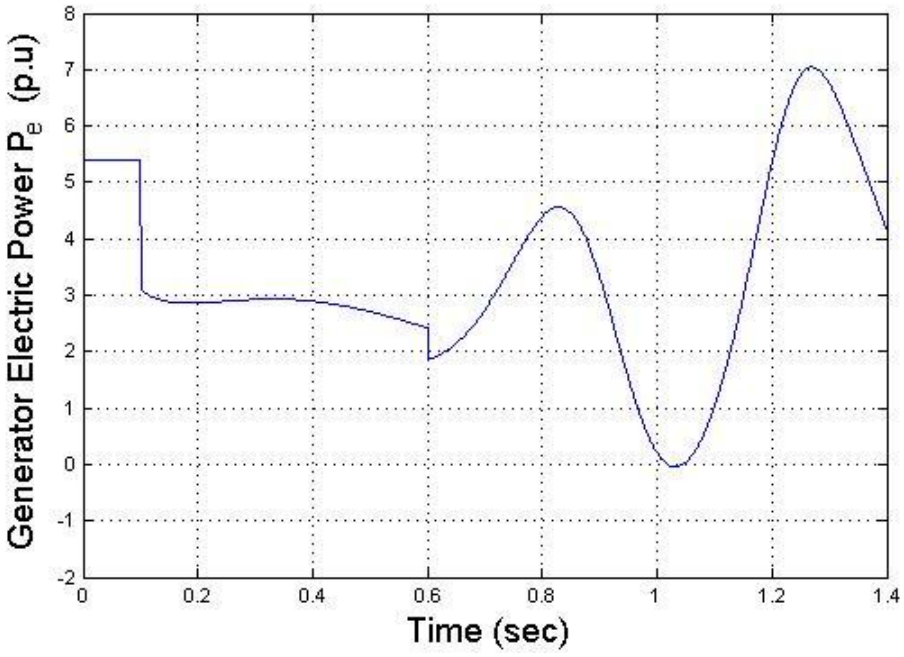

(b)

Fig. 5.14 (a) Electric power output of the generator G8 at bus 37 (RTDS); (b) Electric power output of the generator G8 at bus 37 (PSS/E)

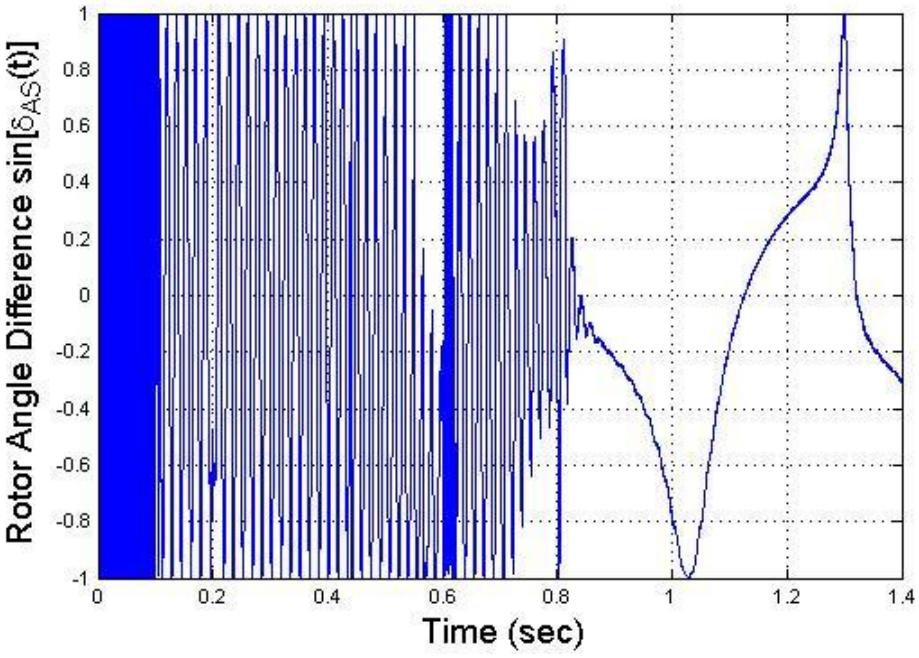

(a)

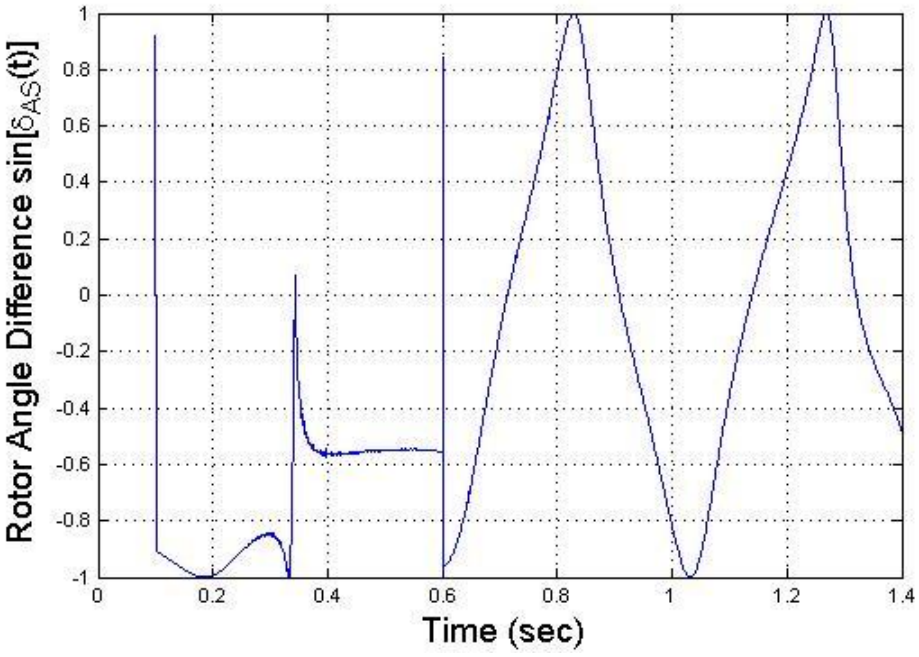

(b)

Fig. 5.15 (a) Rotor angle difference obtained by the proposed method using RTDS data;

(b) Rotor angle difference obtained by the proposed method using PSS/E data

Due to the filter's distortion, the low-pass filter is not recommended with the proposed method. Section 5.3 has demonstrated that the calculation process of the proposed method involves the first order derivative in its calculation. The derivative is very sensitive to the shape of curves. Any minor changes caused by the filter could invalidate the estimation result.

Because of the difficulty of obtaining the generator rotor angles in a large scale power system, simulations are used in this chapter to illustrate the feasibility and effectiveness of the proposed technique. The PSS/E and RTDS are included in section 5.4 for the purpose of improving the credibility of simulation results. Numerical results have showed that even with interference of the sub-transient components, the proposed technique still provides a more reasonable result than the COI for multi-machine power system transient stability studies.

5.5 Conclusions

In this chapter, the use of COI on the on-line analysis of the transient stability in the multi-machine power system has been investigated, and the disadvantage of this approach has been discussed. A novel approach for estimating the generator rotor angle difference has been introduced to replace the COI. The proposed technique directly obtains the rotor angle difference using only the local generator's active and reactive power output, which could be applied easier to real-time applications. The numerical simulations have proved that the rotor angle difference calculated by the proposed

technique is more reasonable than the one produced by COI. In the future, the feasibility of the proposed technique needs to be verified with actual power system operation data.

In addition, the proposed technique potentially provides a new way to evaluate the impact of renewable energy sources on the power system transient stability. Because the common renewable energy sources do not have a rotor or direct electro-magnetic linkage between the rotor and the grid, it is difficult to quantitatively identify the severity of their impact. The proposed technique can be used to obtain a virtual rotor angle difference for renewable energy sources. This could enable new possibilities in power system transient stability related studies.

CHAPTER SIX

TRANSIENT STABILITY CONSTRAINED OPTIMAL POWER FLOW

6.1 Introduction

In recent years there has been more renewable energy integrated into the power system for pursuing clean, sustainable and cheaper energy sources. Among common renewable energy sources, the wind energy is the most popular solution. Since renewable energy has obtained only a small portion of the total generation, its impact on power system operations was neglected because of the tiny effect. However, as the effort of increasing the wind power to 20% of the total generation before 2030 [60], the effect of wind generators on the power system stability has become an important issue. In order to fit for the variable wind speed, the wind generator is designed differently from the regular synchronous generators. In this chapter, before analyzing the impact of wind power generation, a brief comparison on synchronous generator and the most common wind turbines will be given. After this, the technique developed in Chapter Five will be applied in this chapter to evaluate the impact of DIFG on power system transient stability. Then the power system optimal operation with wind energy presents and its related transient stability constrains will be discussed at the end.

6.1.1 Difference between synchronous generator and wind turbine

The synchronous generator was introduced in Chapter Two. For producing 60 Hz AC power, the generator rotor has to be accurately controlled to maintain a constant speed. Because the rotor and the system frequency are synchronous, this kind of

generator is called synchronous generator. The rotor speed is regulated by accurately controlling the steam turbine according to the instantaneous generator power output. Because of this feature, synchronous generators are not compatible with wind. Since there is no way to control the wind speed like controlling the steam turbine, the synchronous generator would produce a wide range of frequency if it is driven by wind. For wind power generation, the common solution is to use the induction generator [61].

There are four types of induction generators for wind power generation showed in Fig. 6.1 [62]: (a) single fed induction generator, (b) wonder rotor induction generator, (c) doubly fed induction generator (DFIG), and (d) full convertor induction generator.

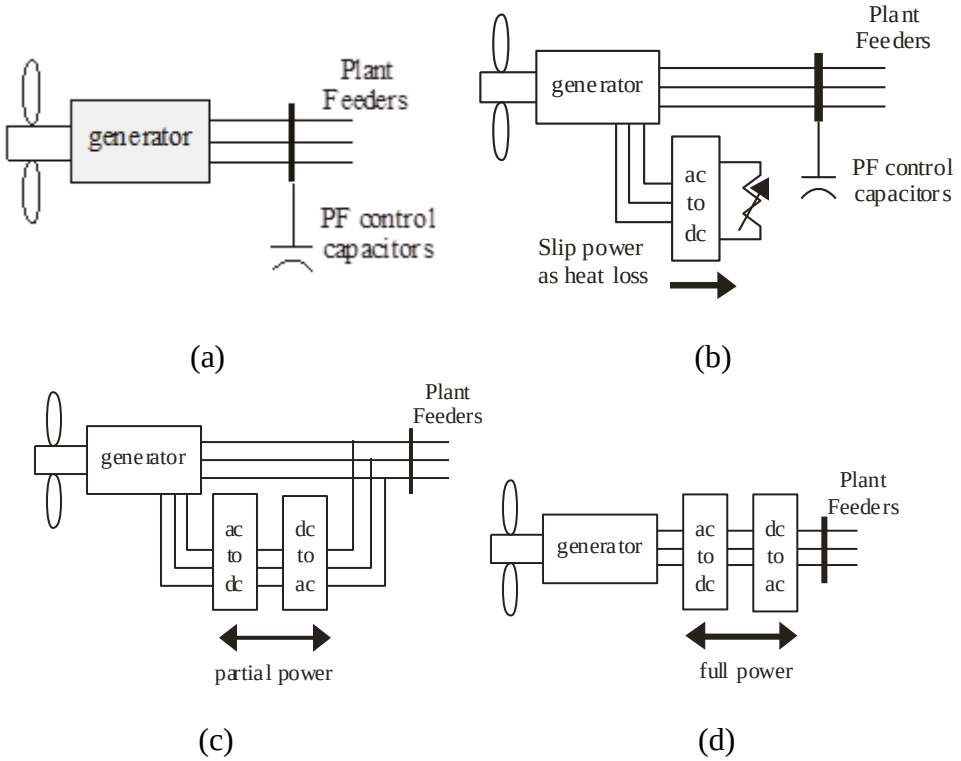

Fig. 6.1 (a) Single fed induction generator; (b) Wonder rotor induction generator; (c) Doubly fed induction generator; (d) Full convertor induction generator.

The type (a) and (b) generators are roughly the reverse use of induction motor. Fundamentals of induction motor can be found in [61]. Type (a) and (b) wind turbines require the rotor speed to lead the electrical speed which is power system frequency. In such case when the wind speed is low, it is operating as an induction motor which does not provide any power to the grid. Type (d) uses a converter to isolate the generator with the power system. This design enables the generator to produce energy with a wide range of wind speed because the convertor will maintain a frequency lower than the turbine shaft speed at the generator side and 60 Hz at the grid side. Power is fed into the convertor and then injected to the grid. The converter is required to have the capacity to allow the rated power to go through. Due to the technical and economical reason, the convertor will limit the size and increase the cost of the wind generator. Type (c) is abbreviated as DFIG which is the most popular wind turbine. The converter of DFIG only conducts small amount of power to the rotor [63-69]. This power allows when the power system frequency is leading the rotor speed, the induction machine can still output power to the grid. In this chapter the study of wind power penetration on power system transient stability is based on DFIG.

The above introduction explained that the electric power of the DFIG is also from the shaft torque. This is the same as the synchronous generator. However, because of the nature of induction machine, the rotor mechanical speed is not synchronous with the electrical speed which is the grid frequency. Therefore, the power system transient stability with DFIG can no longer be investigated by directly studying the rotor angle difference between generators [70-83]. The following section will apply the generator

rotor angle difference estimation technique developed in Chapter Five to study the impact of wind power generation on power system transient stability.

6.1.2 Transient stability constrains for optimal power flow

According to the literature review, the transient stability constrained power flow refers to optimizing the power system operation while maintaining the system within the safety range of transient stability. For determining the safety range with the presence of wind turbine, the rotor angle difference estimation technique proposed in Chapter Five will be employed to find the difference between the wind turbine and the synchronous generator and help to determine the threshold of the transient stability constrains.

It should be noted is that the rotor angle difference estimation technique proposed in Chapter Five is used for comparing the dynamic behavior of DFIG and synchronous generator only. It is not used for determining the transient stability constrains. During the optimal power flow calculation process, transient stability constrained optimal power flow adds stability constrains into the inequality constrain. The transient stability constrains showed in the literature review is the rotor angle difference between each generator and the COI. Chapter Five have demonstrated the ineffectiveness of COI for multi-machine system transient stability studies. Although the rotor angle difference estimation technique proposed in Chapter Five has better performance than COI in power system transient stability studies, it cannot be used for directly obtaining the threshold or stability constrains. Because the optimal power flow is intended for static operation and in this situation generator output power is constant, the time derivatives of generator

active power and reactive power will result in an undefined value in equation (5.11). Thus, the transient stability constrain in this chapter is defined as the terminal voltage angle difference between every two generators.

Although the optimal power flow calculates generator bus voltage angle instead of generator rotor angle, the generator rotor angle of synchronous generator can be determined by the terminal voltage angle. Because the synchronous generator commonly generates reactive power, its output current lags the field armature voltage. Fig. 6.2 shows the phasor diagram of the synchronous generator voltage and current. Due to the lagging current, the generator terminal voltage slightly lags the armature voltage. In Fig. 6.2, V_s and I_s are generator terminal voltage and current phasors; jX_s is the generator synchronous reactance; E_f is the field armature voltage which angle equals to the generator rotor angle. Because generator terminal voltage always lags the armature voltage and the voltage drop from the armature voltage to generator terminal voltage is small, in static power system operation, the angle difference between generator terminal voltages can be approximately replaced by the generator rotor angle.

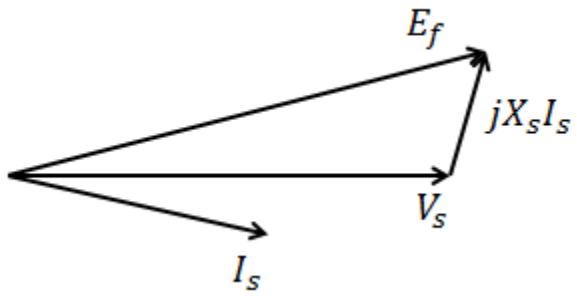

Fig. 6.2 Phasor diagram of synchronous generator

For induction generators, the above conclusion is not valid since the E_f is not synchronous with the V_s. The generator rotor angle difference estimation technique is used to figure out the equivalent rotor angle difference between the induction generator and the power system. Following is the result of dynamic simulations executed in modified IEEE 9-bus system (Fig. 6.3). The system contains two synchronous generators on bus 1 and 2 and one wind farm on bus 10. According to [84], the wind farm is constructed as several wind turbines connecting to a collector bus and then through a step-up transformer to feed power into the power system. In transient stability studies, all wind turbines in a wind farm are usually lumped together as one equivalent generator. The wind farm's rotor angle obtained by the technique proposed in Chapter Five will be compare with the voltage phase angle on the collector bus.

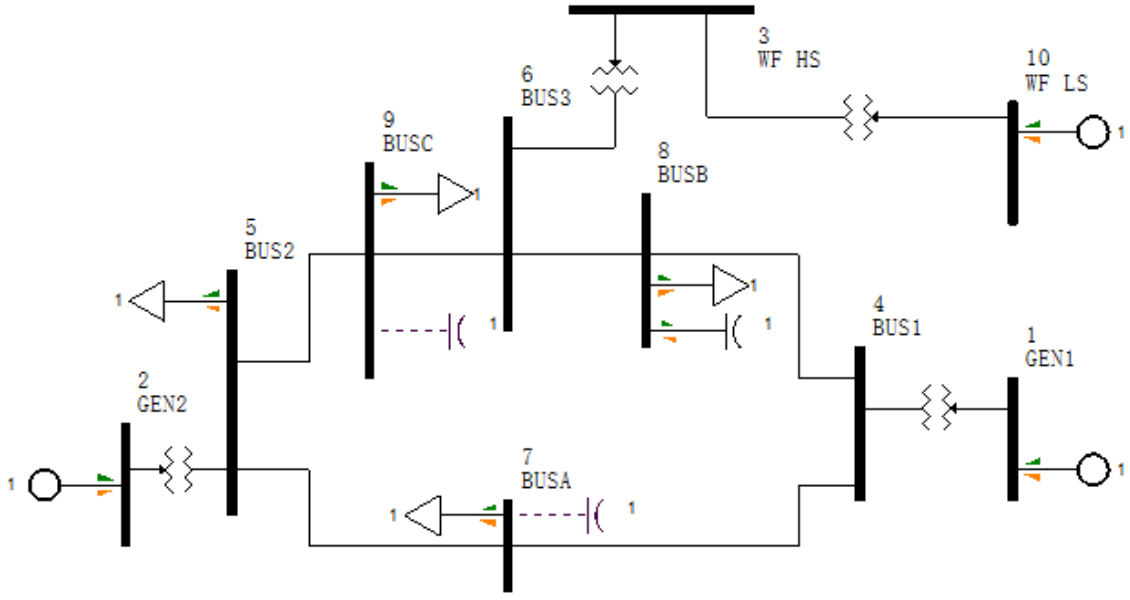

Fig 6.3 Modified IEEE 9 bus system

A three phase fault is applied to the transmission line between bus 6 and 8 for 0.75 second as the disturbance. Then the fault is cleared and the faulty line continues operating all the time. Since there are three generators in the system and one of them is a wind farm, it is not accurate to obtain the angle difference just from the rotor angle difference of two synchronous generators. The rotor angle difference estimation technique is applied to the generator on bus 2 to compare the equivalent generator rotor of synchronous generator with its terminal voltage angle. The same procedure is then executed with the wind farm to compare the equivalent rotor angle of the wind farm and the voltage angle on the collector bus. Fig 6.4 and 6.5 show these comparisons. Due to the reason explained in Chapter Five, the rotor angle showed in Fig 6.4 and Fig. 6.5 are $\sin(\delta)$ where δ is the rotor angle difference.

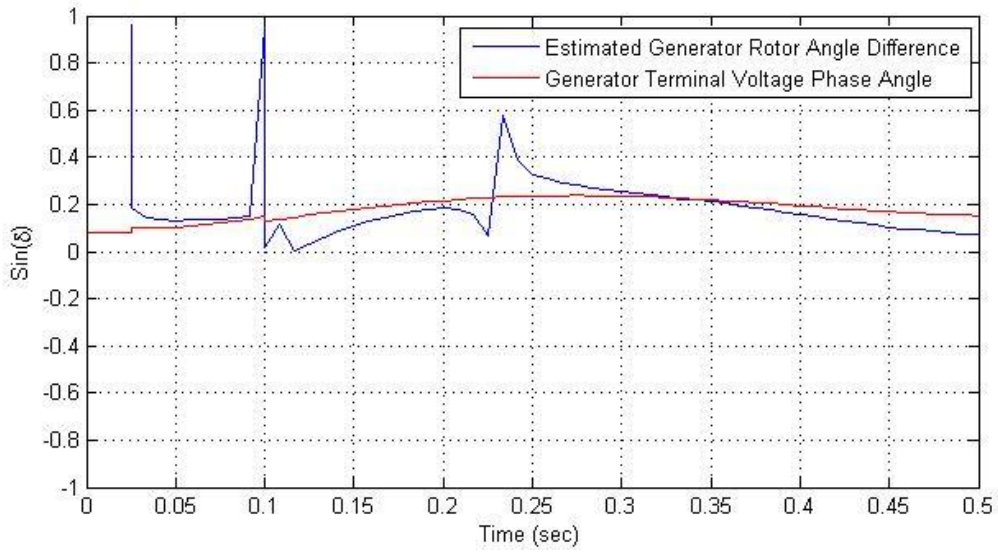

Fig 6.4 Rotor angle difference and generator terminal voltage angle of the synchronous generator

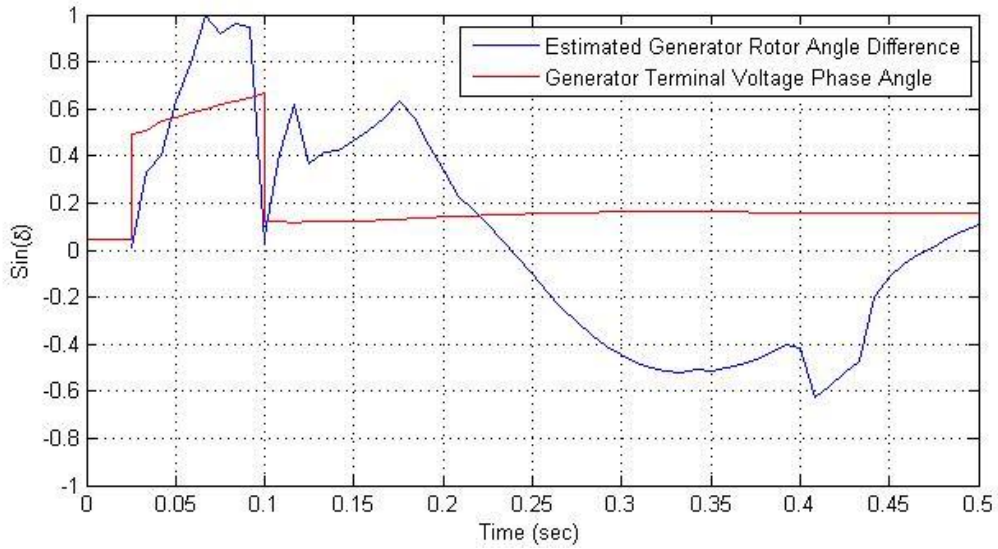

Fig 6.5 Equivalent Rotor angle difference and generator terminal voltage angle of the wind farm

During a short period after the disturbance, the estimated generator rotor angle difference of the synchronous generator is very close to its terminal voltage angle. To the contrary, the equivalent generator rotor angle difference of the wind farm showed violent oscillations when compared with the collector bus voltage angle. Taking account of the wind turbine one mass model [85], if the wind turbine has total inertia H_w, the impact of wind farm on power system transient stability equals a synchronous generator with inertia H_w injecting the perturbation showed in Fig. 6.5 to the power system. For reducing this impact, the transient stability constrain for wind farm should be stricter than that of synchronous generators when the wind farm collector bus voltage angle is used to determine transient stability constrains.

According to the equal area criteria, in a two-machine system when the initial generator rotor angle difference is greater than 180^o, the system will definitely become unstable. Though to use 180^o as the stability constrain will be too risky. Meanwhile the modified 9-bus system example has showed that the value of the estimated wind farm equivalent rotor angle difference is bigger than the collector bus voltage angle. To mitigate the oscillation of the wind farm after the disturbance, it requires a smaller initial rotor angle difference. Therefore, if the maximum voltage angle difference of synchronous generators is set to 90^o, the maximum voltage angle difference of wind farm should be more conservative than 90^o. This chapter is tentatively to use 30^o as the transient stability constrain for wind farms.

6.2 South Carolina offshore wind speed measurement system

Since there will be large scale off-shore wind farms construction planned in South Carolina, in this chapter, the South Carolina off-shore wind speed data is used for demonstrating the proposed technique. The off-shore wind speed data came from CAP2 of Carolinas Costal Ocean Observing and Prediction System (Caro-Coops) [86]. The measurement devices are carried by offshore buoys [87]. Fig. 6.6 is the location of Caro-Coops CAP2 buoy [86].

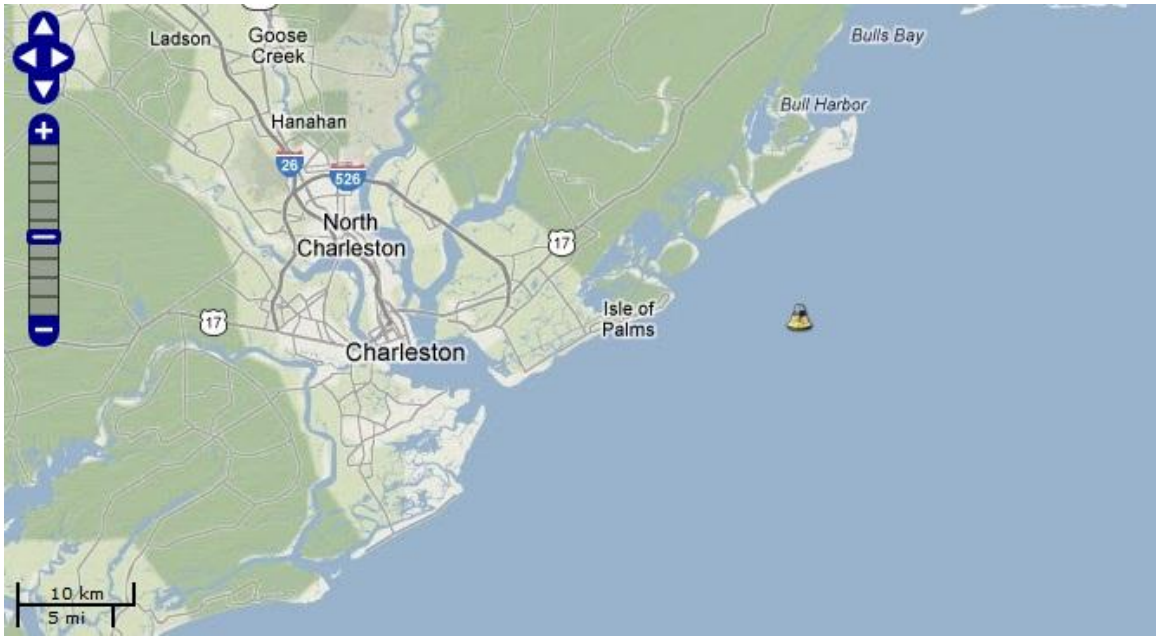

Fig. 6.6 The location of Caro Coops CAP2 buoy

Currently the wind speed data from Caro-Coops is available from 2005 to 2008. Since the data of year 2005 is incomplete, the wind speed data from 2006 to 2008 is used for study. CAP2 buoy captures the wind speed at sea level every two hours. The unit of wind speed is given by knot/hour. For simplicity, it is converted to the metric system as meter per second by multiplying 0.517.

Fig. 6.7 shows the histogram of wind speed recorded by CAP2 buoy at 9:00am in September. It gives a rough idea that the wind speed of CAP2 at that time is usually between 1 – 12 m/s. Since there are only 90 measurement data in Fig. 6.7, the envelope of the histogram is not smooth because the distribution of available data is sparse. The common approach for studying the availability of wind power is the Monte Carlo method

to simulate the randomness of the wind speed [88]. For this purpose, the probability density function (PDF) of the wind speed has to be determined first.

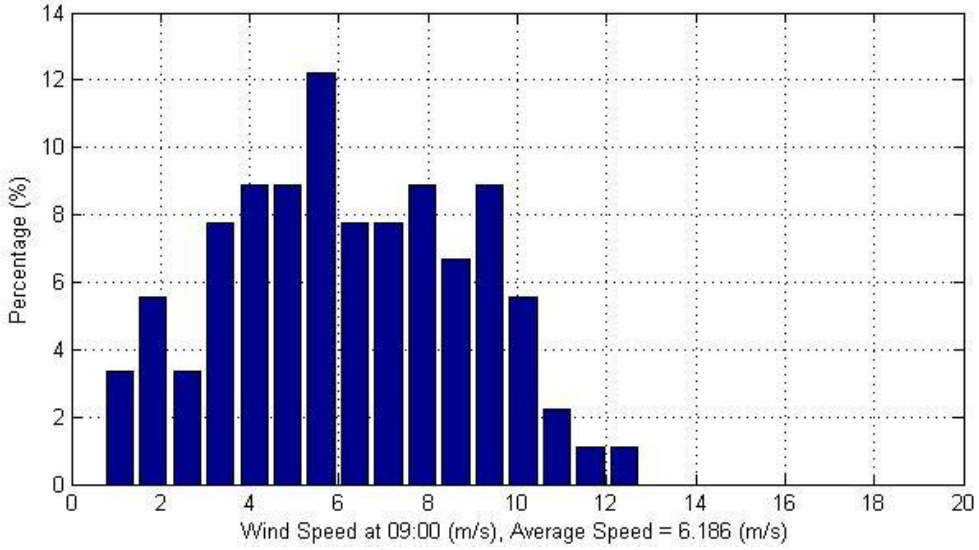

Fig. 6.7 Histogram of wind speed at 9:00 am in September

6.3 Stochastic modeling for wind speed and wind turbine output power

According to [89], the probability density of wind speed generally matches the probability density of Weibull distribution. The PDF of Weibull distribution is given as:

$$f(x;\lambda,k) = \begin{cases} \frac{k}{\lambda}(\frac{x}{\lambda})^{k-1} e^{-(\frac{x}{\lambda})^k} & x \geq 0 \\ 0 & x < 0 \end{cases} \tag{6.1}$$

where

x wind speed

λ Scale parameter (m/s)

k Shape factor

The scale parameter λ and the shape factor k are unknown. They should be obtained by the statics of actual wind speed. However, having the wind speed in Fig. 6.7 and equation (6.1), it is still hard to find the value of λ and k. In this section an approach for obtaining the approximate value of λ and k will be discussed.

The mean of the Weibull distribution is given by (6.2).

$$E(X) = \lambda\Gamma(1 + \frac{1}{k}) \tag{6.2}$$

When the probability of wind speed is believed to match the Weibull distribution, different values of scale parameter and shape factor can be substitute into (6.2) to generate a table of their correlated mean speed of wind. The mean speed from the table is used to compare with the actual mean speed from the measurement to determine the value of λ and k. There will be several combinations of scale parameters and shape factors which give similar mean speed. The scale parameters are very close to each other, but the shape factors vary from a wide range. Fig.6.8 gives an example of the Weibull distribution with different shape factors. Since the probability varies a lot with different shape factors, the shape of wind speed histogram can be used to finally decide the value of the shape factor.

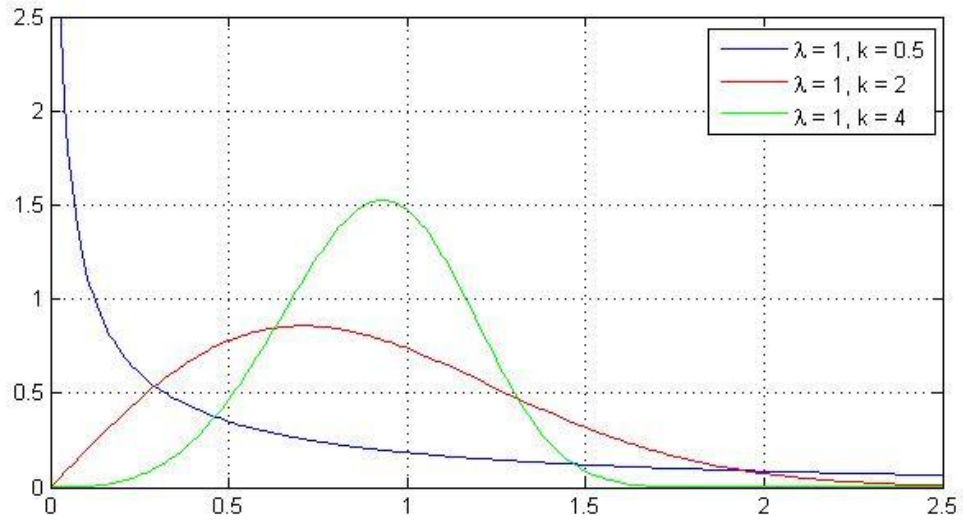

Fig. 6.8 Probability density distribution of Weibull distribution

6.3.1 Stochastic model of wind speed at 9:00 am in September

Table 6.1 gives the mean speed of wind and their correlated λ and k values. The average wind speed at 9:00 am in September is 6.1860m/s. It can be found in Table 6.1 that the possible combinations of scale parameter and shape factor are $\lambda = 6.75, k = 4.84$, $\lambda = 6.80, k = 4.26$, $\lambda = 6.85, k = 3.75$, $\lambda = 6.90, k = 3.26$, $\lambda = 6.95, k = 2.77$.

Table 6.1 Mean speed with scale parameter and shape factor

	$\lambda = 6.75$	$\lambda = 6.80$	$\lambda = 6.85$	$\lambda = 6.90$	$\lambda = 6.95$
$k = 2.76$	6.0073	6.0518	6.0963	6.1408	6.1853
$k = 2.77$	6.0081	6.0526	6.0971	6.1416	6.1861
$k = 3.25$	6.0503	6.0951	6.1399	6.1847	6.2295
$k = 3.26$	6.0512	6.0960	6.1408	6.1856	6.2305
$k = 3.74$	6.0952	6.1403	6.1855	6.2306	6.2758
$k = 3.75$	6.0961	6.1412	6.1864	6.2315	6.2767
$k = 4.25$	6.1395	6.1850	6.2305	6.2759	6.3214
$k = 4.26$	6.1403	6.1858	6.2313	6.2768	6.3223
$k = 4.83$	6.1852	6.2311	6.2769	6.3227	6.3685
$k = 4.84$	6.1860	6.2318	6.2776	6.3234	6.3693

The probabilities of these five combinations are plotted in Fig. 6.9. Compared with the probability density in Fig. 6.7 the combination $\lambda = 6.95, k = 2.77$ is the best fit for the available wind speed histogram.

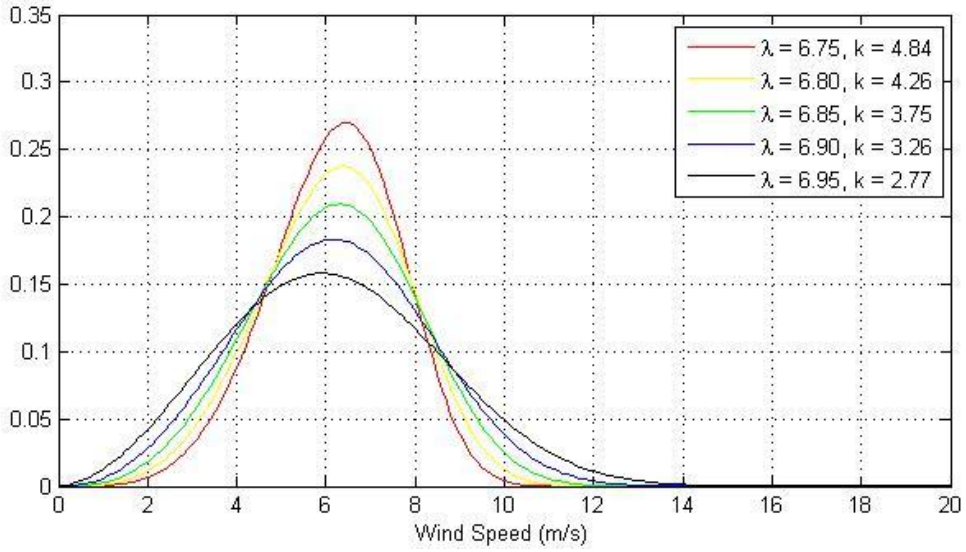

Fig. 6.9 Probability density distribution of different combinations

The Monte-Carlo simulation is applied to generate 1000 data sets for simulating the availability of wind power at 9:00 am in September. The histogram of simulated wind speed data is given in Fig. 6.10.

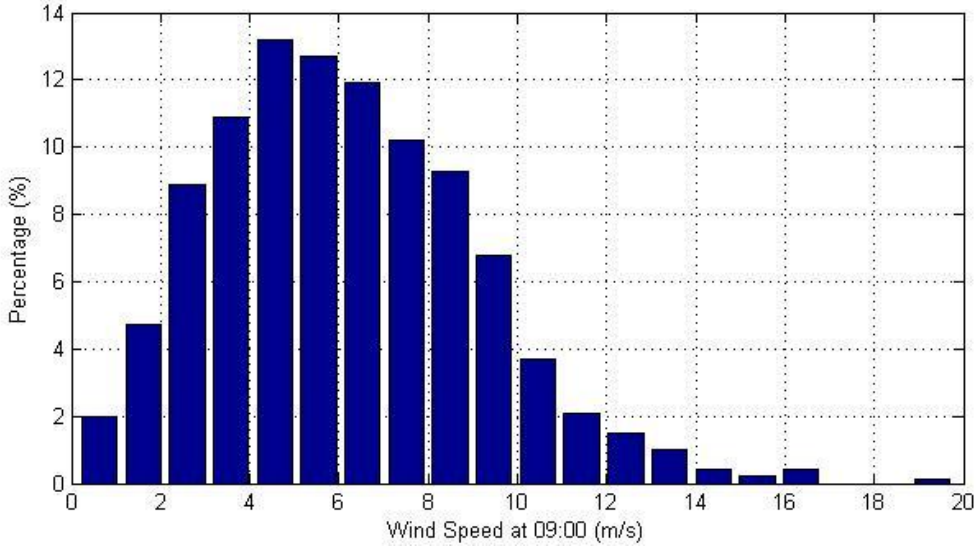

Fig. 6.10 Histogram of simulated wind speed at 9:00 am in September

When the wind speed is simulated, it is substituted to the wind turbine output power equation to obtain the distribution of available wind power.

6.3.2 Output power of wind turbine

According to [90], the relation between wind turbine output power and the wind speed is given by (6.3).

$$P_{max} = \begin{cases} 0.5\rho A C_p V^3 & 3.5 < V < 25 \\ 0 & V < 3.5 \\ 0 & V > 25 \end{cases} \tag{6.3}$$

where

ρ Air density, $\rho = 1.225\ kg/m^3$ at the sea level

A The area wind turbine blade coves

C_p Efficiency of the wind turbine

V Wind speed (m/s)

In this chapter the popular GE 1.5 MW wind turbine is chosen for the wind farm. Its technical manual gives $A = 5342.90\, m^2$ and $C_p = 0.52$ [90]. Substituting these parameters and the wind speed simulated in section 6.2.1, the histogram of wind turbine output power is given in Fig. 6.11.

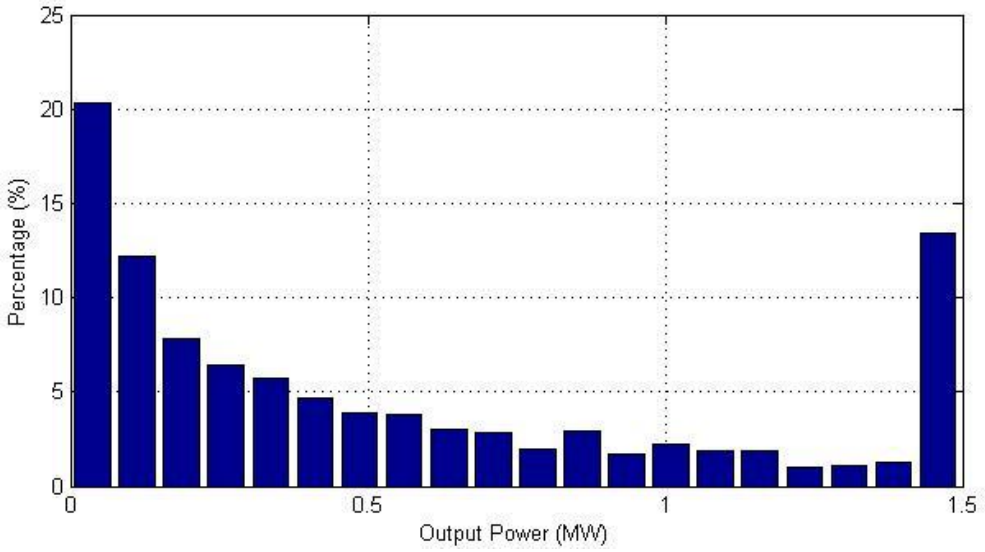

Fig. 6.11 Histogram of the wind power availability at 9:00 am in September

It is inferred from Fig. 6.11 that South Carolina does not have abundant offshore wind power capacity. It can be found in Fig. 6.11 that there are more than 20% chances that the wind turbine cannot provide any power and only less than 15% chances the wind turbine can provide its rated power.

6.4 Optimal power flow with wind energy penetration

In this section, the wind power generation cost is obtained as a quadratic polynomial by the availability of the wind power. This is because the regular generator's generation cost is usually defined by the quadratic polynomial. The popular optimal power flow techniques can be easily used for solving the optimization problem.

6.4.1 Wind power generation cost

Compared with the static and controllable regular power generation, the wind power is a dynamic and random process. The stochastic model of wind power has been discussed in section 6.3. In this section, the cost function of wind power generation will be developed with the wind power model.

According to [91], when the scheduled generation is determined, the actual wind power generation can be divided into shortage and surplus scenarios. If the actual wind speed is low, the available wind power would be less than the schedule. There must be some backup generations such as the spinning reserve to compensate the shortage. These compensation generations should be available at any time and it is costly. Therefore it is better to have fewer backups. On the other hand, if the actual wind speed is high, schedule would be lower than the available wind power. The role of this wasted wind energy is under taken by regular generations which have fuel cost and may have environment impact. In this case, there should be a penalty factor on the cost of wind power surplus. Fig. 6.12 shows the shortage and surplus with the generation schedule.

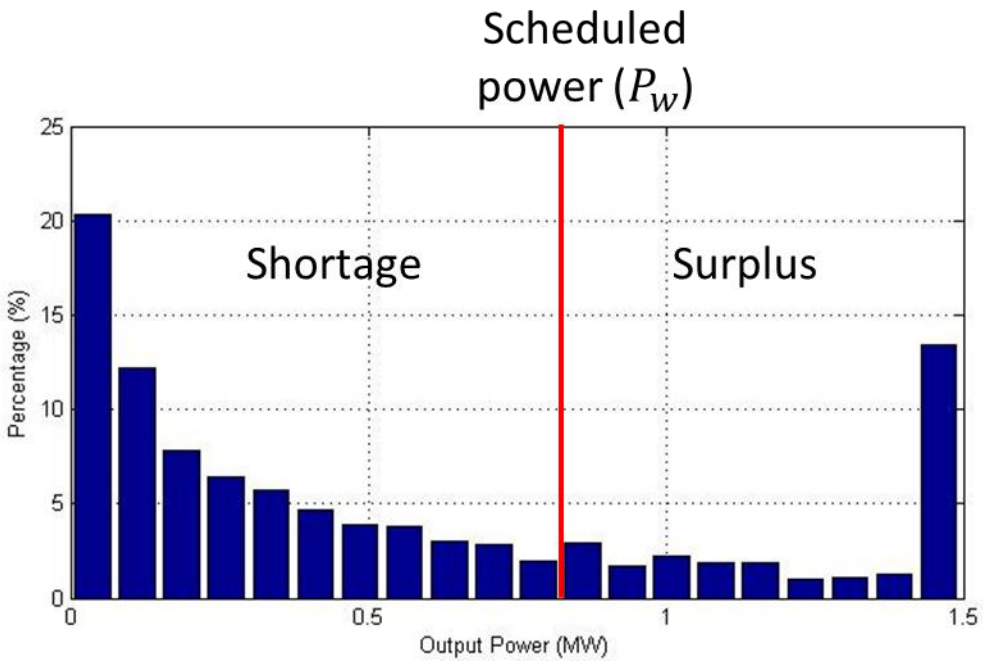

Fig. 6.12 Shortage and surplus of wind power

Reference [89] has explained how to calculate the expected cost of wind power generation. First, the expectance of shortage power and the surplus power according to the scheduled power generation are calculated by (6.4) and (6.5).

$$P_{shortage}(P_w) = \Pr(P_{actual} < P_w)\,[P_w - E(P_{actual}|P_{actual} < P_w)] \tag{6.4}$$

$$P_{surplus}(P_w) = \Pr(P_{actual} > P_w)\,[E(P_{actual}|P_{actual} > P_w) - P_w] \tag{6.5}$$

where

P_w Scheduled wind power generation

P_{actual} Actual available wind power

Then the cost of wind power generation is calculated as:

$$F(P_w) = cost_{shortage} * P_{shortage}(P_w) + cost_{surplus} * P_{surplus}(P_w) \quad (6.6)$$

where

$cost_{shortage}$ Shortage cost factor (R/(h*MW))

$cost_{surplus}$ Surplus cost factor (R/(h*MW))

Equation (6.6) gives the cost function of one wind turbine. In a wind farm which has *n* turbines, the total cost should multiply by *n*. The cost calculated by (6.6) is discrete since the histograms of expected shortage and surplus have limited bins. For finding a continuous cost curve, the curve fitting is needed to obtain a quadratic polynomial so that the optimal power flow can be solved by the available techniques.

6.4.2 Optimal power flow

Optimal power flow belongs to the power system economical operation. It is based on satisfying the requirements of regular power flow to achieve the minimum cost. The OPF problem can be formulated as an objective function (6.7), equality constrains (6.8) and inequality constrains (6.9) [92]:

$$\min f(x,u) \quad (6.7)$$

$$s.t\ H(x,u) = 0 \quad (6.8)$$

$$and\ h(x,u) < 0 \quad (6.9)$$

where

x Vector of state variables

u Vector of control variables

The objective function is the summation of generator fuel costs. Usually the generator fuel cost is a quadratic polynomial (6.10):

$$f(P_{Gi}) = a + bP_{Gi} + cP_{Gi}{}^2 \tag{6.10}$$

where

P_{Gi} Scheduled power generation of generator i

a, b and c Constant values

The equality constrains are power flow equations (6.11) and (6.12):

$$P_{Gi} - P_{Li} - \sum_{j=1}^{n} \left|V_i V_j Y_{ij}\right| cos\left(\theta_{ij} + \delta_j - \delta_i\right) = 0 \tag{6.11}$$

$$Q_{Gi} - Q_{Li} - \sum_{j=1}^{n} -\left|V_i V_j Y_{ij}\right| sin\left(\theta_{ij} + \delta_j - \delta_i\right) = 0 \tag{6.12}$$

where

P_{Gi} and Q_{Gi} Active and reactive power generation at bus i

P_{Li} and Q_{Li} Active and reactive load at bus i

V_i Voltage magnitude at bus i

δ_i Voltage angle at bus i

Y_{ij} Magnitude of admittance matrix term

θ_{ij} Angle of admittance matrix term

The optimization problem can be solved by many approaches. Since the purpose of this work is to develop a practical way to solve transient stability constrained OPF with the presence of wind power, the optimization procedure will be solved by fmincon() function in Matlab.

6.5 Solving the transient stability constrained power flow

The traditional solution for optimal power flow problem described by (6.7)-(6.9) is linear programming. It linearizes the generator fuel cost function and the power flow equations. The linear programming approach is not accurate since the fuel cost curve is linearized by limited segments. Simulation has showed that solving the nonlinear optimization often encounters convergence problem when the system is complex. In this chapter, an alternate approach is taken for the purpose to mitigate the convergence problem while keeping the nonlinear relations of the generation cost functions. Firstly the nonlinear optimization is executed to find the approximate configuration of lowest fuel cost. The equality constrain is the balance between the total generation and the total load. The result is used as the generation demand in the constrained power flow to satisfy the transient stability constrains and obtain the losses. After the stability constrained power flow step, the optimization will be executed again. At this time the equality constrains become the balance between the total generation, the total load and total losses. If the

result from the optimization matches the result of the previous power flow step, it is considered as converged and this result is the final optimized generation schedule. If the optimized generation demand does not match the result of the previous power flow, the optimized generation demand will be substitute to the constrained power flow again to solve the new losses and another optimization process will be executed. After several iterations the calculation will converge. Following is the flow chart of proposed process (Fig. 6.13).

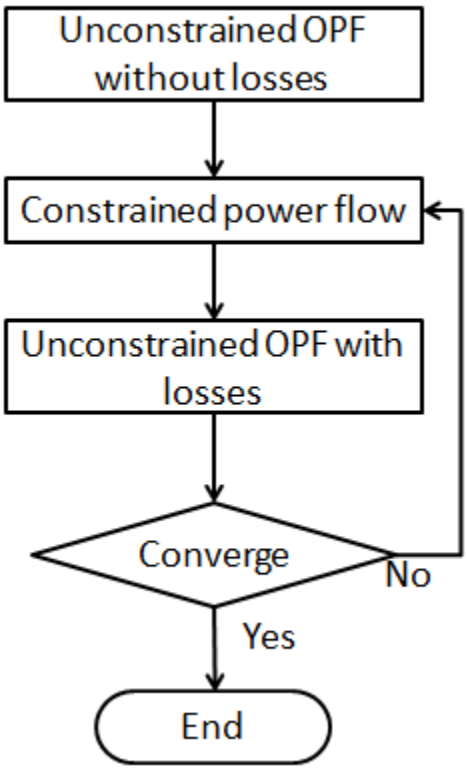

Fig. 6.13 Flow chart of the proposed process

6.6 Numerical example and results

In this section, the proposed transient stability optimal power flow technique will be tested by the IEEE 9-bus system and IEEE 39-bus system.

6.6.1 IEEE 9-bus example

The IEEE 9-bus system is used to illustrate the calculation process of the proposed technique. The system is given in Fig. 6.3. The wind speed analyzed in section 6.4 is used as the wind energy availability for obtaining the generation cost of the wind farm. The wind farm is assumed to have 50 GE 1.5 MW wind turbines and is set to operate within the range of ±0.95 power factor.

According to equation (6.4) and (6.5), the shortage and surplus of GE 1.5 wind turbine at 9:00 am in September are given in Fig. 6.14 and Fig. 6.15.

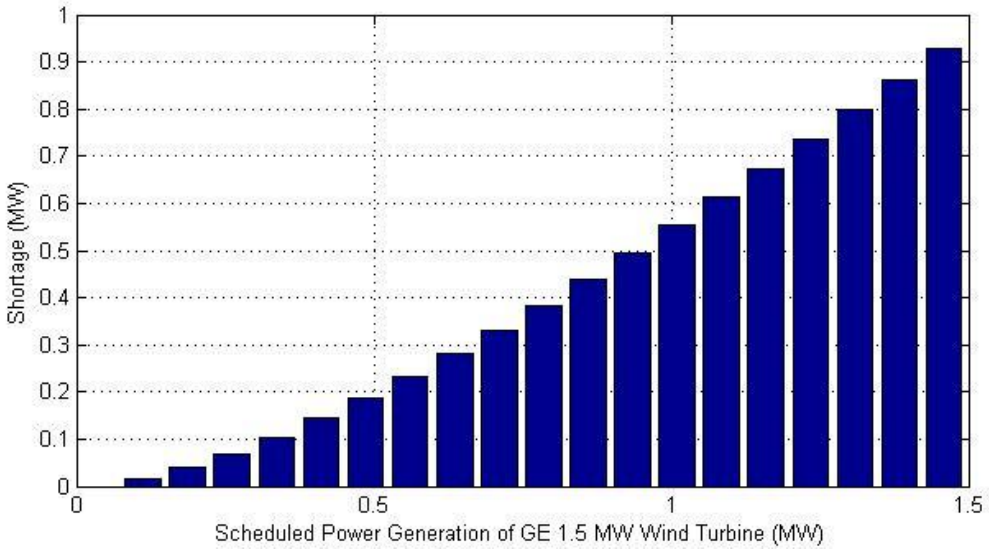

Fig. 6.14 Expected wind power shortage of one GE 1.5 MW wind turbine

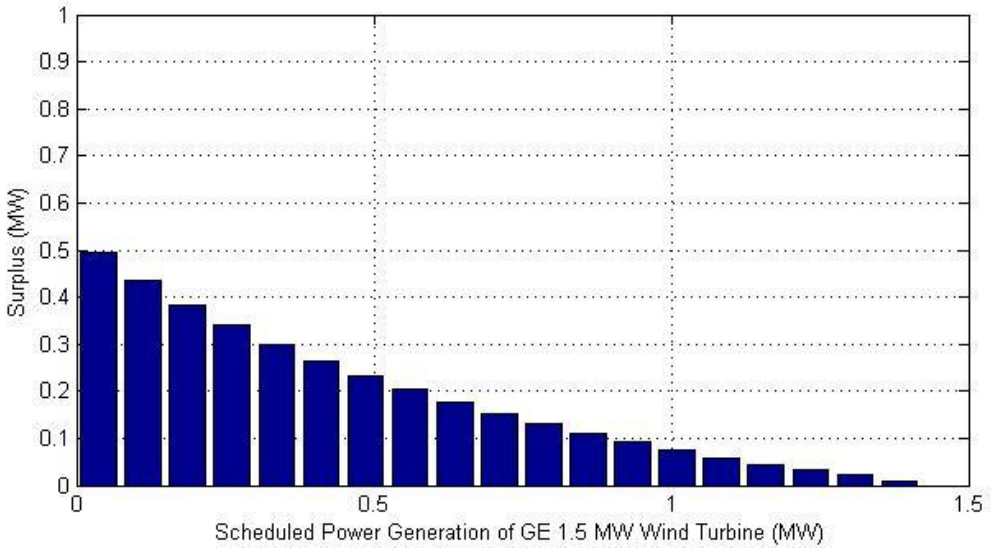

Fig 6.15 Expected wind power surplus of one GE 1.5 MW wind turbine

The curve fitting of shortage and surplus according to the scheduled power are given as:

$$F_{shortage}(P_w) = n * cost_{shortage}(0.2069{P_w}^2 + 0.3629P_w - 0.03173) \quad (6.13)$$

$$F_{surplus}(P_w) = n * cost_{surplus}(0.2069{P_w}^2 - 0.6371P_w + 0.5003) \quad (6.14)$$

The P_w in (6.13) and (6.14) is the scheduled power generation of one wind turbine.

With shortage and surplus cost factor equal to 14 R/MW and 2 R/MW, combining the parameter n with P_w, the cost function of the entire wind farm which has 50 wind turbines is given as:

$$F(P_{wf}) = 0.066208{P_{wf}}^2 + 3.8064P_{wf} + 27.819 \quad (6.15)$$

The P_{wf} in (6.15) is the scheduled power generation of the entire wind farm.

The two other synchronous generators' cost functions are given as:

$$F_1(P_{G1}) = 0.00533{P_{G1}}^2 + 11.669P_{G1} + 213.1 \quad (6.16)$$

$$F_2(P_{G2}) = 0.00889{P_{G1}}^2 + 10.333P_{G1} + 200 \quad (6.17)$$

First iteration starts from the wind farm operating at its rated power and equally distributing the rest of the load to other two synchronous generators. Neglecting the losses, the optimal power flow result is:

$P_{G1} = 128.26\ MW$

$P_{G2} = 152.04\ MW$

$P_{Wf} = 69.70\ MW$

$loss = 0\ MW$

By substituting the scheduled generation into power flow, the new scheduled generation with considering transient stability constrains becomes:

$P_{G1} = 131.58\ MW$

$P_{G2} = 152.04\ MW$

$P_{Wf} = 69.70\ MW$

$loss = 3.3\ MW$

The second iteration will consider the losses. With 3.3 MW losses, the optimal power flow result is:

$P_{G1} = 130.22\ MW$

$P_{G2} = 153.22\ MW$

$P_{Wf} = 69.89\ MW$

$loss = 3.3\ MW$

Substitute the scheduled generation in to power flow, the new generation schedule within the transient stability constrain is:

$P_{G1} = 130.25\ MW$

$P_{G2} = 153.22\ MW$

$P_{Wf} = 69.89\ MW$

$loss = 3.3\ MW$

The calculation converged at this step because the power flow result matches the optimal power flow result in the previous step. The final cost is 4432.1 R/h. When all 75 MW wind power is scheduled and the rest generation is equally distributed to other two synchronous generators, the resulted cost is 4434.6 R/h. This means although the utilization of renewable energy is usually believed to be as much as possible, because of the uncertainty of wind speed, the expected cost of the wind power generation is not

always the lowest. After the optimal power flow, the biggest angle difference between generator buses is 2.4^{o}. This guarantees the operation has reasonable distance away from the stability margin.

6.6.2 IEEE 39-Bus example

The IEEE 39-bus system and the South Carolina offshore wind speed at 9:00 pm in September are used in this section to demonstrate the proposed technique. The power plant at bus 38 has been replaced by a wind farm which contains 200 GE 1.5 MW wind turbines. The rated power of the wind farm is 300MW. The wind farm is set to operate within the range of ±0.95 power factor. The mean speed of wind at 9:00 pm is 5.91354 m/s. This is the lowest speed during a day in September. The scale parameter and shape factor correlated to this mean speed are 6.64 m/s and 2.81. The availability of wind power is given by Fig. 6.16 and related shortage and surplus are given by Fig. 6.17 and Fig. 6.18.

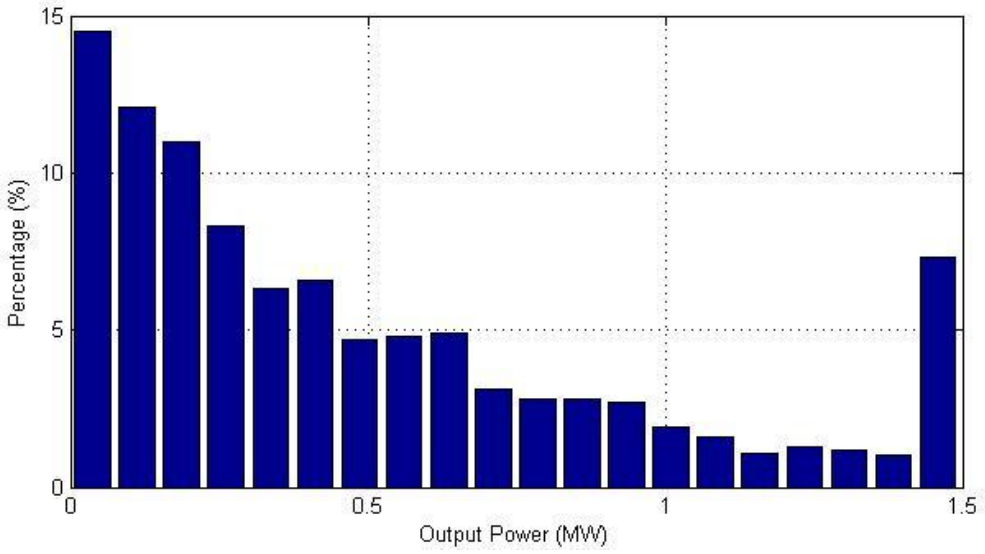

Fig. 6.16 Histogram of the wind power availability at 9:00 pm in September

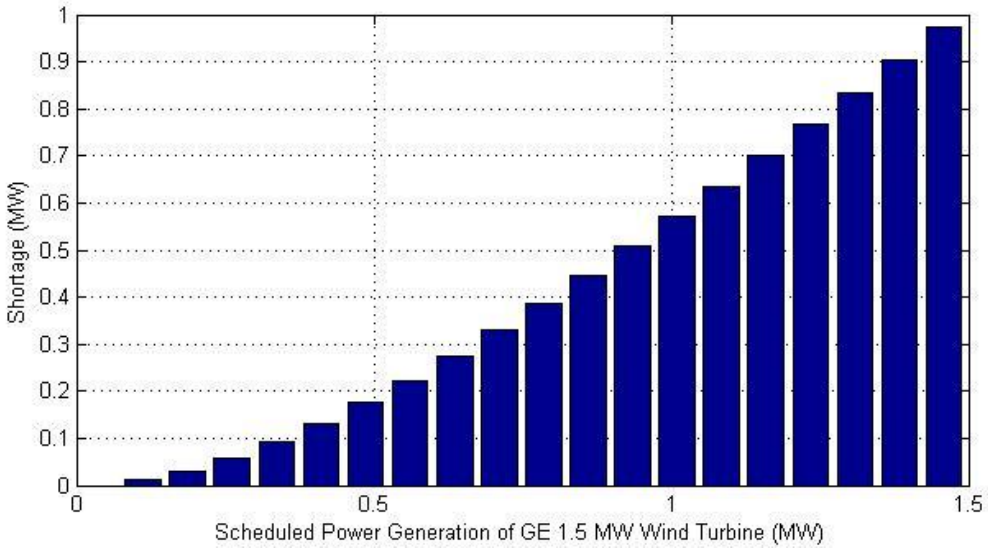

Fig. 6.17 Expected wind power shortage of one GE 1.5 MW wind turbine

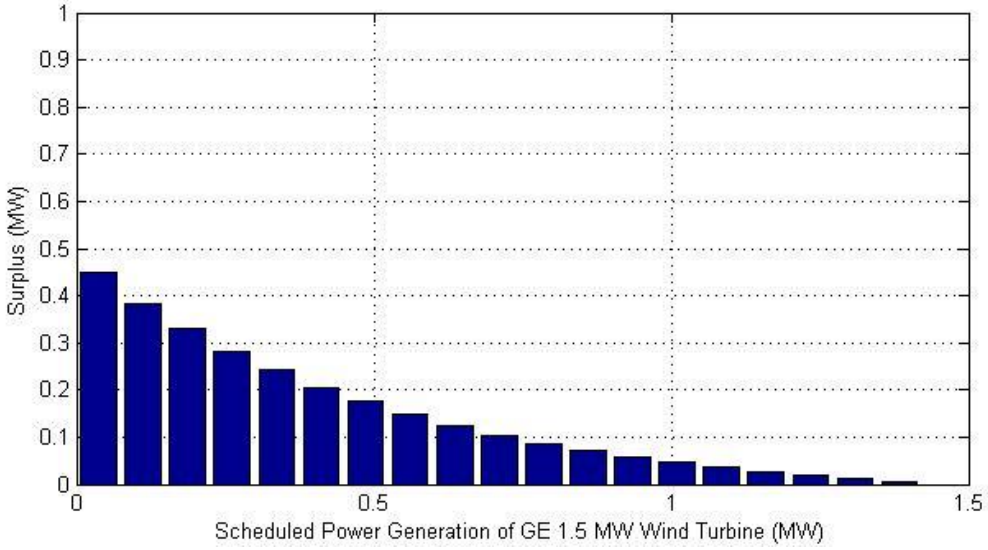

Fig 6.18 Expected wind power surplus of one GE 1.5 MW wind turbine

The curve fitting of shortage and surplus according to the scheduled power are given by:

$$F_{shortage}(P_w) = n * cost_{shortage}(0.2522{P_w}^2 + 0.3355P_w - 0.03619) \quad (6.18)$$

$$F_{surplus}(P_w) = n * cost_{surplus}(0.2522{P_w}^2 - 0.6645P_w + 0.4492) \quad (6.19)$$

The P_w in (6.13) and (6.14) is the scheduled power generation of one wind turbine.

With shortage and surplus cost factor equal to 18 R/MW and 2 R/MW, the cost function of the entire wind farm which has 200 wind turbines is given as:

$$F(P_{wf}) = 0.020176{P_{wf}}^2 + 3.368P_{wf} + 78.348 \quad (6.20)$$

The P_{wf} in (6.20) is the scheduled power generation of the entire wind farm.

The other synchronous generators' cost functions are also quadratic polynomials which has the form in (6.21). Their parameter [93] and initial scheduled power generations are given in Table 6.2.

$$F_i(P_{Gi}) = a{P_{Gi}}^2 + bP_{Gi} + c \quad (6.21)$$

Table 6.2 Generation cost and scheduled power generation

	a	b	c	P_{Gi} (MW)
Gen1	0.0193	6.9	0	250
Gen2	0.0111	3.7	0	690
Gen3	0.0104	2.8	0	650
Gen4	0.0088	4.7	0	700
Gen5	0.0128	2.8	0	600
Gen6	0.0094	3.7	0	700
Gen7	0.0099	4.8	0	600

Gen8	0.0113	3.6	0	600
Gen10	0.0064	3.9	0	300

The optimization is solved similarly as the 9-bus example. The final result of generation schedule is given in Table 6.3.

Table 6.3 Optimal generation schedule

	P_{Gi} (MW)
Gen1	270.79
Gen2	614.98
Gen3	699.64
Gen4	718.90
Gen5	568.46
Gen6	726.20
Gen7	633.97
Gen8	608.52
Wind Farm	250.65
Gen10	300

The initial generation cost and optimized generation cost are 56219 R/h and 56063R/h. The stability constrained optimal power flow has saved 156 R/h. The biggest angle difference between generator buses is 27.08^{o}. This guarantees the operation has reasonable distance from the stability margin.

6.7 Conclusions

This chapter discussed the impact of wind power generation on power system transient stability and the stochastic model of South Carolina offshore wind power. Based on the result of these two studies, a technique for solving the transient stability constrained optimal power flow with wind power penetration has been proposed. The

proposed technique is able to solve the nonlinear optimization problem for better accuracy. At present it can minimize the expected generation cost of the power system while maintaining the system within the safety region to enhance the power system transient stability. Better approaches to solve the nonlinear optimal power flow should be studied in the future to allow the proposed technique more functions such as minimizing the losses, optimizing transformer taps, optimizing reactive power compensators and other proper aspects.

CHAPTER SEVEN

CONCLUSIONS

In this dissertation the power system transient stability assessment technique and its related power system optimal operation with wind power has been discussed. Chapter Four has started with the regular approach and applied the catastrophe theory for large scale power system transient stability assessment. Compared with other techniques, the catastrophe theory can greatly reduce the complexity of power system operating patterns. However the following studies have discovered that the concept of COI for SMIB equivalent system will downgrade the performance of the stability assessment techniques. Chapter Five has further discussed the COI in multi-machine power system transient stability related techniques. Then a new technique for estimating the generator rotor angle difference has been developed to replace the COI. Based on all results and discoveries, Chapter Six has studied the impact of wind power generation on power system transient stability and developed a practical approach for power system economic operation under transient stability constrains with wind farms. Future work would be focused on following areas:

a. Real time power system state estimation with PMU.
b. Stability impact and optimizations on renewable energy sources and new power storage devices.
c. Transient stability studies with micro grid and distributed generation.

APPENDICES

Appendix A

IEEE 9-Bus System Data

Generator Data

	Bus Number	Base kV	Voltage (p.u)	X source (p.u)
Generator 1	1	16.5	1.01	0.040
Generator 2	2	18	1.01	0.089
Generator 3	3	13.8	1.01	0.107

Branch and Transformer Data

From Bus	To Bus	Line R (p.u)	Line X (p.u)	Charging B (p.u)
4	7	0.010	0.085	0.088
4	8	0.017	0.092	0.079
5	7	0.032	0.161	0.153
5	9	0.0085	0.072	0.0745
6	8	0.039	0.170	0.179
6	9	0.0119	0.1008	0.1045
1	4	0	0.0567	0
2	5	0	0.0625	0
3	6	0	0.0586	0

Bus Data

Bus Number	Bus kV	PLoad (MW)	QLoad (Mvar)	BShunt (Mvar)
1	16.5	0	0	0
2	18.0	0	0	0
3	13.8	0	0	0
4	230	0	0	0
5	230	35	10	0
6	230	0	0	0
7	230	125	70	20
8	230	90	40	10
9	230	100	55	20

Appendix B

IEEE 39-Bus System Data

Generator Data

	Bus Number	Base kV	Voltage (p.u)	X source (p.u)
Generator 1	30	100	1.00	0.23
Generator 2	31	100	1.00	0.23
Generator 3	32	100	1.00	0.23
Generator 4	33	100	1.00	0.23
Generator 5	34	100	1.00	0.23
Generator 6	35	100	1.00	0.23
Generator 7	36	100	1.00	0.23
Generator 8	37	100	1.00	0.23
Generator 9	38	100	1.00	0.23
Generator 10	39	100	1.00	0.23

Branch and Transformer Data

From Bus	To Bus	Line R (p.u)	Line X (p.u)	Charging B (p.u)
1	2	0.003500	0.041100	0.349350
1	39	0.001000	0.025000	0.375000
2	3	0.001300	0.015100	0.128600
2	25	0.007000	0.008600	0.073000
3	4	0.001300	0.021300	0.110700
3	18	0.001100	0.013300	0.106900
4	5	0.000800	0.012800	0.067100
4	14	0.000800	0.012900	0.069100
5	6	0.000200	0.002600	0.021700
5	8	0.000800	0.011200	0.073800
6	7	0.000600	0.009200	0.056500
6	11	0.000700	0.008200	0.069450
7	8	0.000400	0.004600	0.039000
8	9	0.002300	0.036300	0.190200
9	39	0.001000	0.025000	0.600000
10	11	0.000400	0.004300	0.036450
10	13	0.000400	0.004300	0.036450
13	14	0.000900	0.010100	0.086150

14	15	0.001800	0.021700	0.183000
15	16	0.000900	0.009400	0.085500
16	17	0.000700	0.008900	0.067100
16	19	0.001600	0.019500	0.152000
16	21	0.000800	0.013500	0.127400
16	24	0.000300	0.005900	0.034000
17	18	0.000700	0.008200	0.065950
17	27	0.001300	0.017300	0.160800
21	22	0.000800	0.014000	0.128250
22	23	0.000600	0.009600	0.092300
23	24	0.002200	0.035000	0.180500
25	26	0.003200	0.032300	0.256500
26	27	0.001400	0.014700	0.119800
26	28	0.004300	0.047400	0.390100
26	29	0.005700	0.062500	0.514500
28	29	0.001400	0.015100	0.124500
2	30	0.000000	0.018100	0
6	31	0.000000	0.025000	0
10	32	0.000000	0.020000	0
11	12	0.001600	0.043500	0
12	13	0.001600	0.043500	0
19	20	0.000700	0.013800	0
19	33	0.000700	0.014200	0
20	34	0.000900	0.018000	0
22	35	0.000000	0.014300	0
23	36	0.000500	0.027200	0
25	37	0.000600	0.023200	0
29	38	0.000800	0.015600	0

Bus Data

Bus Number	Bus kV	PLoad (MW)	QLoad (Mvar)	BShunt (Mvar)
1	100.0	0	0	0
2	100.0	0	0	0
3	100.0	322	2.4	0
4	100.0	500	184	0
5	100.0	0	0	0
6	100.0	0	0	0
7	100.0	233	84	0
8	100.0	522	176	0

9	100.0	0	0	0
10	100.0	0	0	0
11	100.0	0	0	0
12	100.0	8.5	88	0
13	100.0	0	0	0
14	100.0	0	0	0
15	100.0	320	153	0
16	100.0	329	32.3	0
17	100.0	0	0	0
18	100.0	158	30	0
19	100.0	0	0	0
20	100.0	680	103	0
21	100.0	274	115	0
22	100.0	0	0	0
23	100.0	247	84.6	0
24	100.0	308	-92.2	0
25	100.0	224	47.2	0
26	100.0	139	17	0
27	100.0	281	75	0
28	100.0	206	27.6	0
29	100.0	283.5	26.9	0
30	100.0	0	0	0
31	100.0	9.2	4.6	0
32	100.0	0	0	0
33	100.0	0	0	0
34	100.0	0	0	0
35	100.0	0	0	0
36	100.0	0	0	0
37	100.0	0	0	0
38	100.0	0	0	0
39	100.0	1104	250	0

Appendix C

GE 1.5 MW Wind Turbine Parameters

Generator WT3G1

Symbol	Value
X_{eq}	0.8
$K_p ll$	30
$K_{ip} ll$	0
PLLMX	0.1
P_{rated}	1.5

Electrical control WT3E1

Symbol	Value
Tfv	0.15
K_{pv}	18
K_{iv}	5
K_c	0.05
Tfp	0.05
K_{pp}	3
K_{ip}	0.6
PMX	1.12
PMN	0.10
QMX	0.296
QMN	-0.436
IP_{max}	1.10
RPMX	0.45
RPMN	-0.45
T_Power	5.0
K_{qi}	0.0
VMINCL	0.90
VMAXCL	1.20
K_{qv}	40
XIQmin	-0.50
XIQmax	0.40
T_V	0.05
T_p	0.05
Fn	1.0

WPMIN	0.69
W_p20	0.78
W_p40	0.98
W_p60	1.12
Pwp	0.74
W_p100	1.20

Turbine WT3T1

Symbol	Value
VW	1.25
H	4.95
DAMP	0
K_{aero}	0.0070
Theta2	21.98
Htfrac	0.875
Frec1	1.80
DSHAFT	1.50

Pitch control WT3P1

Symbol	Value
Tp	0.30
Kpp	150
Kip	25
Kpc	3.0
Kic	30
ThetaMin	0.0
ThetaMax	27.0
RTeta	10.0
PMX	1.0

REFERENCES

[1] August 14 2003 Blackout Investigation [online]. Available: http://www.nerc.com/~filesz/blackout.html

[2] "promoting Wholesale Competition Through Open Access Non-Discriminatory Transmission Services by Public Utilities; Recovery of Stranded Costs by Public Utilites and Transmitting Utilityes," Decket Nos. RM95-8-000 and RM-7-001, Order No. 888, April, 1996

[3] "Open Access Same-Time Information System (Formerly Real-Time Information Networks) and Standards of Conduct," Docket No. RM95-9-000, Order No. 889, April, 1996

[4] P. M Anderson, A. A. Fouad, "Poewr System Control and Stability," 2nd Edition, Wiley-IEEE press, 2002.

[5] R. SChainker, P. Miller, W. Dubbelday, P. Hirsh, G. Zhang, "Real Time Dynamic Security Assessment: Fast Simulation and Modeling Applied to Emergency Outage Security of the Electric Grid," IEEE Power and Energy Magazing, Vol. 4, pp. 51-58, March, 2006.

[6] P. Kundur; J. Paserba; V. Ajjarapu; G. Andersson; A. Bose; C. Canizares; N. Hatziargyriou; D. Hill; A. Stankovic; C. Taylor; T. Van Cutsem; V. Vittal, "Definition and classification of power system stability IEEE/CIGRE joint task force on stability terms and definitions," IEEE Trans. Power Systems, Vol. 19 , Issue. 3, pp. 1387 - 1401, 2004.

[7] V. Centeno; A.G. Phadke; A. Edris; J. Benton; M. Gaudi; G. Michel, "An adaptive out-of-step relay [for power system protection]," IEEE Trans. Power Delivery, Vol. 12 , Issue. 1, pp. 61 - 71, 1997

[8] Jan Machowski, Janusz W. Bialek, James R. Bumby, "Power System Dynamics: Stability and Control," 2nd Edition, Wiley, 2008

[9] R. Billinton; P.R.S Kuruganty, "A Probabilistic Index for Transient Stability," IEEE Transactions on Power Apparatus and Systems, Vol. PAS-99, Issue. 1, pp. 195 - 206, 1980

[10] K.W. Chan; D.P. Brook; R.W. Dunn; A.R. Daniels, "Time domain simulation based on-line dynamic stability constraint assessment," International Conference on Electric Utility Deregulation and Restructuring and Power Technologies, pp. 384 - 389, 2000.

[11] Chih-Wen Liu; J.S. Thorp, "New methods for computing power system dynamic response for real-time transient stability prediction," IEEE Trans. Circuits and Systems I: Fundamental Theory and Applications, Vol. 47 , Issue. 3, pp. 324 - 337, 2000.

[12] N. Kakimoto; M. Sugumi; T. Makino; K. Tomiyama, "Monitoring of interarea oscillation mode by synchronized phasor measurement," IEEE Trans. Power Systems, Vol. 21 , Issue. 1, pp. 260 - 268, 2006.

[13] Kai Sun; S. Likhate; V. Vittal; V.S. Kolluri; S. Mandal, "An Online Dynamic Security Assessment Scheme Using Phasor Measurements and Decision Trees," IEEE Trans. Power Systems, Vol. 22, Issue. 4, pp.1935 - 1943, Nov, 2007.

[14] Liang-Song Zhou; Bo Peng; Cheng-Jun Xia; Hui-Jun Hu, "Novel hierarchical decision-making transient stability control system based on on-line stability calculation," International Conference on Advances in Power System Control, Operation and Management, vol.2, pp. 332 - 336, 2000.

[15] Zhi-gang Du; Lin Niu; Jian-guo Zhao, "Application of support vector regression model based on phase space reconstruction to power system wide-area stability prediction," International Power Engineering Conference, pp. 1371 - 1376, 2007.

[16] A.W.N. Izzri; A. Mohamed; I. Yahya, "A New Method of Transient Stability Assessment in Power Systems Using LS-SVM," 5th Student Conference on Research and Development, pp. 1 - 6, 2007.

[17] H. Mori; Y. Komatsu, "A hybrid method of optimal data mining and artificial neural network for voltage stability assessment," IEEE Russia Power Tech, pp. 1 - 7, Jun, 2005.

[18] A. Roth; D. Ruiz-Vega; D. Ernst; C. Bulac; M. Pavella; G. Andersson, "An approach to modal analysis of power system angle stability," 2001 IEEE Porto Power Tech Proceedings, Vol. 2, 2001.

[19] Y. Xue; T. Van Cutsem; M. Ribbens-Pavella, "A simple direct method for fast transient stability assessment of large power systems," IEEE Trans. Power Systems, Vol. 3, Issue. 2, pp. 400 - 412, May, 1988.

[20] Michael Sherwood; Dongchen Hu,; Venkatasubramanian, Vaithianathan Mani, "Real Time Detection of Angle Instability Using Synchrophasors and Action Principle," 2007 iREP Symposium Bulk Power System Dynamics and Control - VII. Revitalizing Operational Reliability, pp. 1 - 11, Aug, 2007.

[21] C.-W. Liu; J. Thorp, "Application of synchronised phasor measurements to real-time transient stability prediction," Generation, IEE Proceedings Transmission and Distribution, Vol. 142, Issue. 4, pp. 355 - 360, Jul, 1995.

[22] Yuri Makarov; Carl Miller; Tony Nguenm; Jian Ma, "Characteristic ellipsoid method for monitoring power system dynamic behavior using phasor measurements," 2007 iREP symposium bulk power system dynamics and control VII, revitalizing operational reliability, pp.1 -5, Aug, 2007.

[23] H. Ota; Y. Kitayama; H. Ito; N. Fukushima; K. Omata, K. Morita; Y. Kokai, "Development of transient stability control system (TSC system) based on on-line stability calculation, IEEE Trans. Power Systems, Vol. 11, Issue. 3, pp.1463 - 1472, Aug, 1996.

[24] Ancheng Xue; Chen Shen; Shengwei Mei; Yixin Ni; Wu, F.F.; Qiang Lu, "A new transient stability index of power systems based on theory of stability region and its applications, Power Engineering Society General Meeting, Jun, 2006.

[25] N. Amjady; S.A. Banihashemi, "Transient stability prediction of power systems by a new synchronism status index and hybrid classifier," IET Generation, Transmission & Distribution, Vol. 4, Issue. 4, pp. 509 - 518, 2010.

[26] Da-Zhong Fang; T.S. Chung; Yao Zhang; Wennan Song, "Transient stability limit conditions analysis using a corrected transient energy function approach," IEEE Trans. Power Systems, Vol. 15, Issue. 2, pp. 804 - 810, May, 2000.

[27] F.F. Song; T.S. Bi; Q.X. Yang, "Study on wide area measurement system based transient stability control for power system," The 7th International Power Engineering Conference, Vol. 2, pp. 757 - 760, 2005.

[28] V.N. Avramenko, "Power system stability assessment for current states of the system," IEEE Russia Power Tech, pp. 1 - 6, 2005.

[29] M.H. Haque, "Application of energy function to assess the first-swing stability of a power system with a SVC," IEE Proceedings Generation, Transmission and Distribution, Vol. 152, Issue. 6, pp. 806 - 812, Nov, 2005.

[30] C.D. Vournas; P.W. Sauer; M.A. Pai, "Time-scale decomposition in voltage stability analysis of power systems," Proceedings of the 34th IEEE Conference on Decision and Control, Vol. 4, pp. 3459 - 3464, Dec, 1995.

[31] Tzong-Yih Guo; R.A. Schlueter, "Identification of generic bifurcation and stability problems in power system differential-algebraic model,", IEEE Transa. Power Systems, Vol. 9, Issue. 2, pp. 1032 - 1044, 1994.

[32] T.S. Chung,; K.L. Lo; C.S. Chang, "On the effectiveness of applying online dynamic security assessment in power system optimal operation," International Conference on Advances in Power System Control, Operation and Management, Vol. 1, pp. 158 - 163, Nov, 1991.

[33] S. Bruno; E. De Tuglie; M. La Scala, "Transient security dispatch for the concurrent optimization of plural postulated contingencies," IEEE Trans. Power Systems, Vol. 17, Issue. 3, pp. 707 - 714, 2002.

[34] E. De Tuglie; M. Dicorato; Politecnico di Bari; M. La Scala; P. Scarpellini, "Dynamic Security Dispatch Under Practical Constrains," 14 th PSCC, Sevilla, Session 05, Paper 4, Jun, 2002.

[35] S.A. Soman; T.B. Nguyen; M.A. Pai; R. Vaidyanathan, "Analysis of angle stability problems: a transmission protection systems perspective," IEEE Trans. Power Delivery, Vol. 19, pp. 1024 – 1033, Jun, 2004.

[36] S. Paudyal; G. Ramakrishna; M.S. Sachdev, "Application of Equal Area Criterion Conditions in the Time Domain for Out-of-Step Protection," IEEE Trans. Power Delivery, Vol. 25, pp. 600 – 609, Sep, 2010.

[37] K.R. Padiyar; S. Krishna, "Online detection of loss of synchronism using energy function criterion," IEEE Trans. Power Delivery, Vol. 21, pp. 46 – 55, Dec, 2006.

[38] A. Pizano-Martianez; C.R. Fuerte-Esquivel; D. Ruiz-Vega, "Global Transient Stability-Constrained Optimal Power Flow Using an OMIB Reference Trajectory," IEEE Trans. Power Systems, Vol. 25, pp. 392 – 403, Jan, 2010.

[39] Y. Kato; S. Iwamoto, "Transient stability preventive control for stable operating condition with desired CCT," IEEE Trans. Power Systems, Vol. 1, pp. 1154 – 1161, Nov, 2002.

[40] Saunders; Peter Timothy, An introduction to catastrophe theory, Cambridge University Press, 1980.

[41] A.M. Mihirig; M.D. Wvong, "Transient stability analysis of multi-machine power systems by catastrophe theory," IEE Proceedings, Generation, Transmission and Distribution, Vol. 136, pp. 254 – 258, Jul, 1989.

[42] A.A. Sallam, "Power systems transient stability assessment using catastrophe theory," IEE Proceedings, Generation, Transmission and Distribution, Vol. 136, pp. 108 – 114, Mar. 1989.

[43] K.H. So; J.Y. Heo; C.H. Kim; R.K. Aggarwal; K.B. Song, “Out-of-step detection algorithm using frequency deviation of voltage,” IET Generation, Transmission & Distribution, Vol. 1, pp. 119 – 126, Jan, 2007.

[44] M. D. Wvong; A. M. Mihirig, “Catastrophe theory applied to transient stability assessment of power systems,” IEE Proceedings, Generation, Transmission and Distribution, Vol. 133, pp. 314-318, Sep. 1986.

[45] R. Zarate-Minano; T. Van Cutsem; F. Milano; A.J. Conejo, “Securing Transient Stability Using Time-Domain Simulations Within an Optimal Power Flow,” IEEE Trans. Power Systems, Vol. 2, pp. 243 – 253, Feb, 2010.

[46] E. Ghahremani; M. Karrari; M.B. Menhaj; O.P. Malik, “Rotor angle estimation of synchronous generator from online measurement,” 2008 Universities Power Engineering Conf, pp. 1 – 5, Sep, 2008.

[47] V. Bandal; B. Bandyopadhyay, “Robust decentralised output feedback sliding mode control technique-based power system stabiliser (PSS) for multimachine power system,” IET Control Theory & Applications, Vol. 1, pp. 1512 – 1522, Sep, 2007.

[48] Kejun Mei; S.M. Rovnyak; Chee-Mun Ong, "Clustering-Based Dynamic Event Location Using Wide-Area Phasor Measurements," IEEE Trans. Power Systems, Vol. 23, Issue. 2, pp. 673 - 679, 2008.

[49] K.K. Anaparthi; B. Chaudhuri; N.F. Thornhill; B.C. Pal, "Coherency Identification in Power Systems Through Principal Component Analysis," IEEE Trans. Power Systems, Vol. 20, Issue. 3, pp. 1658 - 1660, 2005.

[50] G. Chicco; R. Napoli; F. Piglione, "Comparisons among clustering techniques for electricity customer classification," IEEE Trans. Power Systems, Vol, 21, Issue, 2, pp. 933 - 940, 2006

[51] E.R. Hamilton; J. Undrill; P.S. Hamer; S. Manson, "Considerations for generation in an islanded operation," Industry Applications Society 56th Annual Petroleum and Chemical Industry Conference, pp. 1 - 10, 2009.

[52] Joe H. Ward, Jr, "Hierarchical Grouping to Optimize an Objective Function," Journal of the American Statistical Association, Vol. 58, Issue. 301, pp.236-244, MAr, 1963.

[53] K.R. Padiyar; S. Krishna, "Online detection of loss of synchronism using energy function criterion," IEEE Trans. Power Delivery, Vol. 21, Issue. 1, pp. 46 - 55, 2006.

[54] Y. Kato; S. Iwamoto, "Transient stability preventive control for stable operating condition with desired CCT," IEEE Trans. Power Systems, Vol: 17, Issue: 4, pp. 1154 - 1161, 2002.

[55] Z. Wang; V. Aravnthan; E. Makram, "Generator cluster transient stability assessment using catastrophe theory," 10th International Conference on Environment and Electrical Engineering, pp. 1 – 4, 2011.

[56] S. Paudyal, G. Ramakrishna; M.S. Sachdev, "Application of Equal Area Criterion Conditions in the Time Domain for Out-of-Step Protection," IEEE Trans. Power Delivery, Vol. 25, pp. 600 – 609, Sep, 2010.

[57] M.H. Haque, "Evaluation of First Swing Stability of a Large Power System With Various FACTS Devices," IEEE Trans. Power Systems, Vol. 23 , Issue. 3, pp. 1144 - 1151, 2008.

[58] http://www.energy.siemens.com/hq/en/services/power-transmission-distribution/power-technologies-international/software-solutions/pss-e.htm

[59] http://www.rtds.com/index/index.html

[60] 20% Wind Energy by 2030 Increasing Wind Energy's Contribution to U.S. Electricity Supply, DOE/GO-102008-2567, July 2008.

[61] P.K. Sen; J.P. Nelson, "Application guidelines for induction generators," IEEE International Electric Machines and Drives Conference Record, pp. WC1/5.1 - WC1/5.3, 1997.

[62] T. Petru; T. Thiringer, "Modeling of wind turbines for power system studies," IEEE Trans. Power Systems, Vol. 17, Issue: 4, pp. 1132 - 1139, 2002.

[63] Yazhou Lei; A. Mullane; G. Lightbody; R. Yacamini, "Modeling of the wind turbine with a doubly fed induction generator for grid integration studies," IEEE Trans. Energy Conversion, Vol. 21, Issue. 1, pp. 257 – 264, Mar, 2006.

[64] Chompoo-inwai Chai; Wei-Jen Lee; P. Fuangfoo; M. Williams; J.R. Liao, "System impact study for the interconnection of wind generation and utility system" IEEE Trans. Industry Applications, Vol. 41, Issue 1, pp. 163 - 168, Jan.-Feb. 2005.

[65] M.A. Poller, "Doubly-fed induction machine models for stability assessment of wind farms," 2003 IEEE Bologna Power Tech Conference Proceedings, Vol. 3, pp. 1 - 6, 2003.

[66] Shuhui Li; T.A. Haskew; J. Jackson, "Power generation characteristic study of integrated DFIG and its frequency converter," Power and Energy Society General Meeting - Conversion and Delivery of Electrical Energy in the 21st Century, pp. 1 – 9, Jul, 2008.

[67] V. Bufano; M. Dicorato; A. Minoia; M. Trovato, "Embedding wind farm generation in power system transient stability analysis," 2005 IEEE Russia Power Tech, pp. 1 – 7, 2005.

[68] N.W. Miller; J.J. Sanchez-Gasca; W.W. Price; R.W. Delmerico, "Dynamic modeling of GE 1.5 and 3.6 MW wind turbine-generators for stability simulations," Power Engineering Society General Meeting, Vol. 3, pp. 1977 - 1983, 2003.

[69] B. Ekanayake; L. Holdsworth; N. Jenkins, "Comparison of 5th order and 3rd order machine models for doubly fed induction generator (DFIG) wind turbines," Electric Power Systems Research, Vol. 67, Issue. 3, pp. 207 - 215, Dec, 2003.

[70] Wei Qiao; R.G. Harley, "Effect of grid-connected DFIG wind turbines on power system transient stability," Power and Energy Society General Meeting - Conversion and Delivery of Electrical Energy in the 21st Century, pp.1 – 7, Jul 2008.

[71] J. Wiik; J.O. Gjefde; T. Gjengedal, "Impacts from large scale integration of wind energy farms into weak power systems," International Conference on Power System Technology, Vol. 1, pp. 49 - 54, Dec, 2000.

[72] K. Elkington; V. Knazkins; M. Ghandhar, "On the rotor angle stability of power systems with Doubly Fed Induction Generators," 2007 IEEE Lausanne Power Tech, pp. 213 - 218, Jul, 2007.

[73] D. Basic; Jian-Guo Zhu; G. Boardman, "Transient performance study of a brushless doubly fed twin stator induction generator," IEEE Trans. Energy Conversion, Vol. 18, Issue 3, pp. 400 – 408, Sep, 2003.

[74] http://www.elec.uow.edu.au/pqc/specs.html

[75] Fei Ye; Xueliang Huang; Chaoming Wang; Gan Zhou; Ping Luo, "The impact and simulation on large wind farm connected to power system," Third International Conference Electric Utility Deregulation and Restructuring and Power Technologies, pp. 2608 – 2614, Apr 2008.

[76] T. Senjyu; N. Sueyoshi; K. Uezato; H. Fujita, "Transient current analysis of induction generator for wind power generating system," Transmission and Distribution Conference and Exhibition 2002: Asia Pacific, Vol. 3, pp. 1647 - 1652, Oct, 2002.

[77] J.J.; N.W. Miller; W.W. Price, "A modal analysis of a two-area system with significant wind power penetration, Sanchez-Gasca," IEEE PES Power Systems Conference and Exposition, Vol.2, pp. 1148 - 1152, Oct, 2004.

[78] J.M. Rodriguez; J.L. Fernandez; D. Beato; R. Iturbe; J. Usaola; P. Ledesma; J.R. Wilhelmi, "Incidence on power system dynamics of high penetration of fixed speed and doubly fed wind energy systems: study of the Spanish case," IEEE Trans. Power Systems, Vol. 17, Issue 4, pp. 1089 – 1095, Nov, 2002.

[79] B. Chitti Babu; K.B. Mohanty; C. Poongothai; Emerging, "Performance of Double-Output Induction Generator for Wind Energy Conversion Systems," First International Conference Trends in Engineering and Technology, pp. 933 – 938, Jul, 2008.

[80] H.R. Najafi; F. Robinson; F. Dastyar; A.A. Samadi, "Transient stability evaluation of wind farms implemented with induction generators," 43rd International Universities Power Engineering Conference, pp. 1 – 5, Sep, 2008.

[81] P. Shi; K.L. Lo, "Effect of wind farm on the steady state stability of a weak grid," Third International Conference Electric Utility Deregulation and Restructuring and Power Technologies, pp. 840 - 845, Apr, 2008.

[82] H. Mohammed; C.O. Nwankpa, "Stochastic analysis and simulation of grid-connected wind energy conversion system," IEEE Trans. Energy Conversion, Vol. 15, Issue 1, pp.85 - 90, Mar, 2000.

[83] S. O. Faried; R. Billinton; S. Aboreshaid, "Probabilistic Evaluation of Transient Stability of a Wind Farm," IEEE Trans. Energy Conversion, pp. 1 – 7, 2009.

[84] J. Cardenas; V. Muthukrishnan; D. McGinn; R. Hunt, "Wind farm protection using an IEC 61850 process bus architecture," 10th IET International Conference on Developments in Power System Protection (DPSP 2010). Managing the Change, pp. 1 - 5, 2010.

[85] H. Li; Z. Chen, "Transient Stability Analysis of Wind Turbines with Induction Generators Considering Blades and Shaft Flexibility," 33rd Annual Conference of the IEEE Industrial Electronics Society, pp. 1604 – 1609, Nov, 2007.

[86] http://carolinasrcoos.org/

[87] E. Holtslag, "Offshore measurements: validation of Buoy vs Met mast," Wind Energie Ontwikkelings Maatschappij (WEOM), The Netherlands.

[88] Libao Shi; Chen Wang; Liangzhong Yao; Yixin Ni; M. Bazargan, "Optimal Power Flow Solution Incorporating Wind Power," IEEE Systems Journal, Vol. 6, Issue. 2, pp. 233 - 241, 2012.

[89] Jing Liu; Yingni Jiang, "A statistical analysis of wind power density based on the Weibull models for Fujian province in China," World Non-Grid-Connected Wind Power and Energy Conference, pp. 1 - 4, 2009.

[90] 1.5 MW Wind Turbine Series - GE Energy, http://http://site.ge-energy.com/prod_serv/products/wind_turbines/en/downloads/GEA14954C15-MW-Broch.pdf

[91] Jabr, R.A.; Pal, B.C., "Intermittent wind generation in optimal power flow dispatching," IET Transmission & Distribution Generation, Vol. 3, Issue. 1, pp. 66 - 74, 2009.

[92] Haiyan Chen; Jinfu Chen; Xianzhong Duan, "Multi-stage Dynamic Optimal Power Flow in Wind Power Integrated System," Transmission and Distribution Conference and Exhibition: Asia and Pacific, pp. 1 - 5, 2005.

[93] G. Yesuratnam; N. Srilatha; P. Lokender Raddy. “Congestion management Technique Using Fuzzy Logic Based on Security and Economy Criteria,” AIKED’12 Proceedings of the 11th WSEAS international conference on Artificial Intelligence, knowledge Engineering and Data Bases, pp. 157- 162, 2012.